DEPARTMENT OF PHYSICS
UNIVERSITY OF JYVÄSKYLÄ
RESEARCH REPORT No. 12/2006

RADIO-FREQUENCY SPECTROSCOPY OF ATOMIC FERMI GAS

BY
JAMI KINNUNEN

Academic Dissertation
for the Degree of
Doctor of Philosophy

To be presented, by permission of the
Faculty of Mathematics and Science
of the University of Jyväskylä,
for public examination in Auditorium FYS-1 of the
University of Jyväskylä on December 15, 2006
at 12 o'clock noon

Jyväskylä, Finland
December 2006

ISBN 978-951-39-3177-3

URN:ISBN:978-951-39-3177-3

Preface

The work presented in this thesis has been carried out during the years 2002-2006 in the Department of Physics at the University of Jyväskylä.

First I would like to thank my supervisor professor Päivi Törmä. She has put a lot of effort in this work, making the four years of my studies very productive. The extremely rapidly advancing field of ultracold quantum gases would be overwhelming without a good active group. I would therefore like to thank Dr. Mirta Rodríguez, Dr. Jani-Petri Martikainen, Dr. Lars Melwyn Jensen, Mr. Timo Koponen and Mr. Mikko Leskinen for the endless hours spent by the whiteboard in our coffee room and in the group meetings. I would also like to thank all the former and present members of the ele-group for the pleasant atmosphere in our group.

I am also indebted to my friends, family, and especially my wife Ulla and son Aarni for giving me something else to think. There is life beyond physics after all!

This work has been supported by the Academy of Finland and National Graduate School in Material Physics.

Jyväskylä, November 2006

Jami Kinnunen

Abstract

This thesis studies radio-frequency spectroscopy of superfluid alkali Fermi gases. Radio-frequency and laser fields provide a coherent and well understood tool for manipulating atomic gases. However, new phenomena are expected and have already been seen experimentally when the alkali atoms become strongly interacting.

Here we use a simple perturbative treatment of the atom-rf-field coupling for studying the spectroscopy of a strongly interacting gas. At ultracold temperatures fermionic atoms become paired in analogy to electrons in superconductors. The resulting binding energy, or the pairing gap, can be observed as a shift in the radio-frequency spectrum. With strong interactions, the fermions begin pairing already above the critical superfluid transition temperature. The radio-frequency spectroscopy grants a way to study these fluctuation effects quantitatively.

The inhomogeneous trapping potential of the atom cloud also adds its own flavour, resulting in distinct mesoscopic effects in the radio-frequency spectra. Our theoretical models are in very good agreement with the experimental results. First order perturbation theory provides qualitatively correct lineshapes, and our generalised perturbative approach gives quantitatively correct magnitudes for the transfer rates.

The inhomogeneity plays an important part also in more exotic systems in which the simple BCS-type pairing of atoms is prevented by polarising the gas. Superfluidity and phase separation in such spin-imbalanced gases has been experimentally observed. We have suggested the use of radio-frequency spectroscopy for observing exotic polarised superfluid states, present at the edges of the atom cloud.

List of publications

The main results of this thesis have been reported in the following articles

B.I J. KINNUNEN, M. RODRÍGUEZ, AND P. TÖRMÄ, *Signatures of superfluidity for Feshbach-resonant Fermi Gases*. Phys. Rev. Lett. **92** 230403 (2004).

B.II J. KINNUNEN, M. RODRÍGUEZ, AND P. TÖRMÄ, *Pairing gap and in-gap excitations in trapped Fermionic superfluids*. Science **305** 1131 (2004).

B.III J. KINNUNEN AND P. TÖRMÄ, *Beyond linear response spectroscopy of ultracold Fermi gases*. Phys. Rev. Lett. **96** 070402 (2006).

B.IV J. KINNUNEN, L. M. JENSEN, AND P. TÖRMÄ, *Strongly interacting Fermi gases with density imbalance*. Phys. Rev. Lett. **96** 110403 (2006).

Other publications to which the author has contributed

C.I J. KINNUNEN, P. TÖRMÄ, AND J. P. PEKOLA, *Measuring charge-based quantum bits by superconducting single-electron transistor*. Phys. Rev. B **68** 020506R (2003).

C.II T. KOPONEN, J.-P. MARTIKAINEN, J. KINNUNEN, AND P. TÖRMÄ, *Sound velocity and dimensional crossover in a superfluid Fermi gas in an optical lattice*. Phys. Rev. A **73** 033620 (2006).

C.III L. M. JENSEN, J. KINNUNEN, AND P. TÖRMÄ, *Non-BCS superfluidity in trapped ultracold Fermi gases*. cond-mat/0604424 (submitted).

C.IV T. KOPONEN, J. KINNUNEN, J.-P. MARTIKAINEN, AND P. TÖRMÄ, *Fermion pairing with spin-density imbalance in an optical lattice*. New J. Phys. **8** 179 (2006).

Contents

1 Introduction

Radio-frequency (RF) spectroscopy provides the standard of time [54, 32]. The caesium standard uses ultracold ^{133}Cs atoms trapped in a laser trap, and a microwave field inducing transitions between two hyperfine states of the atoms. The excellent precision of the laser- and rf-spectroscopies make these ideal tools for studying atomic gases.

Weakly interacting fermionic particles (such as electrons or atoms with odd number of neutrons) will form pairs at low enough temperatures. This phenomenon is underlying the superconductivity of metals [83] and it is well described by the microscopic theory due to Bardeen, Cooper and Schrieffer (BCS) [6]. On the other hand, if the particles are strongly interacting, the assumptions of the BCS theory are broken. For example, high temperature superconductors are in this strongly interacting regime and they still lack a proper microscopic theory. Strongly interacting systems are also found in ^{3}He [50] and nuclear matter [5], and related problems are also encountered in QCD [72], which are very difficult to study experimentally.

The interactions in dilute atom gases are well described by only a single parameter, the scattering length a, making the theory simple. This, the purity of the system, and the possibility of tuning almost all relevant parameters make these systems ideal for studying the effects and phenomena of strong interactions. In this thesis, I will study the effects of strong interactions on the rf-spectroscopy of atom gases [84, 32, 74, 89, 19, 44, 46] (the last two are Publications II and III of this thesis).

1.1 Superfluid atom gas

The Bose-Einstein condensation (BEC) of atoms was predicted by Satyendra Nath Bose and Albert Einstein in 1920's [69]. Einstein speculated that cooling bosonic atoms (atoms with even number of neutrons) to low enough temperatures would cause them to condense into the lowest accessible quantum state. This would lead into a new form of matter, a bosonic superfluid.

The Bose-Einstein condensation in an alkali gas was first observed in 1995 by Eric Cornell and Carl Wieman [2], and Wolfgang Ketterle [23]. Subsequently it has been realised in several places around the world. In principle, the BEC is formed by simply cooling down the atoms. When the temperature drops below a certain critical level, the bosons start to condense into the ground state. Because the atoms

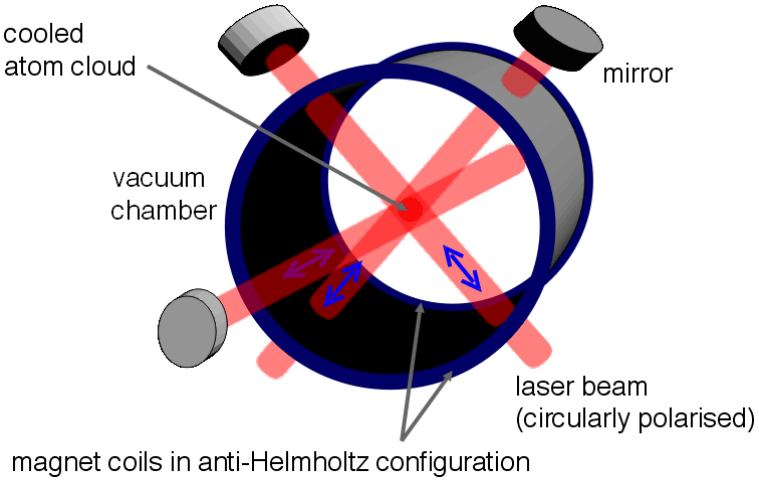

FIGURE 1.1 The magneto-optical trap (MOT) consists of three perpendicular pairs of laser beams and an inhomogeneous magnetic field. The cloud of atoms is trapped in the intersection of the laser beams and cooled down. Typical process produces $10^5 - 10^7$ atoms in the temperature range $10 - 100\,\mathrm{nK}$. Picture by Jan Krieger (in public domain).

are indistinguishable, their phases become locked and they 'behave as one' [69]. In contrast, superfluidity of fermionic atoms is a complicated product of interactions between the atoms. The first results on condensed alkali Fermi gases are from 2003, in which the atoms paired into bosonic molecules that formed a BEC [39, 30]. These were followed by observations of condensates of fermion pairs in the strongly interacting regime [73, 93], cross-over behaviour [9, 11], and other studies on strongly interacting fermions, such as studies on collective excitations [7,41], pairing gap [19], heat capacity [42], molecular fraction [68], and vortices [88].

1.2 Experimental setup

The typical experimental setup of these superfluid atom gas experiments consists of a magneto-optical trap (MOT) formed by six lasers in three perpendicular directions and a magnetic field produced by coils. The intersection of the laser beams forms a potential well in which the atoms become trapped, see Fig. 1.1.

The atoms are produced by heating a piece of metal (for example ^{6}Li) and the vapour is directed into the MOT. The six lasers and the inhomogeneous magnetic field slow and cool down the atoms by radiation pressure and by taking advantage of the Doppler shift. The idea of the Doppler cooling is that the atoms interact only with lasers of correct colour. However, the Doppler shift will change the colour seen by the atom, so that an atom moving towards the laser will see the colour as 'bluer' and an atom moving away from the laser will see the colour as 'redder'. The interaction consists of an absorption of a (colour-shifted) photon from the laser beam

and subsequent emission of a photon of proper colour into arbitrary direction. If the absorbed photon is of lower energy than the emitted one, the energy of the atom is reduced (and hence it is cooled). By using slightly red-detuned lasers, the atoms will be slowed down whenever moving towards any of the six lasers (and the lasers are shining from all directions!).

The Doppler cooling is sufficient for reaching temperatures in the range of 10 - $100\,\mu\mathrm{K}$. At this point the atom cloud becomes too dense and opaque to the lasers and the cooling stops. In order to reach even lower temperatures (such as needed for superfluidity) the atoms are further cooled by using evaporative cooling, in which the most energetic atoms are expelled from the trap by changing their hyperfine states to untrapped ones using a simple laser or radio-frequency field. While depleting the number of atoms in the trap, it will also cool them as the average energy is reduced. The remaining kinetic energy is then distributed among the remaining atoms by two-body collisions. This cooling process can produce temperatures in the range of nK, sufficient for the emergence of superfluidity.

At these temperatures, the stable state of (most) atoms would be a solid. However, the time scale of the condensation (solidification) is long enough to allow the cooling, operation, and measurement of the gas. The crucial point is that the thermalisation required in the cooling depends on two-particle interactions while the solidification requires three-body correlations. In dilute systems, the two-body interactions are much more probable than the three-body interactions. Thus, the ultracold atom gas is in a metastable state, with a sufficiently long lifetime for the experiments.

1.3 Tunable parameters

Almost all of the experimental parameters in the ultracold atom gases can be varied, allowing the study of various and even exotic systems. By choosing different atoms, the masses and the interaction characteristics can be changed and even mixed statistics can be studied by using mixtures of bosons and fermions. Interaction strengths can be varied by the external magnetic field using Feshbach resonances [82] (see Fig. 1.2), allowing the study of the crossover from the BCS-like superfluidity of fermions to the BEC-superfluidity of bosonic molecules [37, 58, 64, 18]. The external trapping potential can be deformed by adding or modifying the lasers and the magnetic field, allowing the study of dimensional crossover from highly elongated 1D cigar-like traps to 2D pancakes [70], but also optical lattices in various geometries [20].

The flexibility of the atomic gases allows connections to several branches of physics. On the other hand, the diluteness and the purity allow avoiding several complicating factors that make similar phenomena hard to observe in other settings. A simple example is the BCS-BEC crossover in high temperature superconductors,

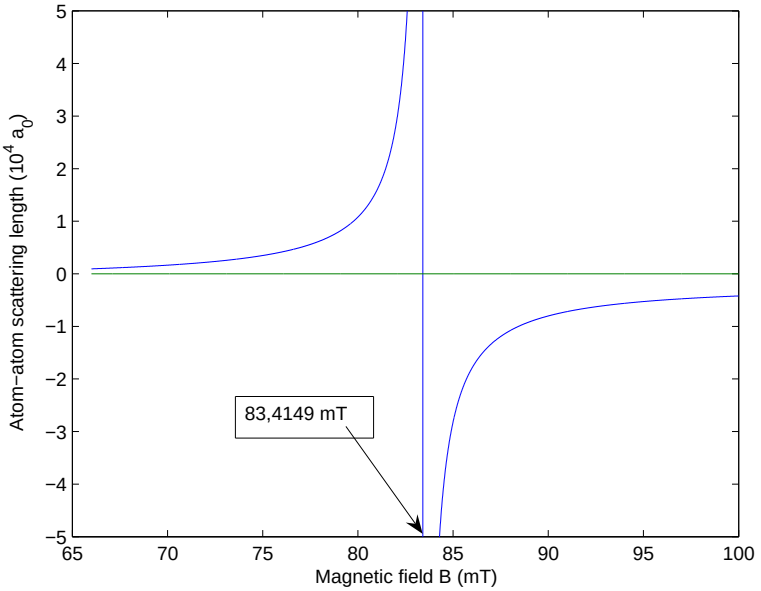

FIGURE 1.2 A Feshbach resonance in a ^{6}Li gas [8]. The interaction strength between the atoms can be tuned by a magnetic field. On resonance ($B_0 = 83.4191\,\mathrm{mT}$), the interaction strength diverges. Below the resonance the atoms pair into bound molecules that can undergo Bose-Einstein condensation. Above the resonance the atoms are described by the BCS theory. Close to the resonance, the atoms are unitary, or strongly interacting.

where the anisotropy of the cuprate sheets and the interactions between the electrons and the ions can hardly be neglected. While these differences make the direct comparison between the atomic gases and the high temperature superconductors difficult, it does allow the study of underlying assumptions about the pair formation, fluctuations, and superfluidity [18].

Fermionic superfluidity in a strongly interacting ultracold Fermi gas was finally observed directly in 2005 by Wolfgang Ketterle's group in MIT [88]. The signature of the superfluidity was a stable hexagonal lattice of quantised vortices in a rotating Fermi gas. With the advent of fermionic superfluidity, the progress for deeper understanding of strongly interacting systems has already begun [91, 65, 90, 66, 92, 76, 20, 75, 67, 1].

2 Atom gases

All elementary particles (neutrons, protons, electrons, photons, etc.) can be divided into two families, fermions and bosons, depending on the symmetry properties of the many-body wavefunctions. These properties are carried onto the composite objects like atoms, allowing us to speak about fermionic or bosonic atoms.

2.1 The two families of particles

The many-body state of identical particles has to satisfy certain symmetry requirements. Being identical means that exchange of any two particles cannot alter the results obtained from a measurement (observables), which is loosely speaking determined by the modulus of a wavefunction $|\Psi|^2$. However, the exchange of the identical particles may affect the phase of the many-body wavefunction that is not directly observable. Fermions are defined as particles that give a phase change of π (that is, the wavefunction Ψ is multiplied by -1) when two fermions are exchanged, whereas exchange of bosons does not affect the phase.

The symmetry properties are taken care of by defining (anti-)commutation relations

$$\begin{aligned}\left[\hat{\Psi}_\sigma(\vec{r}), \hat{\Psi}_{\sigma'}(\vec{r}')^\dagger\right]_\pm &\equiv \hat{\Psi}_\sigma(\vec{r})\hat{\Psi}_{\sigma'}(\vec{r}')^\dagger \pm \hat{\Psi}_{\sigma'}(\vec{r}')^\dagger\hat{\Psi}_\sigma(\vec{r}) = \delta_{\sigma\sigma'}\delta^3(\vec{r}-\vec{r}') \\ \left[\hat{\Psi}_\sigma(\vec{r})^\dagger, \hat{\Psi}_{\sigma'}(\vec{r}')^\dagger\right]_\pm &= 0 \\ \left[\hat{\Psi}_\sigma(\vec{r}), \hat{\Psi}_{\sigma'}(\vec{r}')\right]_\pm &= 0, \end{aligned} \tag{2.1}$$

where $\delta_{\sigma\sigma'}$ is the Kronecker's delta, $\delta^3(\vec{r})$ is the three-dimensional Dirac's delta function and the field operators $\hat{\Psi}_\sigma(\vec{r})^\dagger$ and $\hat{\Psi}_\sigma(\vec{r})$ create and annihilate a particle with spin σ at position $\vec{r}$. Fermionic anticommutation relations are obtained with the plus sign $+$ and the bosonic commutation relations with the minus sign $-$.

In practice the field operators are usually expanded in some basis of mutually orthonormal functions $\{\psi_k(\vec{r})\}_k$

$$\hat{\Psi}_\sigma(\vec{r}) = \sum_k \psi_k(\vec{r})\hat{c}_{k\sigma}, \tag{2.2}$$

where the operator $\hat{c}_{\vec{k}\sigma}$ annihilates a particle with spin σ from state with the quantum

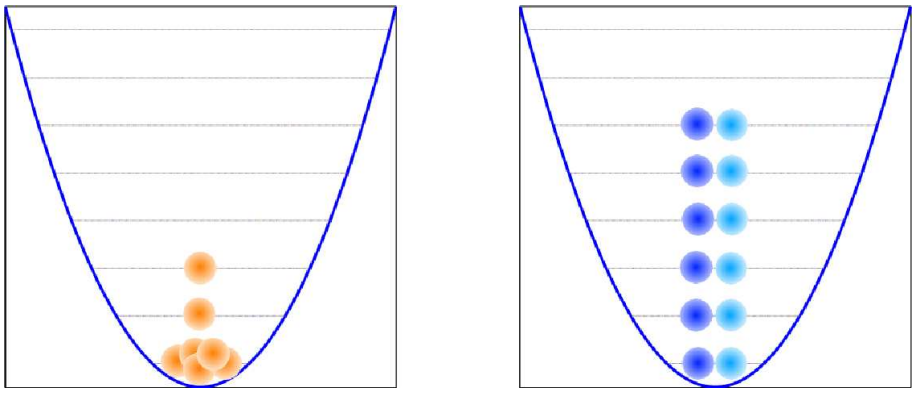

FIGURE 2.1 Several bosons (left picture) can occupy the same state (states shown as the horizontal lines). When the number of particles in any state becomes very large, the system is said to have Bose(-Einstein)-condensed. In contrast, the Pauli exclusion principle forbids two identical fermions from occupying the same state (right picture). The picture shows two-component gas, with each level filled by two fermions of different internal states (and hence not identical), up to the Fermi level.

number $\vec{k}$. For fermions (bosons) the anticommutation (commutation) properties of the field operators are carried onto the $\hat{c}$-operators, and we obtain

$$\left[\hat{c}_{\vec{k}\sigma}, \hat{c}^\dagger_{\vec{k}'\sigma'}\right]_\pm = \delta_{\sigma\sigma'}\delta_{\vec{k},\vec{k}'}, \tag{2.3}$$

and $\left[\hat{c}^\dagger_{\vec{k}\sigma}, \hat{c}^\dagger_{\vec{k}'\sigma'}\right]_\pm = \left[\hat{c}_{\vec{k}\sigma}, \hat{c}_{\vec{k}'\sigma'}\right]_\pm = 0.$

Trying to create two identical fermions ($\sigma = \sigma'$) in the same state ($\vec{k} = \vec{k}'$) gives $\hat{c}^\dagger_{\vec{k}\sigma}\hat{c}^\dagger_{\vec{k}\sigma} = 0$. This means that it is forbidden to place two identical fermions in the same state, a property known as the Pauli exclusion principle. On the other hand bosons do not obey this kind of restriction and hence any number of bosons can be in the same state, see Fig. 2.1. These properties are also reflected as different statistics for the particles, the Fermi-Dirac and Bose-Einstein statistics. This means that the expectation value for the number of bosons in a state with energy E_k in an equilibrium (at a given temperature T) is given by the Bose-Einstein distribution

$$n_{\mathrm{B}}(E) = \frac{1}{e^{\beta(E-\mu)} - 1}, \tag{2.4}$$

where $\beta = \frac{1}{k_{\mathrm{B}}T}$, k_{B} is the Boltzmann constant, and μ is the chemical potential. In contrast, fermions follow the Fermi-Dirac distribution

$$n_{\mathrm{F}}(E) = \frac{1}{e^{\beta(E-\mu)} + 1}. \tag{2.5}$$

These equations can be derived from the quantum statistical partition function describing a thermal equilibrium. As expected, the expectation value for the number

of identical fermions found at any state is at most one whereas the number of bosons is not limited. In particular, the Bose distribution diverges at $E - \mu = 0$. This corresponds to the appearance of a Bose-Einstein condensate.

Whether a particle belongs to the class of fermions or bosons depends on its spin angular momentum. Fermions have half-number spin angular momenta $\frac{1}{2}$, $\frac{3}{2}$, $\frac{5}{2}$, etc. and bosons have integer spin angular momenta 0, 1, 2, etc. Neutrons, protons and electrons are spin one-half particles while photons have spin one.

2.2 Atom gases

The elementary particles that form the atoms (neutrons, protons and electrons) are all fermions. Now one can ask what kind of symmetry properties do identical atoms have? A hydrogen atom consists of a proton-electron pair. Exchange of two hydrogen atoms would therefore correspond to exchange of two protons and two electrons, each exchange yielding a change in the sign of the many-body wavefunction. The sign of the total wavefunction is therefore unchanged, and the hydrogen atom has bosonic characteristics. Moreover, the spins of these two fermions can be combined to form a composite particle with the total spin of 0 or 1. On the other hand, a deuteron atom consists of a proton, neutron and one electron, and the exchange of two deuteron atoms would yield a total sign change of -1. Thus, deuteron atom has fermionic characteristics.

More generally, a group of even number of fermions combines as an integer spin particle and therefore has bosonic properties and a group of odd number of fermions looks like a fermion. Since (neutral) atoms have equal numbers of protons and electrons, the number of neutrons in the atom core (isotope) determines whether the atom should be treated as a boson or a fermion. If the distance between two atoms is very long compared to the size of a typical wavepacket (like in a dilute gas), the atoms do not 'see' the composite nature of each other, and the fermionic/bosonic description is adequate.

Since the atoms consist of several elementary particles, there are lot of internal degrees of freedom, and hence a multitude of internal states. This corresponds to having several different pseudospin states σ in Eq. (2.1). In the Fermi gas experiments so far, one is usually interested in mixtures of atoms in two different hyperfine states, effectively forming a two-component system analogous to the two spin states of the electrons in metals and superconductors. The hyperfine energy splitting of an atom arises from the spin-orbit interaction between the spin of the atom nucleus and the orbital motion of the electrons and the spin-spin interaction between the nucleus and the electrons' spins.

As an example, a hydrogen atom consists of an electron and a proton, each having a spin of $1/2$. These combine either into a total spin of $F = 0$ when the proton and the electron have opposite spins, or $F = 1$ when the spins are aligned. These

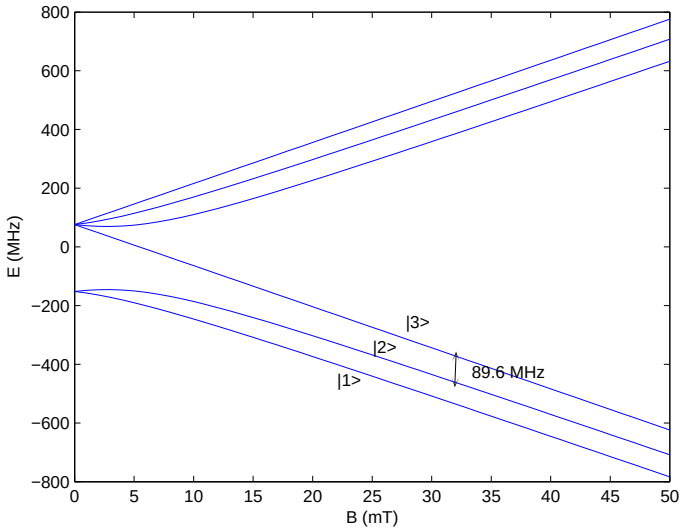

FIGURE 2.2 The energies of different hyperfine states of ^{6}Li in the presence of a magnetic field B. In this work, I will consider only the three high field seeking states denoted as $|1\rangle$, $|2\rangle$, and $|3\rangle$.

total spin states are $(2F+1)$-fold degenerate, and the different degenerate states are defined by the magnetic moment $m_\mathrm{f} = -F, -F+1, \ldots, F-1, F$. These are the hyperfine states usually used in atomic gas experiments and they are denoted as $|F, m_\mathrm{f}\rangle$. The presence of an external magnetic field lifts the degeneracy and the typical energy splittings between the different hyperfine states are of the order of $10-100\,\mathrm{MHz}$, see Fig. 2.2. Notice that the presence of the external magnetic field is required not only to trap the atoms but also to create the energy splitting between the hyperfine states, thus suppressing the spontaneous transitions of the atoms between the different internal states. As the typical energy and temperature scales studied in the experiments are of the order of $1-100\,\mathrm{kHz}$, these transitions can be safely neglected.

A dilute atomic gas is a weakly interacting gas, in which the interatomic scattering length a is much smaller than the average interatomic distance R, i.e. $|a/R| \ll 1$. For strongly interacting gases, this requirement is not usually met. However, the simple description of the atom-atom interactions using only the scattering length has turned out to be sufficient in many cases. The reason is that bound states that are connected with strong interactions are very short lived close to the resonance because of a very strong coupling between the molecular state and the state with free (unbound) atoms [82]. Neglecting these bound states recovers the simple theory also for the strongly interacting atoms.

3 Paired atoms and superfluidity

Superconductivity in metals and superfluidity in Fermi gases require attractive interactions between fermions (electrons in superconductors, fermionic atoms in Fermi gases). The BCS-theory explains that even a weak attractive interaction is sufficient for the fermions to start pairing at low enough temperatures. These pairs, called Cooper pairs, undergo a Bose-Einstein condensation.

Nowadays one has several possible approaches for microscopic description of the superconductivity and superfluidity: the original variational principle was used by Bardeen, Cooper and Schrieffer [6], canonical transformation yields an easy, but not so transparent path to superconductivity [27], and Green's function techniques are used in many modern extensions of the BCS theory [53]. Here I will start with the first approach, since there the underlying phenomena are most easily understood. I will also describe briefly the second approach, as I will use a similar technique for solving the Bogoliubov-deGennes equations in a harmonic trap. Finally, I will apply the Green's function techniques in order to explain some of the extensions of the BCS theory but also to get acquinted with the techniques as they will be useful when discussing the radio-frequency spectroscopy of atomic gases.

3.1 Interacting fermions

I start the description of the interacting many-body fermion system with the definition of the (grand canonical) Hamiltonian

$$\begin{aligned}\hat{H} = \sum_{\sigma=\downarrow,\uparrow} \int d^3\vec{r}\, \hat{\Psi}^\dagger_\sigma(\vec{r}) \hat{K}(\vec{r}) \hat{\Psi}_\sigma(\vec{r}) \\ + \int d^3\vec{r} \int d^3\vec{r}'\, \hat{\Psi}^\dagger_\uparrow(\vec{r}) \hat{\Psi}^\dagger_\downarrow(\vec{r}') U(|\vec{r}' - \vec{r}|) \hat{\Psi}_\downarrow(\vec{r}') \hat{\Psi}_\uparrow(\vec{r}).\end{aligned} \tag{3.1}$$

The field operator $\hat{\Psi}_\sigma(\vec{r})$ destroys a particle with spin σ at position $\vec{r}$ and $U(\vec{r} - \vec{r}')$ describes the particle-particle interaction. The operator $\hat{K}(\vec{r}) = -\frac{\hbar^2\nabla^2}{2m} + V_{\text{ext}}(\vec{r}) - \mu$ describes the kinetic energy of the particles and the external trapping potential, and μ is the chemical potential. Notice that we have neglected here any three-body correlations. In metallic superconductors this is well grounded due to weak interactions and in ultracold atom gases because the gas is very dilute, so that the probability of

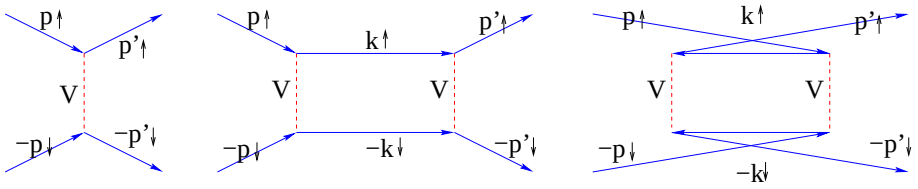

FIGURE 3.1 The first (left) and second (middle and right) Born approximations for the scattering of two particles from state $\vec{p}$,$-\vec{p}$ to state $\vec{p}'$,$-\vec{p}'$. In the second order process, the scattering takes place through an intermediate state $\vec{k}$, $-\vec{k}$, the middle diagram describing scattering through an empty intermediate state and the right diagram describing an intermediate state that is initially occupied.

having three or more atoms at the same place is small. In addition, we have assumed that the interactions do not flip the (hyperfine) spin states of the particles.

Hamiltonian in Eq. (3.1) will be encountered again later, but here I will restrict the discussion to a box-like external potential

$$V_{\text{ext}}(\vec{r}) = \begin{cases} 0 & \text{if } |x|, |y|, |z| < L \\ \infty & \text{elsewhere,} \end{cases} \tag{3.2}$$

where the size of the box L^3 is eventually made infinite. The eigenstates of the non-interacting fermions in the box potential are plane waves. Expanding the field operators in this basis gives

$$\hat{H}_{\text{box}} = \sum_{\vec{p}\sigma=\uparrow,\downarrow} \varepsilon_p \hat{c}^\dagger_{\vec{p}\sigma} \hat{c}_{\vec{p}\sigma} + \frac{1}{L^3} \sum_{\vec{k}\vec{p}\vec{q}} U_{\vec{k}-\vec{p}} \hat{c}^\dagger_{\vec{k},\uparrow} \hat{c}^\dagger_{-\vec{k}+\vec{q},\downarrow} \hat{c}_{-\vec{p}+\vec{q},\downarrow} \hat{c}_{\vec{p},\uparrow}, \tag{3.3}$$

where $U_{\vec{k}-\vec{p}} = \int d^3\vec{r} U(r) e^{i(\vec{k}-\vec{p})\cdot\vec{r}}$ and $\varepsilon_p = \frac{\hbar^2 p^2}{2m}$, and $\vec{p} = \frac{2\pi}{L}(n_x, n_y, n_z)$ with $n_x, n_y, n_z \in \mathbb{Z}$.

Short-range interaction potentials $U(r)$ (such as in dilute atom gases) give $U_{\vec{k}-\vec{p}} \approx U$, that is, a constant interaction. This approximation does not describe correctly the scatterings of high momentum states, resulting in ultraviolet divergences in various integrals, as will be seen later. For the discussions below, I will assume an attractive ($U < 0$) delta function (zero range) interaction.

3.2 Cooper instability

As a prelude to the microscopic theory of superconductivity, Cooper [22] showed that at zero temperature the Fermi sea is unstable to an attractive interaction between the fermions. Even if the interaction is arbitrarily weak, at low enough temperatures the fermions near the Fermi surface will form stable pairs.

The first Born approximation describes a single scattering event between the particles. Fig. 3.1 shows also the second Born approximation, that corresponds to

a double scattering. The diagrams describe the scattering of two particles with opposite momenta $\vec{p}$ and $-\vec{p}$ into the final state with momenta $\vec{p}'$ and $-\vec{p}'$. The second order process occurs through an intermediate state with momenta $\vec{k}$ and $-\vec{k}$ (with energy ϵ). The effective scattering can now be written as an integral equation

$$U_{\text{eff}}(\vec{p},\vec{p}') = U + U^2 \int_{-\mu}^{\hbar\omega_{\text{c}}} d\epsilon\, N(\epsilon) \left[\frac{\left(1-n_{\text{F}}(\epsilon)\right)^2}{2\varepsilon_p - 2\epsilon} + \frac{n_{\text{F}}(\epsilon)^2}{2\epsilon - 2\varepsilon_p} \right], \tag{3.4}$$

where $N(\epsilon)$ is the density of (intermediate) states, $\varepsilon_p = \frac{\hbar^2 p^2}{2m} - \mu$, μ is the chemical potential, $n_{\text{F}}(\epsilon)$ is the Fermi distribution, and ω_{c} is some cutoff that removes the ultraviolet divergence of the integral. For the weakly interacting gas at zero temperature the chemical potential μ equals the Fermi energy E_{F}. The integration variable ϵ is the energy of the intermediate state. The first term is the first Born approximation and the second term contributes if the intermediate state $(\vec{k},-\vec{k})$ is unoccupied. In this case the two atoms $(\vec{p},-\vec{p})$ scatter to this empty state and then scatter to the final state $(\vec{p}',-\vec{p}')$. The last term describes a process, in which atoms in state $(\vec{k},-\vec{k})$ scatter to $(\vec{p}',-\vec{p}')$ and then the atoms in the initial state $(p,-p)$ scatter to state $(\vec{k},-\vec{k})$. The last two terms correspond to the second Born approximation.

For the sake of simplicity, I will assume that the density of states is constant $N(\epsilon) = N_0$. This assumption is usually done in BCS theory but it does not hold for strong interactions. However, the essential physics that follow will be unchanged (a sufficient condition is that the density of states does not have 'too many' zeroes around the Fermi surface).

At zero temperature and for a large cutoff $\hbar\omega_{\text{c}} \gg \mu$, the integral in Eq. (3.4) yields

$$U^2 N_0 \ln\left(\frac{-\varepsilon_p}{\sqrt{(\varepsilon_p+\mu)\,\hbar\omega_{\text{c}}}} \right). \tag{3.5}$$

For particles close to the Fermi surface, we can approximate $\varepsilon_p + \mu \approx \mu$. Going to higher orders in the Born approximation gives a geometric series

$$U_{\text{eff}} = U \sum_{n=0}^{\infty} \left[U N_0 \ln\left(\frac{-\varepsilon_p}{\sqrt{\mu\hbar\omega_{\text{c}}}} \right) \right]^n = \frac{U}{1 - U N_0 \ln\left(\frac{-\varepsilon_p}{\sqrt{\mu\hbar\omega_{\text{c}}}} \right)}. \tag{3.6}$$

This corresponds to the ladder approximation, shown in the Fig. 3.2, and it will be encountered again later.

The effective interaction U_{eff} has a pole when the denominator becomes zero, i.e.

$$\varepsilon_p = \varepsilon_0 \equiv \sqrt{\mu\hbar\omega_{\text{c}}}\, e^{1/N_0 U}. \tag{3.7}$$

Because of the exponential factor $e^{1/N_0 U}$, where U is small and negative, the pole is located very close to the Fermi surface $\varepsilon_p \approx 0$. This means that fermions close

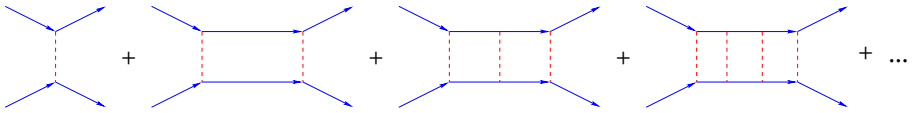

FIGURE 3.2 The ladder approximation corresponds to a series of higher and higher ordered scattering events.

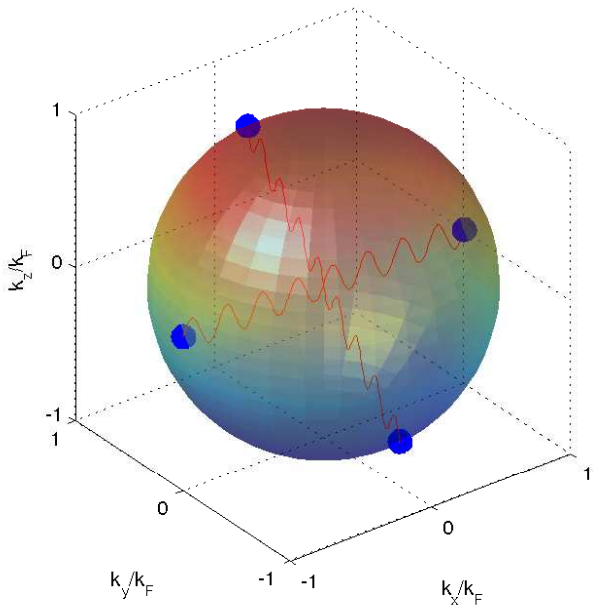

FIGURE 3.3 The Cooper instability occurs in the scattering of two fermions on the Fermi surface with equal but opposite momenta. The system avoids the instability by forming an energy gap at the Fermi energy. This signals the phase transition to the superfluid phase.

to the Fermi surface will interact resonantly with their pair on the opposite side of the Fermi sphere. The many-body system reacts to the divergence by forming zero-momentum pairs from fermions on the Fermi surface, see Fig. 3.3. The pair formation lowers the energies of the fermions, leaving a gap in the density of states around the Fermi energy. This is the Cooper instability, showing that even a weak attractive interaction is sufficient for breaking the normal Fermi sea. The energy gap or the binding energy Δ of the Cooper pairs can be measured, and it will be encountered below frequently.

Notice that the appearance of the Cooper instability depends on the fact of having a filled Fermi sea as the resonance vanishes for $\mu = 0$. Indeed, the energy of the Cooper pair can be shown to be positive but less than the Fermi energy. Therefore only atoms close to the Fermi surface will find the bound state as really 'bound', allowing them to reduce their energy by binding. This is in contrast to stable molecular states that correspond to negative energy pairs, and therefore do not require the

presence of a many-body system.

3.3 BCS theory

The microscopic theory of superconductivity was formulated by Bardeen, Cooper and Schrieffer [6]. The BCS theory starts with the assumption that fermions (for example electrons in a superconducting metal) feel an attractive interaction and they can form pairs. As the previous section on Cooper instability hinted, the pairing occurs mostly between atoms of equal (but opposite) momenta.

The theory starts with an ansatz for the ground state wavefunction

$$|\Psi_{\mathrm{BCS}}\rangle = \prod_{\vec{k}} \left(u_k + v_k \hat{c}^\dagger_{\vec{k}\uparrow} \hat{c}^\dagger_{-\vec{k}\downarrow} \right) |0\rangle, \tag{3.8}$$

where u_k and v_k are variational parameters (Bogoliubov coefficients), and each pair of the creation operators $\hat{c}^\dagger_{\vec{k}\uparrow} \hat{c}^\dagger_{-\vec{k}\downarrow}$ creates a zero-momentum pair (Cooper pair) into the vacuum state $|0\rangle$. Notice that the number of atoms (or pairs) in the BCS ground state is not fixed, as the trial wavefunction is not an eigenstate of the number operator.

The variational parameters u_k and v_k are determined by minimizing the energy of the system and by the normalisation $u_k^2 + v_k^2 = 1$. The energy is given by the BCS Hamiltonian operator

$$\hat{H}_{\mathrm{BCS}} = \sum_{\vec{k}\sigma} \epsilon_k \hat{c}^\dagger_{\vec{k}\sigma} \hat{c}_{\vec{k}\sigma} + U \sum_{\vec{k},\vec{q}} \hat{c}^\dagger_{\vec{k}\uparrow} \hat{c}^\dagger_{-\vec{k}\downarrow} \hat{c}_{-\vec{k}-\vec{q}\downarrow} \hat{c}_{\vec{k}+\vec{q}\uparrow}, \tag{3.9}$$

where $\epsilon_k = \frac{\hbar^2 k^2}{2m} - \mu$ is the single particle energy of a non-interacting fermion, μ is the chemical potential, and U is the interaction energy (attractive, hence U is negative) between the fermions of different spins. This is the same Hamiltonian as in Eq. (3.3) but for zero-momentum Cooper pairs.

The energy of the trial wavefunction (3.8) is now

$$E = \langle \Psi_{\mathrm{BCS}} | \hat{H}_{\mathrm{BCS}} | \Psi_{\mathrm{BCS}} \rangle = \sum_{\vec{k}} \left(2\epsilon_k v_k^2 + U u_k v_k \sum_{\vec{q}} u_{\vec{k}+\vec{q}} v_{\vec{k}+\vec{q}} \right). \tag{3.10}$$

The q-sum on the right hand side does not depend on $\vec{k}$ for periodic boundary conditions or an infinite system, and we can define $\Delta = -U \sum_{\vec{q}} u_q v_q$. Minimizing the

energy yields

$$\begin{aligned} u_k^2 &= \frac{1}{2}\left(1+\frac{\epsilon_k}{E_k}\right) \\ v_k^2 &= \frac{1}{2}\left(1-\frac{\epsilon_k}{E_k}\right), \end{aligned} \tag{3.11}$$

and

$$u_k v_k = \frac{\Delta}{2E_k}, \tag{3.12}$$

where $E_k = \sqrt{\epsilon_k^2 + \Delta^2}$ is a quasiparticle energy. These equations will be encountered also later, but now it is important to understand that these equations follow from the assumptions on the two-body scattering process and the presence of the Fermi sea. The Δ turns out to be the superfluid order parameter that vanishes above some critical temperature T_c. The order parameter Δ has also the role of an energy gap, producing a region with a zero density of states around the Fermi energy. This gap allows the system to avoid the Cooper instability, and it can be solved from its definition as an implicit integral equation. Generalised to finite temperatures, it reads

$$1 = -U \int d^3\vec{k} N(k) \frac{1-2n_\mathrm{F}(E_k)}{2E_k}, \tag{3.13}$$

where $n_\mathrm{F}(x) = \frac{1}{1+e^{\beta x}}$ is the Fermi-Dirac distribution and $N(k)$ is the density of momentum states [3]. Notice that the integral is ultra-violet divergent. This is an artifact from the assumption of delta function interaction. The integral is often regularised by simply removing the divergent part [51] or by introducing a high energy cut-off [47].

For a deeper understanding of the superfluidity, it is useful to derive it also using the canonical transformation (and later also diagrammatically with Green's functions). However, I will only list the results here and discuss a few points.

3.3.1 Canonical transformation

The objective of the canonical transformation [27] is to diagonalise the BCS Hamiltonian (3.9). This is done in the mean-field approximation, where the four-operator product in the interaction term is replaced by two operators and an expectation value. This decomposition can be written as

$$\hat{c}_{\vec{k}\uparrow}\hat{c}_{-\vec{k}\downarrow} = \langle \hat{c}_{\vec{k}\uparrow}\hat{c}_{-\vec{k}\downarrow}\rangle + \left(\hat{c}_{\vec{k}\uparrow}\hat{c}_{-\vec{k}\downarrow} - \langle \hat{c}_{\vec{k}\uparrow}\hat{c}_{-\vec{k}\downarrow}\rangle\right), \tag{3.14}$$

where the latter term on the right hand side is the fluctuations around the mean field. Keeping the fluctuations only to the first order results in the following mean-

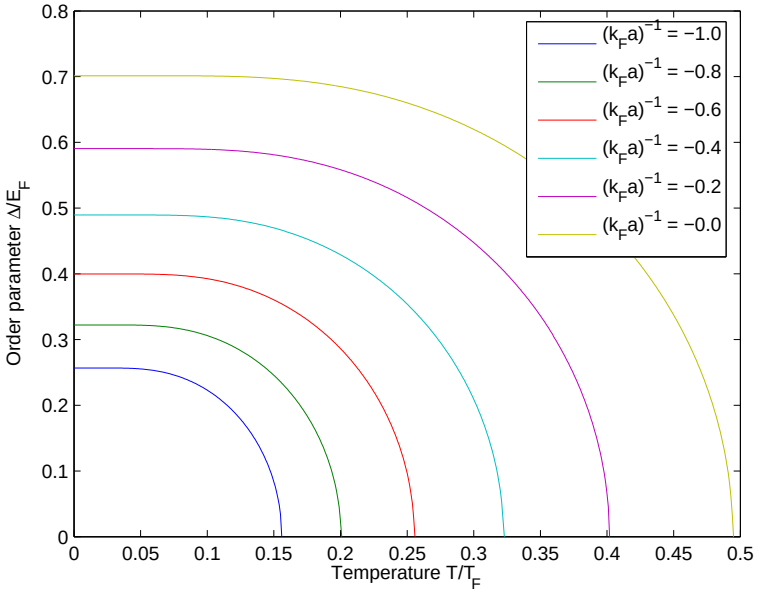

FIGURE 3.4 The superfluid order parameter (the pairing gap) as a function of temperature for several interaction strengths $(k_{\mathrm{F}}a)^{-1}$. The temperature dependence shows the second-order phase transition at the critical temperature T_{c} where the order parameter vanishes. The curves have been obtained using simple BCS theory that does not describe properly strongly interacting systems. Thus the plots must be considered only at a qualitative level.

field Hamiltonian

$$\hat{H}_{\mathrm{HF}} = \sum_{\vec{k}\sigma} \epsilon_k \hat{c}^\dagger_{\vec{k}\sigma} \hat{c}_{\vec{k}\sigma} + \sum_{\vec{k}} \left[U \sum_{\vec{q}} \langle \hat{c}^\dagger_{\vec{q}\uparrow} \hat{c}^\dagger_{-\vec{q}\downarrow} \rangle \hat{c}_{-\vec{k}\downarrow} \hat{c}_{\vec{k}\uparrow} + h.c. \right], \tag{3.15}$$

where the subscript HF stands for Hartree-Fock approximation. Here we denote $-U \sum_{\vec{q}} \langle \hat{c}^\dagger_{\vec{q}\uparrow} \hat{c}^\dagger_{-\vec{q}\downarrow} \rangle = \Delta$, which is the same order parameter Δ obtained above. This allows the interpretation of the order parameter as the strength of the Cooper pair condensate field. This is an analogy to the Bose-Einstein condensate order parameter $\langle \hat{b} \rangle$, where $\hat{b}$ is the annihilation operator of a boson. In this mean-field approximation, the ground state is not an eigenstate of the number operator.

The diagonalisation of the above Hamiltonian operator is a straightforward task, as it separates into mutually commuting operators for each $\vec{k}$-state. This is performed by the Bogoliubov transformation [27]

$$\begin{aligned} \hat{c}_{\vec{k}\uparrow} &= u_k \hat{\gamma}_{\vec{k}\uparrow} + v_k \hat{\gamma}^\dagger_{-\vec{k}\downarrow} \\ \hat{c}^\dagger_{-\vec{k}\downarrow} &= u_k \hat{\gamma}^\dagger_{-\vec{k}\downarrow} - v_k \hat{\gamma}_{\vec{k}\uparrow}, \end{aligned} \tag{3.16}$$

where $\hat{\gamma}_{\vec{k}\sigma}$ are (fermionic) quasiparticle operators and the Bogoliubov coefficients (the same as the variational parameters above) are to be determined from the diag-

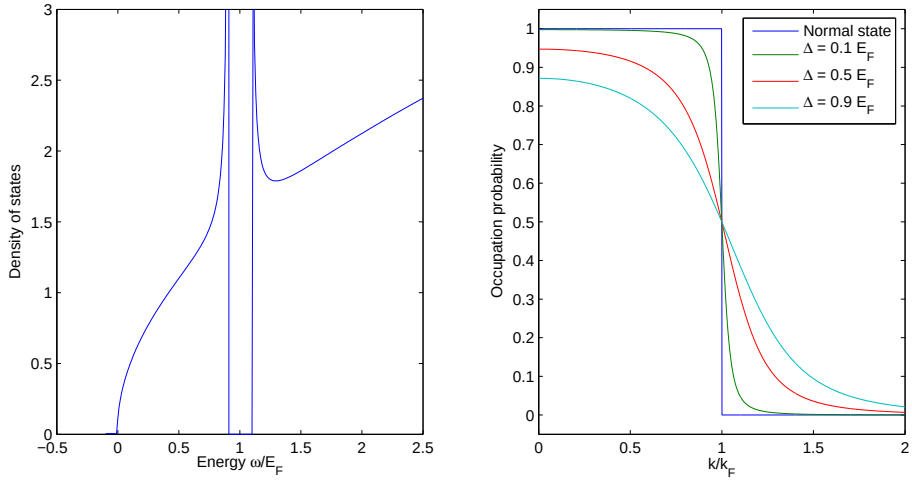

FIGURE 3.5 The density of states (left picture) of a fermionic superfluid shows the appearance of a gap at the Fermi energy (here $\Delta = 0.1\, E_{\rm F}$. The increase of the gap is reflected as broadening of the Fermi surface (right picture). For noninteracting gas ($\Delta = 0$) the Fermi surface is sharp.

onalisation and from the normalisation $u_k^2 + v_k^2 = 1$. The result is

$$\hat{H}_{HF} = C + \sum_{\vec{k}\sigma} E_k \hat{\gamma}^\dagger_{\vec{k}\sigma} \hat{\gamma}_{\vec{k}\sigma}, \tag{3.17}$$

where $E_k = \sqrt{\epsilon_k^2 + \Delta^2}$ and C is a real number. The operator $\hat{\gamma}_{\vec{k}\sigma}$ destroys a quasiparticle with momentum $\vec{k}$. However, the spin index σ should not be mixed with the spin of the real particles, as the quasiparticle operators are combinations of the both (real) spin states.

The canonical transformation allows the study of single particle excitations of the superfluid. The quasiparticle energies E_k are the eigenenergies of the system, and the excitations correspond to creation of these quasiparticles. Notice that while the number of real particles is not fixed in the system, the number of quasiparticles is fixed as the quasiparticle number operator commutes with the Hamiltonian. The quasiparticle spectrum, or the density of states, can be experimentally determined by measuring the I-V curve across a normal metal - superconductor tunnel junction (for a metallic superconductor), or by using radio-frequency spectroscopy [84] (for atomic Fermi gas).

Both the variational approach and the canonical transformation are more or less limited to the BCS region, meaning weakly interacting fermions. In order to be able to describe strong interactions, the BCS theory needs to be extended to include also the fluctuations of the Cooper pair field. This is the region where most of the experiments with superfluid Fermi gases have been done, and therefore we need to consider also the Green's function approach.

3.4 Green's function

The Green's function tells the probability that a particle initially (at time t') in a state i will end up in state f after a time $t - t'$. That is,

$$G(i, t'; f, t) = \langle \Psi | \mathcal{T} \hat{c}_f(t) \hat{c}_i^\dagger(t') | \Psi \rangle, \tag{3.18}$$

where $\mathcal{T}$ is the time ordering operator and the expectation value is calculated in some given state $|\Psi\rangle$ of the total system. The state $|\Psi\rangle$ can be some specific state (often a ground state) if one knows it, but often one does not know the state of the system beforehand and the point of the Green's function technique is to find it. This kind of solution where the Green's function also determines the state $|\Psi\rangle$ is called self-consistent.

I will now introduce a diagrammatic representation as the underlying physics is often easier to explain in this representation. The starting point is the interaction picture presentation of the Green's function. Starting with the mean-field Hamiltonian in Eq. (3.15), we write it in the form $\hat{H} = \hat{H}_0 + \hat{V}$, where $\hat{H}_0 = \sum_{\vec{k}\sigma} \epsilon_k \hat{c}^\dagger_{\vec{k}\sigma} \hat{c}_{\vec{k}\sigma}$ and

$$\hat{V} = \sum_{\vec{k}} \left[U \sum_{\vec{q}} \langle \hat{c}^\dagger_{\vec{q}\uparrow} \hat{c}^\dagger_{-\vec{q}\downarrow} \rangle \hat{c}_{-\vec{k}\downarrow} \hat{c}_{\vec{k}\uparrow} + h.c. \right]. \tag{3.19}$$

The Green's function in Eq. (3.18) was written in the Heisenberg picture, where the states do not depend on time. In the interaction picture the same Green's function is

$$G(i, t'; f, t) = \langle \phi | \hat{S}(t, -\infty)^\dagger \hat{c}_f(t) \hat{S}(t, t') \hat{c}_i^\dagger(t') \hat{S}(t', -\infty) | \phi \rangle, \tag{3.20}$$

where the time evolution is treated using the scattering S-matrix

$$\hat{S}(t, t') = \mathcal{T} \exp \left[\frac{-i}{\hbar} \int_{t'}^{t} dt_1 \, \hat{V}(t_1) \right]. \tag{3.21}$$

In the interaction picture, the state is $|\Psi\rangle = \hat{S}(0, -\infty)|\phi\rangle$ and the time dependence of the operators is $\hat{\mathcal{O}}(t) = e^{i\hat{H}_0 t/\hbar} \hat{\mathcal{O}}(0) e^{-i\hat{H}_0 t/\hbar}$. The purpose of the scattering matrices $\hat{S}(t, -\infty)$ is to make sure that the system is in the ground state when Green's function is evaluated. If the state $|\phi\rangle$ is the ground state of the Hamiltonian $\hat{H}_0$, the adiabatic switching on of the perturbation $\hat{V}$ will bring the system into the ground state of the full Hamiltonian $\hat{H}$ [27]. In principle one would like to have also an adiabatic switching factor $e^{-\nu|t|/\hbar}$ in the perturbation $V(t)$. On the other hand, if the state at $t' = 0$ is known, then parts from the $t = -\infty$ to $t = t'$ can be neglected. This is the case of radio-frequency spectroscopy, where the pulse begins at some time $t' = 0$, lasting for time T. At the beginning of the pulse, the state is given by the equilibrium BCS-type calculation and the effect of the rf-pulse is to drive the system out of equilibrium.

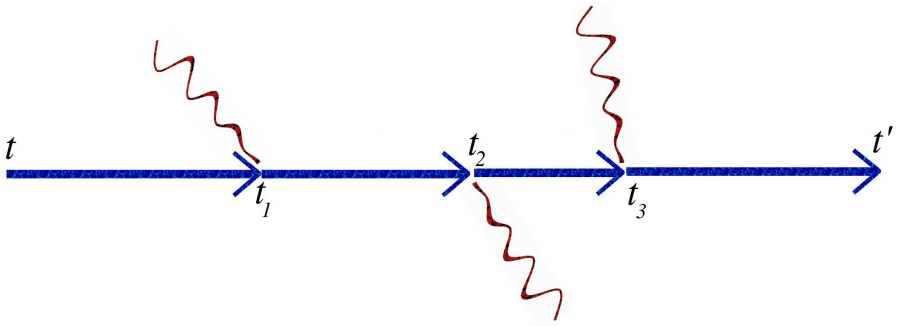

FIGURE 3.6 The expanded S-matrix describes paths where the perturbation $\hat{V}$ operates at a set of discrete times $t_1, t_2, \ldots, t_n$. Rest of the time the system propagates as governed by the unperturbed Hamiltonian H_0, giving a simple phase factor when in the basis of H_0.

The S-matrix can be expanded as a time ordered series

$$\hat{S}(t,t') = \sum_{n=0}^{\infty} \left(\frac{-i}{\hbar}\right)^n \int_t^{t'} dt_n \int_t^{t_n} dt_{n-1} \ldots \int_t^{t_2} dt_1 \, \hat{V}(t_n) \ldots \hat{V}(t_1). \tag{3.22}$$

This can be interpreted as follows: the S-matrix operates on a state $|\Psi_0\rangle$ at time t' and takes it into a new state by the time t. From time t' to time t_1 the system does the trivial time-evolution as governed by the Hamiltonian $\hat{H}_0$. This is a simple process, as the operator $\hat{H}_0$ is diagonal. Then at time t_1 the system is perturbed by the interaction operator $\hat{V}$ and we get to a new state $|\Psi_1\rangle$. This state is again easy to evolve for a time $t_2 - t_1$ and the process is then repeated until in the end the state has propagated to time t'. As one already sees, this simple process (or a path) is hard to describe by words, so it is easier to make a picture of it. This leads us to the diagrammatic representation as shown in Fig. 3.6.

The perturbative approach alone is not sufficient for explaining superfluidity, as even the simple BCS theory requires terms of arbitrary high order. This problem is overcome by doing resummations of sets of diagrams. The starting point is the Dyson's equation, which can be formally written as

$$G = G_0 + G_0 \Sigma G. \tag{3.23}$$

Here G_0 is called bare Green's function (or propagator), and it describes the propagation of a particle in the absence of any interactions, G is the full (often called dressed) Green's function from Eq. (3.20), and the self-energy Σ describes interactions. The Dyson's equation can be drawn diagrammatically as shown in Fig. 3.7. As is evident from Eq. (3.23), even a simple form for the self-energy generates an infinite series of terms to the full Green's function. In order to avoid counting same terms twice, we assume that the self-energy is connected, meaning that what ever diagrams are included in the bubble, they cannot be split in two by cutting a single

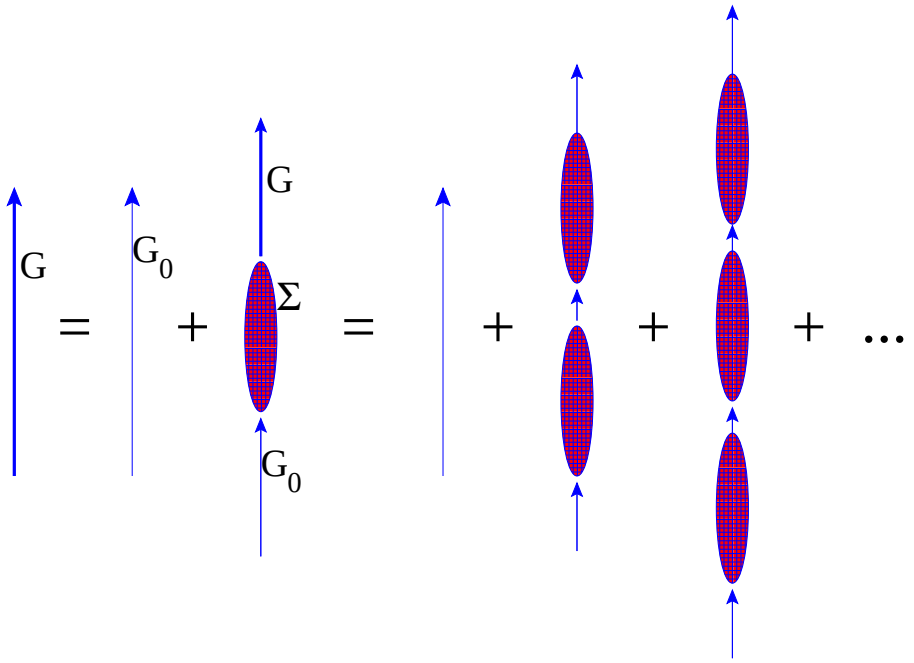

FIGURE 3.7 The Dyson's equation in real-time Green's functions. The full Green's function is depicted as a bold arrow and the free propagation (in the absence of any interactions) is drawn as a thin arrow. The interactions are described by the bubbles called self-energy Σ. The equation generates an infinite series of terms as shown in the right hand side of the diagrammatic equation.

particle line, see Fig. 3.8.

The full diagrammatic representation of the BCS-theory is shown in Fig. 3.9 [53]. It is not explicitly in the form of the Dyson's equation, but it can be written in that form by using Nambu formalism which replaces the Green's functions by 2x2 matrices. The diagonal elements describe the single particle propagators and the off-diagonal parts are called anomalous propagators. In the BCS limit, the anomalous propagator is $F(t',t) = \langle \hat{c}^\dagger_\uparrow(t)\hat{c}^\dagger_\downarrow(t')\rangle$, and it is denoted in the BCS diagrams in Fig. 3.9 by double headed arrow. It describes the Cooper pair field and how the interactions bind or break pairs from/to two particles.

The simple mean-field BCS theory that has now been discussed from three different points of view (using variational approach, canonical transformation, and the Green's function technique) can now be extended for strongly interacting systems by choosing different forms for the self-energy.

3.4.1 Beyond the mean-field approximation

An alternative approach to the Dyson's equation is to calculate equations of motion for the annihilation and creation operators, $c_{\vec{k}\sigma}$ and $c^\dagger_{\vec{k}\sigma}$. The interaction term in the Hamiltonian couples these to the single-particle Green's functions, and these in turn are coupled to two-particle Green's functions [40]. This produces an infinite series

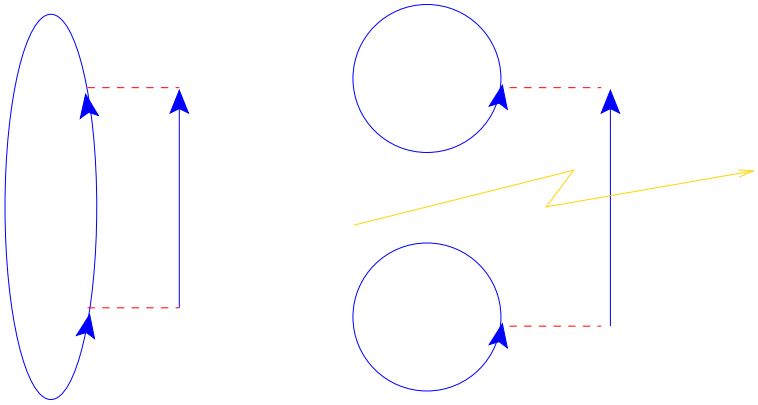

FIGURE 3.8 In order to avoid counting same terms twice, the self-energy needs to be connected (or proper). A connected self energy (left) cannot be split into two by simply cutting a single particle line. The self-energy on the right is not connected.

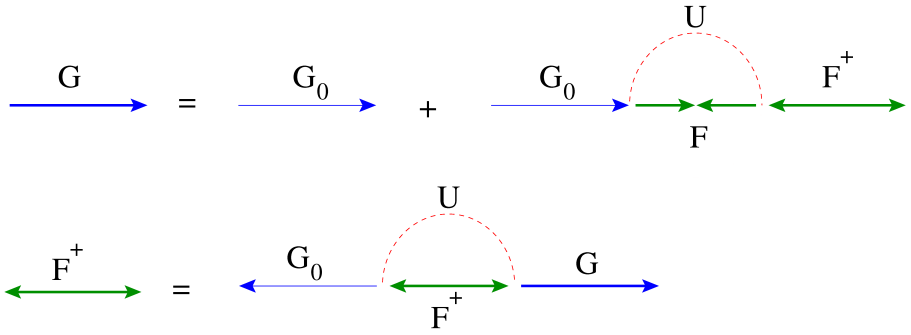

FIGURE 3.9 The diagrammatic representation of the BCS theory consists of two coupled equations for the two Green's functions: dressed single-particle Green's function and the anomalous Cooper pair field.

that needs to be cut or truncated at some point. The two-particle Green's function is

$$G_2^{\alpha'\beta';\alpha\beta}(t_1', t_2'; t_1, t_2) = \langle \Psi | T_t \hat{c}_\alpha(t_1) \hat{c}_\beta(t_2) \hat{c}^\dagger_{\beta'}(t_2') \hat{c}^\dagger_{\alpha'}(t_1)' | \Psi \rangle \tag{3.24}$$

where T_t is a time-ordering operator and the states α, β, α', and β' correspond to the spin and momentum indices. This has actually been met before in conjunction with the Born approximation in the two-particle scattering although without the Green's function language. However, the connection becomes clear when doing the ladder approximation to the two-particle propagator as shown in Fig. 3.10. The effective scattering of two particles in state $p+q, -p+q$ into state $p'+q, -p'+q$ is given by the T-matrix that satisfies the relation [57, 59]

$$T(Q) = U - U \sum_P G(P+Q) G(-P+Q) T(Q), \tag{3.25}$$

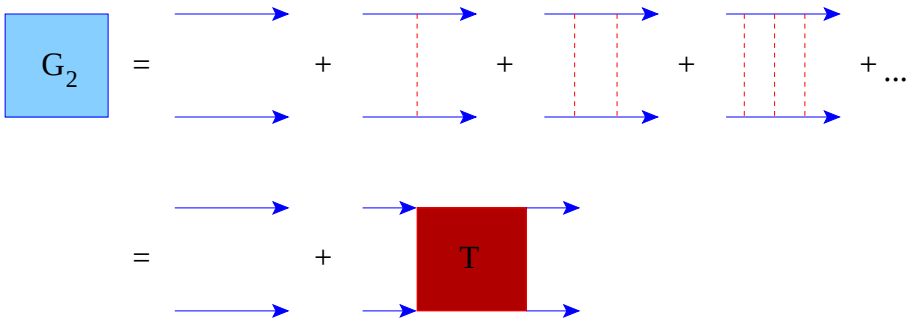

FIGURE 3.10 The two-particle Green's function in the ladder approximation. The T-matrix functions as an effective interaction between the particles.

where the variables P and Q contain both momenta $\vec{p}$, $\vec{q}$ and fermionic and bosonic Matsubara frequencies $i\omega_n$, $i\Omega_m$, respectively (in order to keep discussion simple here, I am not going to any details of Matsubara technique). The T-matrix can be solved to give

$$T(Q) = \frac{U}{1+\chi(Q)}, \tag{3.26}$$

where $\chi(Q) = U\sum_P G(P+Q)G(-P+Q)$ is called the pair susceptibility. Using the T-matrix, the self-energy of the single-particle Green's function can be written as

$$\Sigma(P) = \sum_P T(Q)G(Q-P), \tag{3.27}$$

and the single-particle Green's function is now

$$G(P) = G_0(P) + G_0(P)\sum_Q T(Q)G(Q-P)G(P). \tag{3.28}$$

Upon writing the self-energy Eq. (3.27), the two Green's function approaches are connected. Different approximations for the Green's functions in the pair susceptibility $\chi(Q)$ and the self-energy produce different generalisations of the BCS theory [77, 18]. In addition, the above discussion can be repeated using the Nambu formalism and the 2x2-matrix Green's functions, leading into a different set of theories [57, 71, 33, 58].

According to the Kosterlitz-Thouless criterion, the superfluid phase transition takes place when the T-matrix generates a pole at zero momentum (and Matsubara energy) $T(0)^{-1} = 0$ in analogy to the Cooper instability discussed earlier. Neglecting the uncorrelated parts of the two-particle propagator, the T-matrix has the form of a boson propagator. The appearance of the pole at zero momentum corresponds to a zero chemical potential in a Bose gas and hence the creation of a BEC. The fermionic superfluidity can now be understood as a Bose-Einstein condensation of fermion pairs [26, 51].

4 Trapped Fermi gases

A trapped Fermi gas does not feel a box-like confinement but an approximatively harmonic potential. Therefore the external potential in the Hamiltonian in Eq. (3.1) is replaced by

$$V_{\mathrm{ext}}(\vec{r}) = \frac{1}{2} m\omega^2 r^2, \tag{4.1}$$

where ω is the trapping frequency of the (spherically symmetric) trap. Expanding the field operators in the eigenstates of the potential leads to the Bogoliubov-deGennes (BdG) equations [24] in the harmonic oscillator basis. Another option is to treat the system in local density approximation (LDA), where the system is treated locally as a uniform system but the chemical potential becomes position dependent $\mu \to \mu - V_{\mathrm{ext}}(\vec{r})$. This approach will be described first.

4.1 Local density approximation

In the local density approximation, the spatially inhomogeneous system is locally approximated as a homogeneous system. Assuming a grid of M points in the position space, the variables to be solved are the chemical potential μ and the gap for each M points $\Delta(r)$. However, the gap equations for different points do not explicitly depend on each other, but only through the chemical potential. This simplifies the problem significantly, as fixing the chemical potential separates the solutions for the gaps.

How the gap equation and the densities are solved, depends on the given theory. LDA allows an easy way to implement different generalisations of the BCS theory on trapped gases as it is sufficient to solve the problem for a uniform system. The validity of the approximation depends on the different length scales of the system, such as the extent of the atom wavefunctions $1/k_{\mathrm{F}}$, the interaction range, and the pair size. All these length scales tell the range at which atoms are correlated. If the length scale of the external potential is much larger than these correlation length scales, it is reasonable to assume that atoms do not feel the gradient of the trapping potential. Hence they can be treated as in a uniform system. Often all these length scales boil down to the Fermi scale, giving for the region of validity $k_{\mathrm{F}} r_{\mathrm{osc}} \gg 1$, where $r_{\mathrm{osc}} = \sqrt{\hbar/m\omega}$ is the oscillator length of the trapping potential of frequency ω.

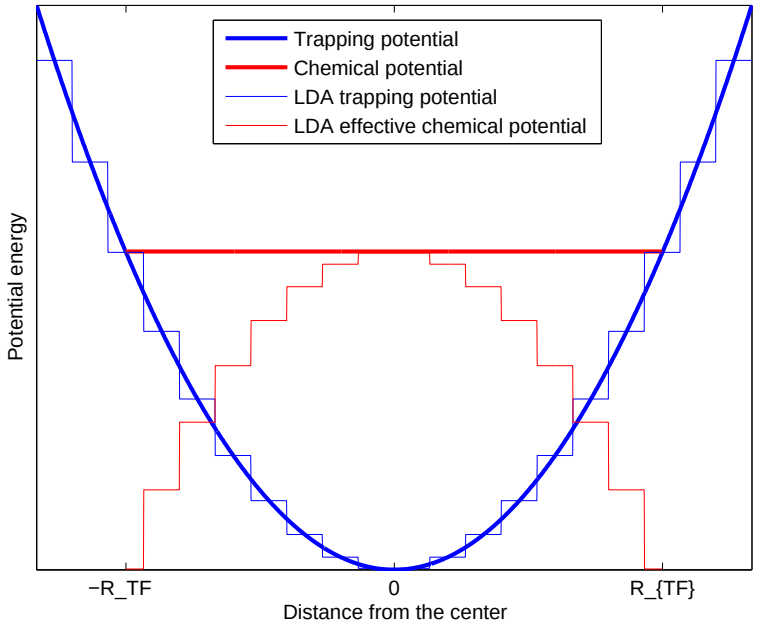

FIGURE 4.1 In local density approximation, the atom cloud is divided into a set of 'bins'. In each bin the system is assumed to be locally uniform, with the effective chemical potential $\mu(r) = \mu - V(r)$ varying as a function of position, where $V(r)$ is the external trapping potential. The number of bins is then increased to get continuous density and gap profiles. R_{TF} is the radius of the atom cloud.

For systems with large numbers of atoms, this condition is usually satisfied. In the limit of small numbers of atoms, the local density approximation is unable to describe the nonlocal nature of atomic wavefunctions. A similar problem arises at the edges of the traps, where the density of the gas is very low. Here the effective kinetic energy of the atoms is low (or the effective local Fermi energy is small) so that the wavefunctions are spread over large distances. However, the local density approximation calculations are very useful because of the simplicity but also as a benchmark for other approaches. For example, the Bogoliubov-deGennes (BdG) approach discussed below is good in the limit of small atom numbers. Comparisons with the local density approximation can be used to find out how strongly the BdG results depend on finite size effects that should vanish in the limit of large systems [12, 29].

4.2 Bogoliubov-deGennes equations

If one does not want to resort to the local density approximation, one ends up with the Bogoliubov-deGennes equations in some basis. The main difference is that now the values of the gap or the order parameter at different points explicitly depend on each other.

Analogously to the canonical transformation for the ordinary BCS-theory, I

start by doing the mean-field approximation for the order parameter [61,62]

$$\Delta(\vec{r}) := -U\langle\hat{\Psi}_\uparrow(\vec{r})\hat{\Psi}_\downarrow(\vec{r})\rangle \tag{4.2}$$

and the density

$$n_\sigma(\vec{r}) := \langle\hat{\Psi}^\dagger_\sigma(\vec{r})\hat{\Psi}_\sigma(\mathbf{r})\rangle. \tag{4.3}$$

This gives the following mean-field Hamiltonian

$$\begin{aligned}\hat{H}_{\mathrm{MF}} =& \sum_\sigma \int d^3\vec{r}\,\hat{\Psi}_\sigma(\vec{r})^\dagger K_\sigma(\vec{r})\hat{\Psi}_\sigma(\vec{r}) + \int d^3\vec{r}\,\Delta(\vec{r})\hat{\Psi}^\dagger_\uparrow(\vec{r})\hat{\Psi}^\dagger_\downarrow(\vec{r}) + h.c. \\ &+ U\sum_\sigma \int d^3\vec{r}\, n_\sigma(\vec{r})\hat{\Psi}^\dagger_{\bar{\sigma}}(\vec{r})\hat{\Psi}_{\bar{\sigma}}(\vec{r}) - \int d^3\vec{r}\,\frac{|\Delta(\vec{r})|^2}{U},\end{aligned} \tag{4.4}$$

where the third term describes the Hartree interaction between atoms of opposing spins σ and $\bar{\sigma}$. Here I have added spin-dependence to the $K_\sigma(\vec{r})$ operator by replacing the chemical potential μ by the chemical potential of the different spin states μ_σ. The purpose is to be able to describe also polarised gases with different numbers of atoms in the two components.

Still following the path of the canonical transformation, I expand the field operators in the basis of the eigenstates of the symmetric 3D-harmonic oscillator (compare with the plane wave expansion in the uniform case)

$$\hat{\Psi}_\sigma(\vec{r}) = \sum_{nlm} R_{nl}(r)Y_{lm}(\Theta)\hat{c}_{nlm\sigma}, \tag{4.5}$$

where

$$R_{nl}(r) = \sqrt{2}\,(m\omega)^{3/4}\sqrt{\frac{n!}{(n+l+1/2)!}}e^{-\frac{r^2}{2}}r^l L_n^{l+\frac{1}{2}}(r^2), \tag{4.6}$$

where $L_n^{l+1/2}(r^2)$ is the Laguerre polynomial, $Y_{lm}(\Theta)$ are the spherical harmonics, and the operator $\hat{c}_{nlm\sigma}$ destroys an atom with the spin σ from the state nlm. Inserting these into the Hamiltonian gives

$$\begin{aligned}\hat{H}_{\mathrm{MF}} =& \sum_\sigma\sum_{nl}(2l+1)\epsilon_{nl\sigma}\hat{c}^\dagger_{nl\sigma}\hat{c}_{nl\sigma} + \sum_{nn'l\sigma} J^l_{nn'\bar{\sigma}}\hat{c}^\dagger_{nl\sigma}\hat{c}_{n'l\sigma} \\ &+ \sum_{nn'l} F^l_{nn'}\hat{c}^\dagger_{nl\uparrow}\hat{c}^\dagger_{n'l\downarrow} + h.c - \int d^3\vec{r}\frac{|\Delta(\vec{r})|^2}{U}.\end{aligned} \tag{4.7}$$

where I have used the spherical symmetry of the trap to get rid of the spherical harmonics $Y_{lm}(\Theta)$ and the angular m quantum numbers. The single particle energies

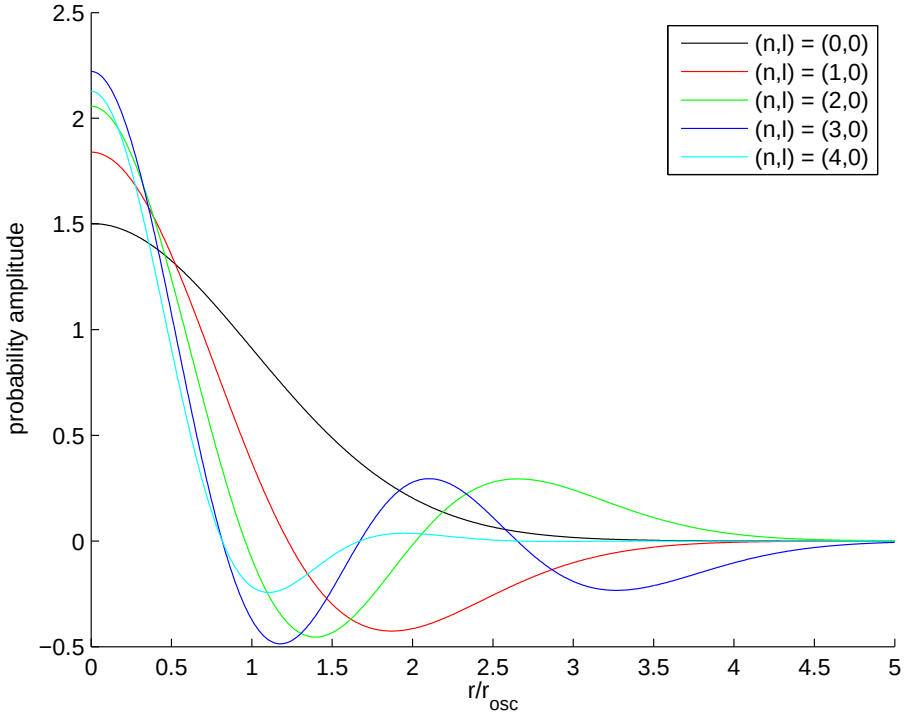

FIGURE 4.2 The field operators, and hence all spatial profiles (such as density and gap profiles) are expanded in the basis of the eigenstates of the harmonic potential. Here are shown the radial parts $R_{nl}(r)$.

are $\epsilon_{nl\sigma} = \hbar\omega(2n + l + 3/2) - \mu_\sigma$, the condensate interaction factor

$$F^l_{nn'} = \int_0^\infty dr\, r^2 R_{nl}(r)\Delta(r)R_{n'l}(r), \tag{4.8}$$

and the Hartree interaction factor

$$J_{nn'l\sigma} = U\int_0^\infty dr\, r^2 R_{nl}n_\sigma(r)R_{n'l}(r). \tag{4.9}$$

As in the usual BCS theory, the gap equation has an ultra-violet divergence that can be regularised by using a cutoff energy $\hbar\omega_c$. Thus, we truncate the Hilbert space by keeping only the single-particle states with the energy $\epsilon_{nl} \leq \hbar\omega_c$. However, introduction of the cutoff requires also a renormalisation of the interaction parameter. In Ref. [12] the regularisation was taken care of by using pseudopotentials. Here I will use the regularisation procedure proposed in Ref. [16], see also [29].

The resulting finite dimensional Hamiltonian can now be diagonalised, by noting that it separates for different l-quantum numbers. Thus, I write $\hat{H} = C + \sum_l \hat{H}_l$,

where

$$\hat{H}_l = \begin{pmatrix} \epsilon_{0l\uparrow} + J^l_{00} & \dots & J^l_{0N} & F^l_{00} & \dots & F^l_{0N} \\ \dots & \dots & \dots & \dots & \dots & \dots \\ J^l_{00} & \dots & \epsilon_{Nl_\uparrow} + J^l_{NN} & F^l_{N0} & \dots & F^l_{NN} \\ F^l_{00} & \dots & F^l_{0N} & -\epsilon_{0l\downarrow} - J^l_{00} & \dots & -J^l_{0N} \\ \dots & \dots & \dots & \dots & \dots & \dots \\ F^l_{N0} & \dots & F^l_{NN} & -J^l_{N0} & \dots & -\epsilon_{Nl\downarrow} - J^l_{NN} \end{pmatrix}, \tag{4.10}$$

where N is the highest n-quantum number satisfying $\epsilon_{nl} \leq \hbar\omega_c$ (notice that it does depend on the value of l) and the constant

$$C = \sum_{nl}(2l+1)\epsilon_{nl\downarrow} + J^l_{nn} - \int d^3\vec{r}\frac{|\Delta(\vec{r})|^2}{U}. \tag{4.11}$$

Each $\hat{H}_l$ can now be diagonalised separately, giving the eigenvalues E_{jl}, where $j = 1, \dots, 2N$, and the corresponding eigenstates $\left(W^l_{n,j}\right)_{n=1,\dots,2N}$. Now we can derive the following self-consistent equations for the order parameter

$$\Delta(r) = U\sum_{nn'l}\frac{2l+1}{4\pi}R_{nl}(r)R_{n'l}(r)\sum_{j=0}^{N}W^l_{N+n,N+j}W^l_{n',N+j} \tag{4.12}$$

and the densities

$$n_\uparrow(r) = \sum_{nn'l}\frac{2l+1}{4\pi}R_{nl}(r)R_{n'l}(r)\sum_{j=0}^{N}W^l_{n,N+j}W^l_{n',N+j} \tag{4.13}$$

and

$$n_\downarrow(r) = \sum_{nn'l}\frac{2l+1}{4\pi}R_{nl}(r)R_{n'l}(r)\sum_{j=0}^{N}W^l_{N+n,j}W^l_{N+n',j}. \tag{4.14}$$

These equations are solved iteratively and the chemical potentials μ_σ are varied in order to keep the numbers of atoms fixed. The density and gap profiles for a unitary Fermi gas at zero temperature obtained using both local density approximation and Bogoliubov-deGennes approach are shown in Fig. 4.3. The excellent agreement between the LDA and BdG results shows that the finite size effects of the BdG approach do not play a major role. On the other hand, the BdG results can be used as a benchmark for the LDA calculations in more complicated systems, for example in polarised gases [43, 38] (Publications IV and V).

Now we can solve the ground state of the system, and at least in the local density approximation we can even calculate the critical temperature of the superfluid phase transition. In the perturbative approach discussed in this thesis, this equilibrium state is the basis for all further studies. What we need is tools to study the

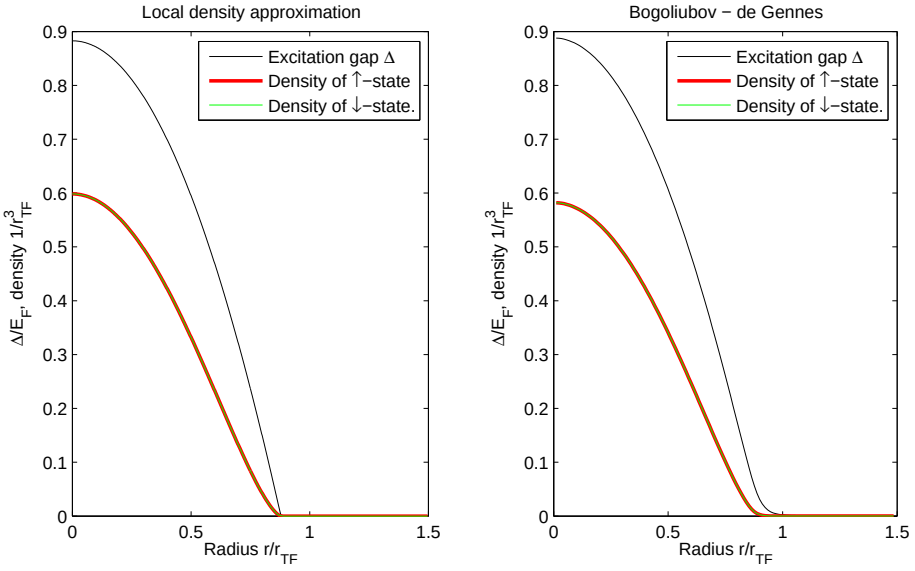

FIGURE 4.3 The density and gap profiles obtained from the LDA (left) and BdG (right) calculations for a resonantly interacting (unpolarised) Fermi gas ($(k_{\mathrm{F}}a)^{-1} = 0.0$). BdG calculations were done for 18000 atoms.

various properties of the superfluid Fermi gas experimentally, thus confirming or rejecting our underlying assumptions on superfluidity. Lasers and radio-frequency fields are ideal tools for pinching, poking, drilling, and banging the atom cloud, and even for simply taking a picture of it. In the next chapter, I will describe the interactions between atoms and electromagnetic radiation.

5 Radio-frequency spectroscopy

5.1 The nature of atom-light interaction

Lasers and radio-frequency fields are used extensively in the atom gas experiments. They are essential for trapping, cooling, and imaging the atoms, but they are also used in many ways for perturbing the cloud in order to see dynamic as well as static properties. I will first study a single atom in an electromagnetic field.

5.1.1 Atom in an electromagnetic field – the dipole approximation

To start with, a system of charged particles (the nucleus and the electrons that compose the atom) in an electromagnetic field is described by the Hamiltonian [21]

$$\hat{H} = \sum_\alpha \frac{1}{2m_\alpha}\left[\hat{\vec{p}}_\alpha - q_\alpha \hat{\vec{A}}\left(\hat{\vec{r}}_\alpha\right)\right]^2 + \sum_\alpha \left(-g_\alpha \frac{q_\alpha}{2m_\alpha}\right) \mathbf{S}_\alpha \cdot \hat{\vec{B}}(\hat{\vec{r}}_\alpha) + \hat{V}_{\text{atoms}} + \hat{H}_{\text{light}}, \quad (5.1)$$

where the first term describes the kinetic energy of a particle α with charge q_α in the presence of the vector potential $\hat{\vec{A}}(\hat{\vec{r}})$. The second term represents the interaction energy of the spin magnetic moments in the magnetic field $\hat{\vec{B}}(\hat{\vec{r}})$. This term is often (for low-energy photons or long wavelength electromagnetic field) much smaller than rest of the terms and therefore neglected. The last two terms describe the particle-particle interactions (for example the interactions between the electron and the nucleus) and the energy of the electromagnetic (light) field in the absence of any particles.

Assuming a cubic box (of size L^3) with periodic boundary conditions, the possible states of the electromagnetic field become discrete modes characterised by wave vectors $\frac{2\pi}{L}(n_x, n_y, n_z)$. Denoting the different modes and polarizations by j, the vector potential $\hat{\vec{A}}$ can be written as (and we take it here as a definition, for a more thorough discussion, see Ref. [21])

$$\hat{\vec{A}}(\hat{\vec{r}}) = \sum_j \sqrt{\frac{\hbar^2}{2\varepsilon_0 \hbar\omega_j L^3}}\vec{\epsilon}_j \left(\hat{a}_j e^{i\vec{k}_j \cdot \hat{\vec{r}}} + \hat{a}_j^\dagger e^{-i\vec{k}_j \cdot \hat{\vec{r}}}\right) \quad (5.2)$$

where ε_0 is the permittivity of free space, $\hbar\omega_j$ is the energy of the mode j, $\vec{\epsilon}_j$ is the

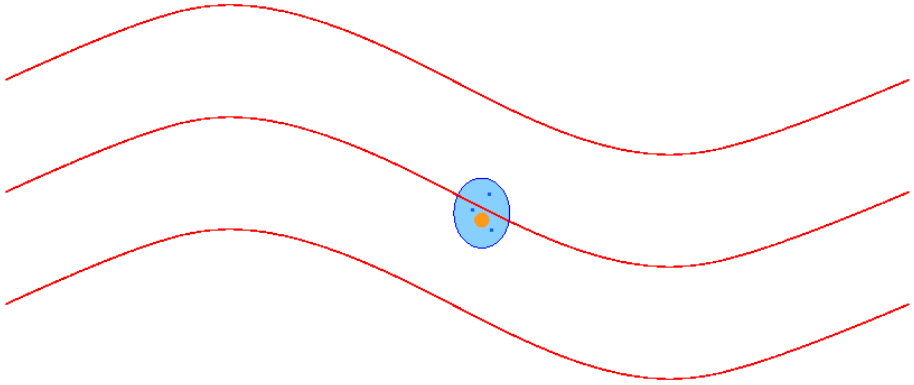

FIGURE 5.1 If the wavelength of the light is much longer than the size of an atom, the atom behaves as if it were a single large dipole. This is the dipole approximation.

polarization, and the operators a_j and $a_j^\dagger$ annihilate and create photons in the state j. In the same way we can write the electric field (will be needed later)

$$\hat{\vec{E}}(\hat{\vec{r}}) = \sum_j i\sqrt{\frac{\hbar\omega_j}{2\varepsilon_0 L^3}}\vec{\epsilon}_j\left(\hat{a}_j e^{i\vec{k}_j\cdot\hat{\vec{r}}} - \hat{a}_j^\dagger e^{-i\vec{k}_j\cdot\hat{\vec{r}}}\right). \tag{5.3}$$

If the wavelength of the light field is much longer than the typical size of an atom (already true for ultraviolet light), all particles inside the atom will feel the same field justifying approximation $\hat{A}_\perp(\hat{\vec{r}}_\alpha) = \hat{A}_\perp(\mathbf{R})$, where $\vec{R}$ is the position of the atom (chosen to be the origin). Defining the electric dipole moment operator [21]

$$\hat{\vec{d}} = \sum_\alpha q_\alpha \hat{\vec{r}}_\alpha, \tag{5.4}$$

the above Hamiltonian can be written in the form (here I have neglected the spin magnetic moments)

$$\begin{aligned}\hat{H}' = &\sum_\alpha \frac{\vec{p}_\alpha^{\,2}}{2m_\alpha} + \epsilon_{\text{dip}} + \vec{d}\cdot\sum_j \mathcal{E}_{\omega_j} i\vec{\epsilon}_j\left(\hat{a}_j^\dagger - \hat{a}_j\right)\\ &+ \sum_j \hbar\omega_j\left(\hat{a}_j^\dagger\hat{a}_j + \frac{1}{2}\right) + \hat{V}_{\text{atoms}} + \hat{H}_{\text{light}},\end{aligned} \tag{5.5}$$

where the constant

$$\epsilon_{\text{dip}} = \sum_j \frac{\left(\vec{\epsilon}_j\cdot\vec{d}\right)^2}{2\varepsilon_0 L^3}, \tag{5.6}$$

and $\mathcal{E}_{\omega_j} = \sqrt{\hbar\omega_j/2\varepsilon_0 L^3}$. The interaction between the atoms and the light field is now

described by

$$\hat{H}_{\mathrm{a-l}} := \hat{\vec{d}} \cdot \sum_j \mathcal{E}_{\omega_|} i\vec{\epsilon}_j \left(\hat{a}_j^\dagger - \hat{a}_j\right) = -\hat{\vec{d}} \cdot \hat{\vec{E}}(\vec{0}), \tag{5.7}$$

where a-l subscript is short for 'atom-light'. This can be generalised to any number of atoms, by replacing $\hat{\vec{E}}(0) \to \hat{\vec{E}}(\vec{R}_n)$, where $\vec{R}_n$ is the position of atom n, and summing over all atoms n.

5.1.2 A two-level atom

Let us consider a single atom for a moment longer. Assume a two-level atom with the ground state $|g\rangle$ and an excited state $|e\rangle$ coupled by a monochromatic (meaning that only one mode j is present) electromagnetic field with energy $\hbar\omega_j = \hbar\omega_{\mathrm{EM}}$, i.e.

$$\hat{\vec{E}}(\vec{r}) = \sqrt{\frac{\hbar\omega_{\mathrm{EM}}}{2\epsilon_0 L^3}}\vec{\epsilon}\left(\hat{a}e^{i\vec{k}\cdot\vec{r}} - \hat{a}^\dagger e^{-i\vec{k}\cdot\vec{r}}\right). \tag{5.8}$$

Writing then the electric dipole operator in the form [21]

$$\hat{\vec{d}} = \vec{d_{\mathrm{ge}}}\left(|g\rangle\langle e| + h.c.\right), \tag{5.9}$$

the atom-light interaction Hamiltonian becomes (assuming the atom is at the origin)

$$\hat{H}_{\mathrm{a-l}} = -\Omega\left(\hat{a}|e\rangle\langle g| + \hat{a}^\dagger|g\rangle\langle e| + \hat{a}|g\rangle\langle e| + \hat{a}^\dagger|e\rangle\langle g|\right), \tag{5.10}$$

where the constant $\Omega = \sqrt{\frac{\hbar\omega_{\mathrm{EM}}}{2\epsilon_0 L^3}}\vec{d_{\mathrm{ge}}} \cdot \epsilon$.

The first two terms on the right describe processes in which the atom absorbs a photon and becomes excited or vice versa. The last two terms describe processes in which either the atom absorbs a photon *and* drops from the excited state to the ground state or emits a photon *and* gets excited. When considering resonant processes (that is, processes in which the energy is conserved) the latter two events are very improbable. Neglecting the last two terms is called the *rotating wave approximation* (reason for the name will become clear below). If the number of photons is large, adding or removing one does not affect the electromagnetic field but simply gives (or takes) an energy $\hbar\omega_{\mathrm{EM}}$ from the atom. Therefore we can remove the photon operators $\hat{a}$ and $\hat{a}^\dagger$ (a semiclassical approximation) but in order to get the energies correct, we will add factors $Ne^{i\omega_{\mathrm{EM}}t}$ and $Ne^{-i\omega_{\mathrm{EM}}t}$. The exponential functions guarantee the correct phase (the additional phase shift comes from the energy shift of $\pm\hbar\omega_{\mathrm{EM}}$ caused by the creation/annihilation of one photon) and N is the photon density, determined by the intensity of the field. Often the absolute value of N is not known.

The total time-dependent Hamiltonian $\hat{H}(t) = \hat{H}_0 + \hat{H}_{\mathrm{a-l}}(t)$ describing the two-

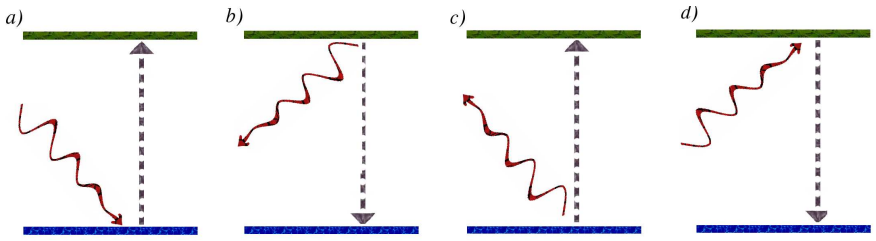

FIGURE 5.2 The two-level atom can a) excite to state $|e\rangle$ (the dashed arrow) by absorbing a photon (the wiggly line), b) drop to the ground state $|g\rangle$ by emitting a photon, c) excite while emitting a photon, or d) drop to ground state while absorbing a photon. The last two processes violate the energy conservation and are neglected in the rotating wave approximation.

state atom is now

$$\begin{aligned}\hat{H}(t) &= \epsilon_{\mathrm{g}}|g\rangle\langle g| + \epsilon_{\mathrm{e}}|e\rangle\langle e| - \Omega\left(e^{i\omega_{\mathrm{EM}}t}|e\rangle\langle g| + e^{-i\omega_{\mathrm{EM}}t}|g\rangle\langle e|\right) \\ &= \begin{pmatrix} \epsilon_{\mathrm{g}} & \Omega e^{i\omega_{\mathrm{EM}}t} \\ \Omega e^{-i\omega_{\mathrm{EM}}t} & \epsilon_{\mathrm{e}} \end{pmatrix},\end{aligned} \tag{5.11}$$

where we have included the photon density N in the atom-field coupling Ω that is now proportional to the intensity of the electromagnetic field. This equation can also be derived by starting from a classical electromagnetic field. In that picture, the rotating wave approximation corresponds to taking time average of the field. Terms that wildly violate the energy conservation will be very rapidly oscillating and therefore average out.

The time-dependent Hamiltonian can be written in a time independent form by rotating the coordinate system at the frequency ω_{EM}. Writing the Hamiltonian in the basis of Pauli spin matrices $\hat{\mathcal{S}}_i$

$$\hat{H} = \frac{\epsilon_g + \epsilon_e}{2}\hat{\mathcal{I}} + \frac{\epsilon_g - \epsilon_e}{2}\hat{\mathcal{S}}_z + \cos(\omega_{\mathrm{EM}}t)\hat{\mathcal{S}}_x + \sin(\omega_{\mathrm{EM}}t)\hat{\mathcal{S}}_y, \tag{5.12}$$

the x,y and z components can be interpreted as components of a magnetic field, around which the dipole rotates. The rotating wave approximation corresponded to neglecting the component of the 'magnetic field' that rotated in the opposite direction to the dipole.

In the rotating coordinate system the rotation of the dipole around the z axis is slower. Therefore the z-component of the magnetic field is lower, see Fig 5.3, meaning that the energy difference between the two spin states is reduced. This means that the field can supply the atom with energy for inducing transitions between the two states. Simple algebra leads to the time independent Hamiltonian (up to a constant)

$$\hat{H} = \begin{pmatrix} -\frac{\delta}{2} & \Omega \\ \Omega & \frac{\delta}{2} \end{pmatrix}, \tag{5.13}$$

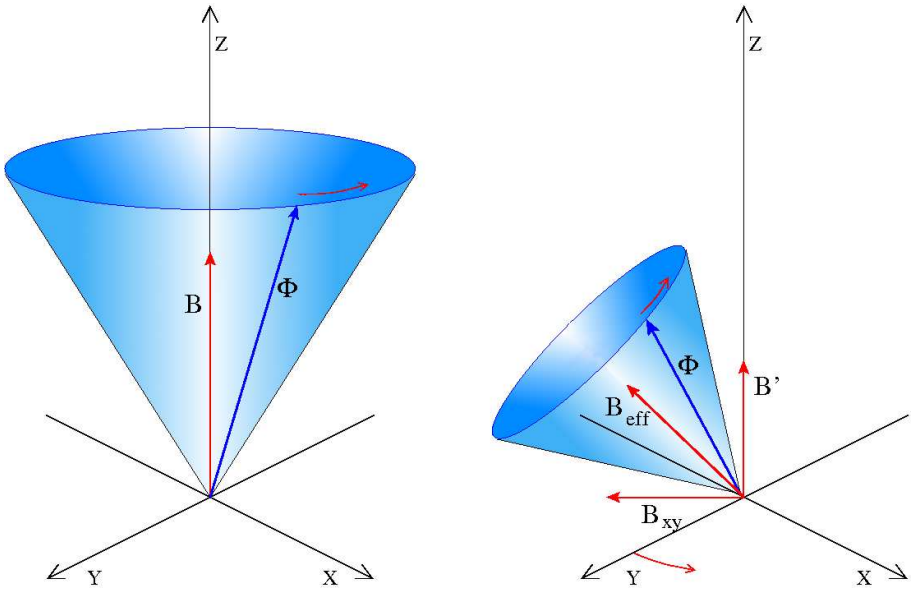

FIGURE 5.3 A dipole Φ in a magnetic field B rotates around the magnetic field axis (left figure). The dipole rotates slower in a rotating coordinate system, meaning that effectively it feels a weaker magnetic field B' (right figure). In addition, the xy-component of the magnetic field tilts the rotation axis. These effects induce transitions between the different spin-states.

where $\delta = \frac{\epsilon_g - \epsilon_e}{2} - \hbar\omega_{\mathrm{EM}}$ is the detuning energy of the field. The detuning energy δ can be varied by changing the frequency of the field ω_{EM}, and the coupling strength Ω is determined by the intensity of the field. This Hamiltonian describes the simplest possible (nontrivial) quantum mechanical system, the two-state system. Solving the time evolution, the probability for an atom initially (at $t = 0$) in state $|g\rangle$ to be found after a time t in state $|e\rangle$ is

$$P_e(t) = \left| \frac{\Omega}{\sqrt{\delta^2 + \Omega^2}} \sin\left(\frac{\sqrt{\delta^2 + \Omega^2}\, t}{2\hbar} \right) \right|^2 , \tag{5.14}$$

This describes coherent Rabi oscillations [21] between the two states at the Rabi frequency $\omega_{\mathrm{R}} = \sqrt{\delta^2 + \Omega^2}/\hbar$, see Fig. 5.4. The amplitude of the oscillations follows the Lorentzian form $L(x) = \frac{1}{\pi} \frac{\Gamma}{x^2 + \Gamma^2}$, where the linewidth Γ is given by the coupling strength Ω.

To summarise, the external electromagnetic field induces transitions between different states of the atom. The field provides both the coupling Ω and the required energy δ that can be varied by controlling the intensity and the frequency of the field. This simple model can be used to create more elaborate models.

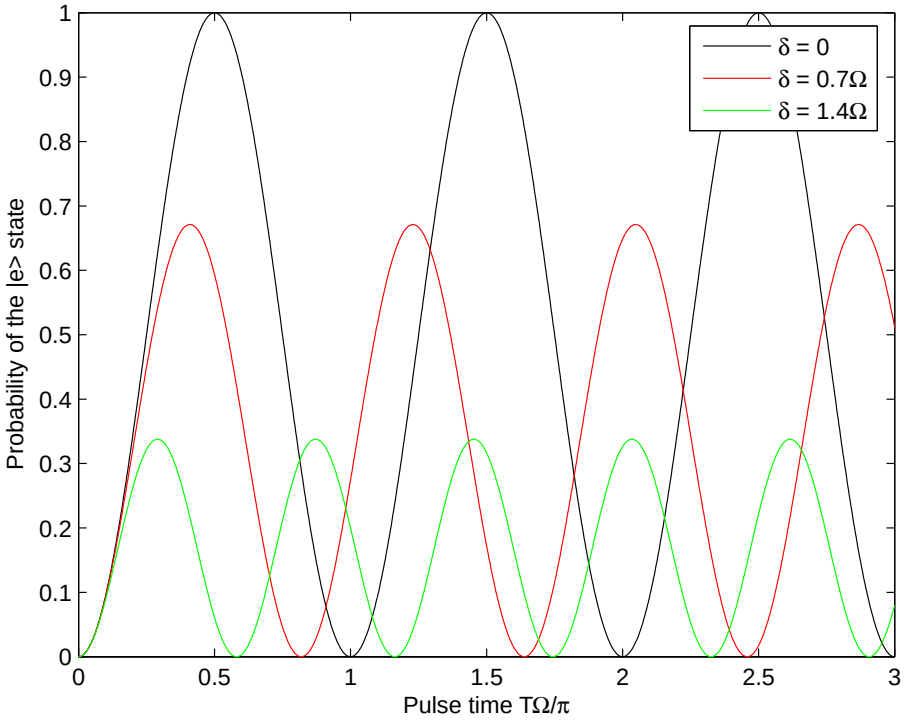

FIGURE 5.4 The probability of finding the atom in the excited state $|e\rangle$ as a function of time shows Rabi oscillations. The amplitude and the frequency of the oscillations changes with the detuning δ.

5.1.3 Decoherence

The effect of decoherence [85] can be introduced to our simple model by measuring the state at random moments. This dampens the coherent Rabi oscillations, see Fig. 5.5. In general, decoherence arises from interactions with a continuum of states (or at least a very large number of states). This can be described by a density matrix ρ, that for a two-level atom is a 2x2-matrix

$$\rho = \begin{pmatrix} p_g & C \\ C^* & p_e \end{pmatrix}. \tag{5.15}$$

The diagonal elements p_g and p_e give the probabilities that the state of the atom, if measured, would yield eigenstate $|g\rangle$ or $|e\rangle$. The off-diagonal elements are called coherences, and they tell the amount of coherence left in the state of the atom. Maximally coherent states are called pure states and they satisfy $|C|^2 = p_g p_e$. In contrast, a completely decoherent sample (i.e. $C = 0$) corresponds to a statistical mixture of the two states. When the state of the system is measured, it loses its coherence and the off-diagonal terms vanish. However, since the density matrix formalism is used in context of ensembles of quantum systems, the diagonal elements are in principle unchanged.

If the two-level atom is interacting with a large number of degrees of free-

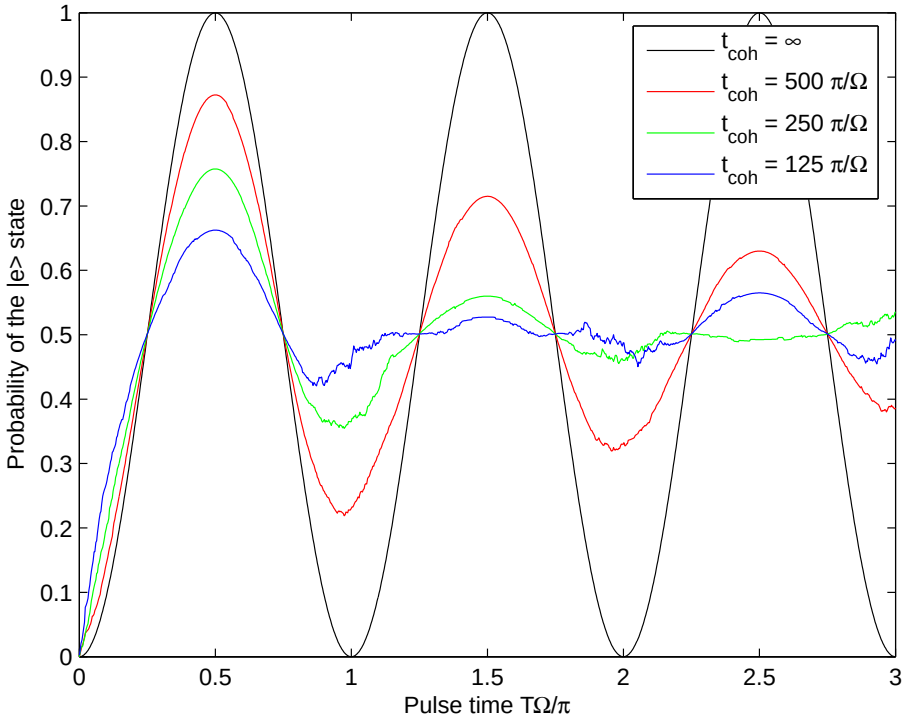

FIGURE 5.5 Introducing decoherence by measuring the state on average at every $t = t_{\mathrm{dec}} = t_{\mathrm{coh}}$ dampens the Rabi oscillations. The curves are obtained by averaging over a large number of simulations. A single simulation would produce a curve that would be jumping between the two states, as a measurement necessarily collapses the state of the atom into either of the two eigenstates.

dom (the continuum), the system is in principle described by a huge density matrix, spanned by the whole Hilbert space of the total system. However, the density matrix of the single atom can be obtained by tracing over the continuum of states. However, for most kinds of interactions, this will cause a decay of the off-diagonal elements of the density matrix in Eq. (5.15). Often the decay is exponential, i.e. $C(t) = C(0)e^{-t/t_{\mathrm{dec}}}$ [21], where the decoherence time t_{dec} gives the characteristic timescale in which the quantum state of the atom will collapse. This decay can be interpreted as a measurement, with the 'observer' being the continuum of states. Reversing this, the effect of decoherence can be described by randomly measuring the state of the system (in an ensemble of systems) with the expectation value for the time between the measurements given by t_{dec} (this too gives an exponential damping to coherences C).

Usually, atom gas experiments boast very long coherence times, giving raise to phenomena such as Rabi oscillations and other interference effects. By using coherent light or radio-frequency field, the atoms are coupled to only a few degrees of freedom, helping to conserve the coherence of the atom states. On the other hand, atom-atom interactions themselves are a source of decoherence as each atom is coupled to all other atoms. However, for degenerate fermionic gases, meaning gases at

very low temperatures, the Pauli blocking helps to conserve coherence even with very strongly interacting gases, by forbidding most of the possible scattering processes.

However, interactions between the atoms produce important correlations that cannot be described with the simple picture used above. As the time evolution becomes more complicated, we will need better tools for describing it. Describing the atom-light interaction perturbatively allows us to include the atom-atom interactions in more detail. Thus, in the following, I will discuss the simple time-dependent perturbation theory.

5.2 Perturbative approach to rf-spectroscopy

In the perturbative approach, the time evolution of the system is expanded in terms of some perturbing potential V. Here we choose as the perturbation the off-diagonal elements of the Hamiltonian (5.13) that describe the coupling between the two atomic states, generated by the surrounding electromagnetic field.

5.2.1 First-order perturbation theory

Usually, the perturbative approach is valid when the 'effect of the perturbation' is small. That is, when the perturbation V is weak as compared to other energy scales in the system H_0 and the state of the system does not change significantly due to the perturbation. In the present context this basically means that $\Omega T/\hbar \ll 1$. With these assumptions, the lowest order terms dominate and the higher order terms can be neglected. These requirements are met by short and weak rf-pulses. However, later we will extend this simple treatment to account for longer and stronger pulses.

Assume that the rf-pulse lasts for time T, i.e. the coupling Ω is turned on at $t = 0$ and off at $t = T$

$$\Omega(t) = \begin{cases} \Omega, & \text{for } 0 \leq t \leq T \\ 0, & \text{otherwise} \end{cases} . \tag{5.16}$$

In the lowest (or the first) order, the time evolution of the system is governed by the unperturbed Hamiltonian H_0 and a single operation of the perturbation V at some time $t \in [0, T]$. The probability amplitude for the transition $|g\rangle \rightarrow |e\rangle$ is now

$$A_e^1(T) = \frac{1}{\hbar} \int_0^T dt \, \langle e| e^{iH_0(T-t)/\hbar} V e^{iH_0 t/\hbar} |g\rangle, \tag{5.17}$$

where perturbation V transfers the atom from $|g\rangle$ to state $|e\rangle$ at time t. Assuming the energies of the two hyperfine states are E_g and E_e, we obtain

$$A_e^1(T) = \frac{\Omega}{\hbar} e^{iE_e T/\hbar} \int_0^T dt \, e^{i(E_g - E_e)t/\hbar}. \tag{5.18}$$

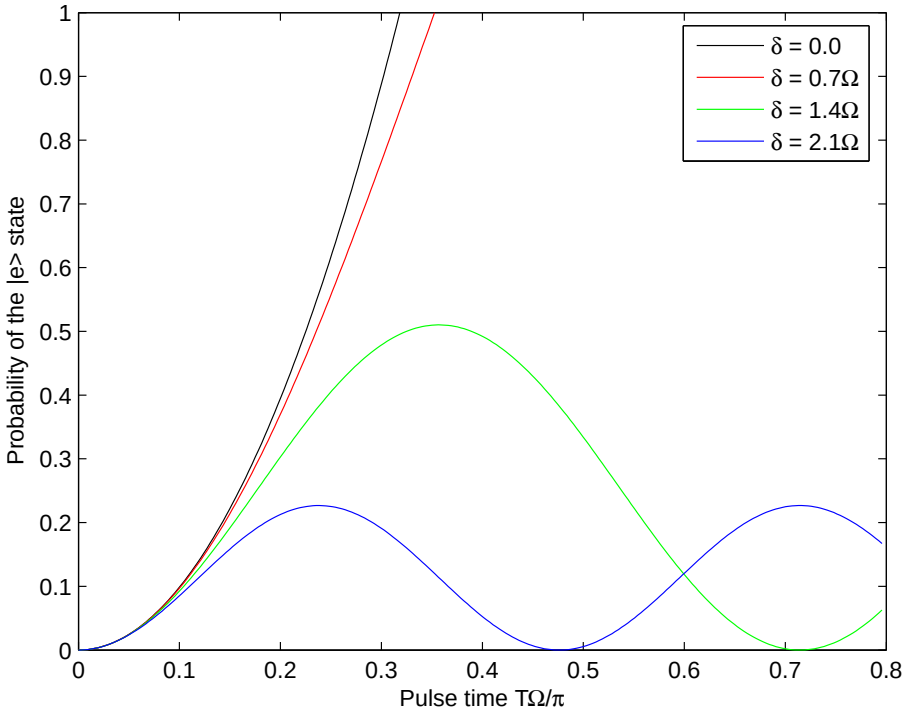

FIGURE 5.6 The probability of finding the atom in the excited state as a function of time, calculated using the first order perturbation theory. For $\delta = E_g - E_e \gg \Omega$, the first order perturbation theory regains the correct Rabi oscillations. For on-resonant atoms, it is valid only in the beginning of the pulse $T \ll \Omega/\pi$.

The energies E_g and E_e are assumed to include also the rf-field energy δ. Doing the integration, the probability of finding the atom (initially in the ground state $|g\rangle$) in the excited state $|e\rangle$ after the pulse is obtained as

$$P_e^1(T) = |A_e^1(T)|^2 = \frac{4\Omega^2 \sin^2\left(\frac{(E_g - E_e)T}{2\hbar}\right)}{(E_g - E_e)^2}, \tag{5.19}$$

which resembles the exact result in Eq. (5.14), the only thing lacking is the linewidth. Clearly, the first-order perturbation theory is valid in the limit of small Ω (as compared to the energy difference $E_g - E_e$), see Fig. 5.6.

In the limit of a very long and weak pulse, a cutoff $e^{-\eta t}$ can be introduced in the perturbing potential $V(t)$ to guarantee a converging solution. In this limit, the diffraction function $\sin^2(x/2)/x^2$ is replaced by the delta function $\delta(x)$, showing that the energy of the atom must be conserved and yielding the Fermi Golden Rule for the transition probability.

A few remarks can be made here that clarify the underlying physics. Firstly, it is interesting that the first-order perturbation theory already gives the Rabi-like oscillations, albeit with the wrong frequency when the coupling Ω is not negligible, see Fig. 5.6. For time $T_1 = \frac{\pi\hbar}{E_g - E_e}$, the probability of finding the atom in the excited

state is maximal. However, a moment later the probability decreases, until at time $T_2 = \frac{2\pi\hbar}{E_g - E_e}$ it is zero. On the other hand, the first-order perturbation theory does not include a process where the atom would be able to excite and then come back to the ground state, since that would be of the second order in the coupling V! The oscillatory behaviour arises from interference of different paths. In the first-order perturbation theory, the different paths (leading to state $|e\rangle$) amount to different times $t < T_1$ and $t' > T_1$ when the atom is transferred to the excited state. If the field is off-resonant, the two states $|e\rangle$ and $|g\rangle$ have different energies E_e and E_g, and hence the different paths will have different phases at the end of the pulse at time T. For $T = T_2$, all paths that describe a transfer of the atom to the state $|e\rangle$ will sum up to zero, meaning that the atom is not transferred. The oscillations seen in the first-order perturbation theory follows from the destructive interference between these paths.

The second important point is that on-resonance ($E_g = E_e$), the oscillatory nature vanishes and the probability is simply $P_e^1 = \left|\frac{\Omega T}{\hbar}\right|^2$. This is related to the limitation of the perturbative approach, as it does not include the broadening caused by the coupling (the Ω^2 term in the square root in the Rabi oscillation frequency). This broadening originates from the back and forth oscillations between the states $|e\rangle$ and $|g\rangle$, and is therefore of higher order in Ω. Furthermore, there is no destructive interference between different paths since both states $|e\rangle$ and $|g\rangle$ have the same energy. On the other hand, the first-order perturbation theory is valid even on-resonance if the pulse is simply short enough (basically $\Omega T/\hbar \ll 1$). This is because in short timescales high order processes are exponentially suppressed, and thus there is no destructive interference from paths describing oscillations between the states $|e\rangle$ and $|g\rangle$. The first-order perturbation theory treatment of the rf-spectrum holds therefore in the whole spectrum: away from the resonance the description is adequate already for long times and in the beginning of the rf-pulse it is valid also on resonance.

5.2.2 Regime of validity of perturbative approach

This is a good point to discuss the regime of validity of the perturbative approach in a more general setting. As discussed above, the perturbative approach is expected to be valid in short timescales. Under certain conditions, the method is valid in any timescale.

If the decoherence time of the system is very long, the atoms will conduct Rabi oscillations, requiring terms of high order in the perturbative expansion. However, if the decoherence time t_{dec} is much shorter than the Rabi oscillation timescale, given by $t_{\mathrm{Rabi}} = \Omega/\hbar$, the Rabi oscillations become strongly suppressed as seen in Fig. 5.5. In this case, the system begins the Rabi oscillations but these are interrupted by the effective measurement due to the decoherence. This measurement collapses the state of the atom into either of the two eigenstates ($|e\rangle$ or $|g\rangle$), the probability given by the corresponding probability amplitudes of the superposition state prior to the

measurement. After the measurement, the atom will restart the Rabi oscillations, beginning from either of the eigenstates.

If the decoherence time is short $t_{\mathrm{dec}} \ll t_{\mathrm{Rabi}}$, the perturbative approach provides correct transition probabilities for this short interval (although rigorous description of the decoherence may be difficult). By dividing the whole pulse into time intervals of the size t_{dec}, and applying the perturbative approach to each interval separately (sequentially), the validity of the approach can be extended to the whole pulse.

5.2.3 Higher-order perturbation theory

The first-order perturbation theory can be improved by including terms of higher order. Resummation of the perturbative expansion will eventually give the exact time evolution. This can be easily seen for on-resonant Rabi oscillations.

The second order term in the perturbative expansion necessarily vanishes, since two operations of the coupling V necessarily return the atom back to the ground state. However, the third order term gives as the (complex) probability amplitude

$$A_e^3 = -\frac{\Omega^3}{\hbar^3}\int_0^T dt_1 \int_{t_1}^T dt_2 \int_{t_2}^T dt_3\, e^{-iE_g t_1/\hbar} e^{-iE_e(t_2-t_1)/\hbar} e^{-iE_g(t_3-t_2)/\hbar} e^{-iE_e(T-t_3)/\hbar}. \tag{5.20}$$

On resonance $E_e = E_g$, this gives $A_e^3 = -e^{iE_eT/\hbar}\frac{\Omega^3T^3}{3!\hbar^3}$. Together with the first order term, we get

$$P_e^3 = \left|\frac{\Omega T}{\hbar} - \frac{\Omega^3 T^3}{3!\hbar^3}\right|^2, \tag{5.21}$$

which is the beginning of the Taylor series of $\sin^2\left(\frac{\Omega T}{\hbar}\right)$, in agreement with the (on-resonant) Rabi oscillations obtained from the exact solution in Eq. (5.14).

Even higher order terms can be obtained from the recursive relation

$$A_e^n(t,T) = \frac{1}{\hbar}\int_t^T dt'\, A_e^{n-2}(t,t')\Omega A_e^1(t',T), \tag{5.22}$$

where

$$A_e^1(t,T) = \frac{1}{\hbar}\int_t^T dt'\, e^{-iE_e(T-t')/\hbar}\Omega e^{-iE_g(t'-t)/\hbar}. \tag{5.23}$$

Now the probability of the transition $g \to e$ in $(2N+1)$-order perturbation theory is

$$P_e^N = \left|\sum_{n=0}^{N} A^{2n+1}(0,T)\right|^2, \tag{5.24}$$

and, indeed, this recursive relation does reproduce the Taylor expansion of the Rabi oscillations. Fig. 5.7 shows the transition probabilities up to the fifth order.

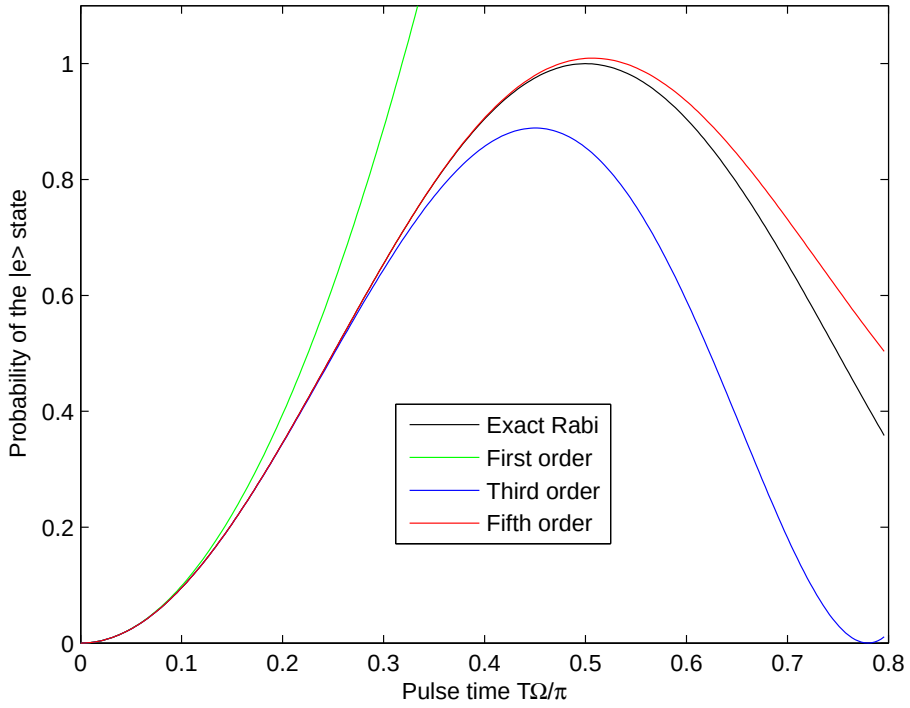

FIGURE 5.7 The probabilities of finding the atom in the excited state as a function of time, calculated using the first, third, and fifth order perturbation theories. High-order terms regain the on-resonant Rabi oscillations.

Now it is time to generalise our model to a many-body system. The full coupling term can be written using the creation and annihilation operators as

$$\hat{H}_{\mathrm{a-l}} = \sum_k \left(\Omega \hat{c}^\dagger_{ke} \hat{c}_{kg} + \Omega \hat{c}^\dagger_{kg} \hat{c}_{ke} \right), \tag{5.25}$$

where I have assumed a pulse with a long wavelength (radio-frequency pulse) that conserves the momentum of each atom state. In the absence of atom-atom interactions, the full Hamiltonian ($\hat{H} = \hat{H}_0 + \hat{V}$, where $\hat{H}_0$ is the kinetic energy of the atoms) separates into mutually commuting parts for different momentum states k, and the time evolution of the total system is therefore a simple product of the time evolutions of each state, i.e. $e^{i\hat{H}t} = \prod_k e^{i\hat{H}_k t}$. Diagonalising each $\hat{H}_k = \hat{H}^k_0 + \hat{V}_k$ separately, it becomes evident that all atoms undergo Rabi oscillations independent of each other. Notice that there is no Pauli blocking since the momentum of atoms is conserved. In this trivial case, the perturbative approach is unnecessary but in principle applicable. When interactions are switched on, the picture changes.

5.2.4 Experiment 1, absence of the mean-field shift

The first nontrivial complication is the introduction of a mean-field energy shift (or Hartree shift). Assuming a two-component Fermi gas populating both the states

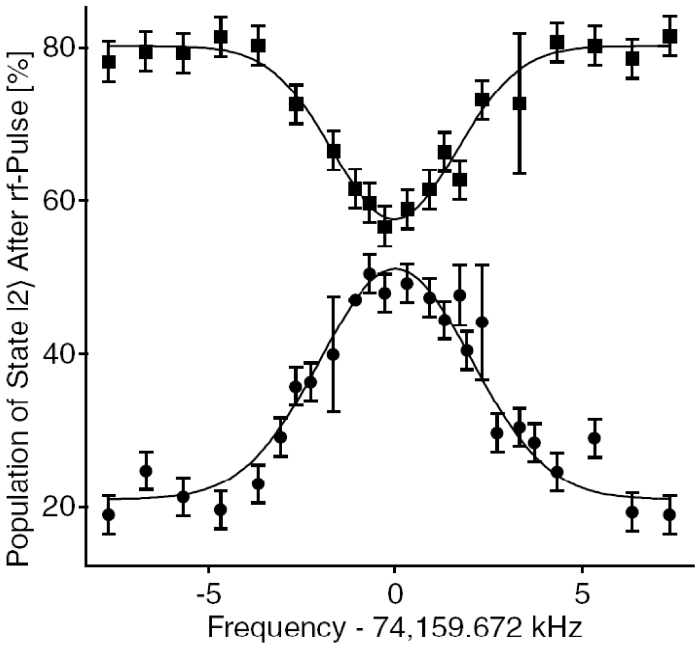

FIGURE 5.8 The absence of the mean-field shift in a rf-transition of a binary Fermi system [89]. Mean-field theory predicts a shift of $20\,\mathrm{kHz}$ in the position of the peak relative to the dip.

$|g\rangle$ and $|e\rangle$, the interactions between the atoms produce a shift in the energy levels of the atoms. If the densities of the two species are n_g and n_e, with the interaction parameter $U = \frac{4\pi\hbar^2 a}{m}$, the energy levels of $|g\rangle$-atoms are shifted by Un_e and the energy levels of $|e\rangle$-atoms are shifted by Un_g. Trivially, one would now assume that the detuning energy would be shifted by the difference in the Hartree energies $Un_e - Un_g = U(n_e - n_g)$. However, this is not the case, as shown both experimentally and theoretically in Ref. [89], see Fig. 5.8. Instead, there is no mean-field energy shift what so ever. The experiment will be discussed in more detail later.

The problem is that the simple perturbative approach above is misleading as it misses the correlations between the atoms. The interpretation given in [89] is that the atoms undergo coherent rotations between the two states. Coherent means here that the states of all atoms are rotated at the same rate (hence they are strongly correlated by the field). In the semiclassical picture this is called the rotation of a Bloch vector. The rotation is described by a unitary operator $\hat{\mathcal{U}}(t)$. Now the interaction energy of the system at any moment t is

$$E_{\mathrm{int}}(t) = \langle\Psi|\hat{\mathcal{U}}(t)^\dagger \hat{H}_{\mathrm{int}}\hat{\mathcal{U}}(t)|\Psi\rangle. \tag{5.26}$$

However, it can be shown that the rotation $\hat{\mathcal{U}}(t)$ commutes with the Hamiltonian $\hat{H}_{\mathrm{int}}$ so that the total interaction energy is necessarily time independent, and therefore the resonant detuning energy is unaffected by the mean-field energy shift.

However, we already understood from the discussion above, that the perturbative approach should produce correct results if one simply includes terms of high enough order. On the other hand, the mean-field interaction Hamiltonian

$$\hat{H}_{\rm int}^{\rm MF} = U \sum_k \left(n_e \hat{c}_{kg}^\dagger \hat{c}_{kg} + n_g \hat{c}_{ke}^\dagger \hat{c}_{ke} \right) \tag{5.27}$$

separates, just like the noninteracting Hamiltonian $\hat{H}_0$, into mutually commuting parts $\hat{H}_k$. Now the perturbative treatment can be done to each atom separately, with the energy difference for the $|g\rangle \rightarrow |e\rangle$-transition

$$\Delta E = E_g + UN_e - E_e - UN_g, \tag{5.28}$$

where E_g and E_e are the single-particle energies of the atoms (neglecting hyperfine energy splitting, $E_g = E_e = \frac{\hbar^2 k^2}{2m}$, where k is the momentum of the atom).

However, this produces the wrong resonant detuning energy δ. The problem is that the mean-field approximation does not describe coherence effects properly. As pointed out in Ref. [89], the Bloch rotation does not add entropy to the system as the atoms remain in identical states. The build up of the mean-field energy requires that this symmetry is broken due to effect of decoherence. Measurement of the system will collapse the superposition states of the atoms, some ending up in the $|e\rangle$ state and some in $|g\rangle$, according to the corresponding probability amplitudes. The mean-field approximation for the $|g\rangle - |e\rangle$ interaction is not valid for a sample where the atoms are in a superposition of the these states. The resonant frequency is determined by the energy change in the coherent sample, which is beyond the reach of the mean-field approximation. These issues underline the importance of describing the atom-atom interactions and atom-light interactions properly using the full interaction Hamiltonian $\hat{H}_{\rm int}$.

5.2.5 Experiment 2, probing of the pairing gap

Radio-frequency or laser spectroscopies have been suggested to be used for detecting the pairing gap in a superfluid Fermi gas [84] and the theory has been generalised to a strongly interacting gas in Ref. [45] (Publication I). The scheme was applied in the experiment in Ref. [19]. In the experiment, a two-component Fermi gas (populating states $|g\rangle$ and $|g'\rangle$) was cooled down to low enough temperatures for the atoms to form pairs. A radio-frequency field was used to transfer atoms from the state $|g\rangle$ to an excited state $|e\rangle$ (the terminology of an excited state can be somewhat misleading. The $|g\rangle$, $|g'\rangle$, and $|e\rangle$ states are simply different hyperfine states.) The transfer of an atom required breaking of a $|g\rangle$-$|g'\rangle$ pair and in this way the rf-field was used to probe the binding energy of these pairs.

The experimental spectra are shown in Figs. 5.9 and 5.10. The spectra show a

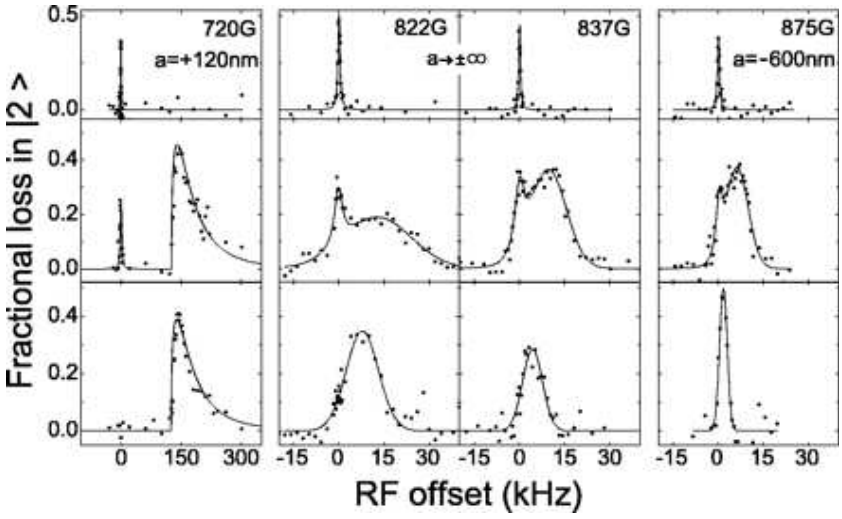

FIGURE 5.9 The measured radio-frequency spectra of a superfluid ^{6}Li Fermi gas [19] at several magnetic field values. The figures in the left are in the BEC regime while rest of the figures are in the strongly interacting regime. The Feshbach resonance is located at $834\,\mathrm{G} = 83.4\,\mathrm{mT}$. Lower figures are for very low temperatures while the upper figures are for higher temperature. The spectra exhibit a broad peak shifted from the zero detuning (RF offset) corresponding to the paired atoms. The figures show the increase in the pairing gap when the interactions become stronger and temperature lower (however, the Fermi energy scale decreases for lower temperatures, yielding smaller pairing gap in absolute units). At higher temperatures, a narrow peak appears at zero detuning, originating from weakly bound atoms at the edge of the trap.

broad shifted peak at very low temperatures, with a narrow peak appearing at the zero detuning at higher temperatures. In addition, increasing temperature (or decreasing interaction strength by tuning the atoms away from the Feshbach resonance into the BCS side) moves the broad peak closer to zero detuning, finally merging the two peaks into a single narrow peak. The experimental setup was studied theoretically in Ref. [44] (Publication II), and Fig. 5.11 shows the rf-spectra obtained using the first order perturbation theory. In the theory, the effects of the inhomogeneous trapping potential were incorporated through the use of local density approximation. The results were in qualitative agreement, the theory producing a similar structure of a single shifted broad peak at very low temperatures and the appearance of an additional narrow peak at higher temperatures. The shifted peak corresponds to the paired atoms and the narrow peak corresponds to atoms at the edge of the trap in Andreev in-gap states that are only weakly bound. At finite temperatures, these weakly bound atoms become thermally excited and in addition the pairing gap decreases at these low density regions. These two factors contribute in producing the narrow finite temperature peak at the zero detuning.

The experimental spectra did not show any mean-field shifts, as can be deduced from the spectra at high temperatures (where pairing effects were absent). Due to the limitations of the perturbative approach discussed above, the theory was

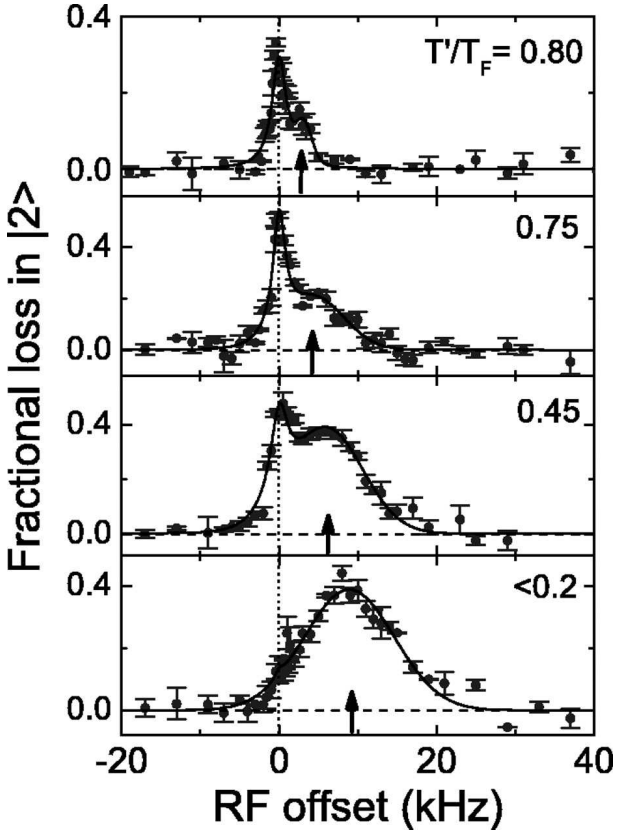

FIGURE 5.10 The radio-frequency spectra at various temperatures T' show the emergence of the narrow peak when the temperature is increased [19]. In addition, the shifted peak becomes narrower and approaches the zero detuning as the pairing gap decreases with increasing temperature. The temperatures shown in the figure are measured after a sweep to the BEC side of the resonance and are not directly related to the temperature of the superfluid on (Feshbach) resonance. The Fermi energy is roughly $52\,\mathrm{kHz}$.

unable to explain the absence of these shifts. However, neglecting these Hartree-type interactions, the experimental and theoretical spectra are in good agreement.

The theoretical calculations assumed the excited state $|e\rangle$ to be non-interacting. However, this was not the case in the experiment, and the possible pair formation between the $|e\rangle$ and $|g\rangle$, or $|e\rangle$ and $|g'\rangle$ atoms could not be ruled out, especially in a rapidly decohering sample. Including these interactions would move the broad pairing peak towards lower detuning energies. This is because the energy levels of the final state $|e\rangle$ would also be shifted down due to appearance of a pairing gap. The interactions of the state $|e\rangle$ can in principle be incorporated (at least in a qualitative level) in the perturbative theory by calculating the energy spectrum of the excited state and calculating the transfer into these states. In the following, I will describe how the perturbative approach can be improved to include the coherence effects and the absence of the mean-field shift.

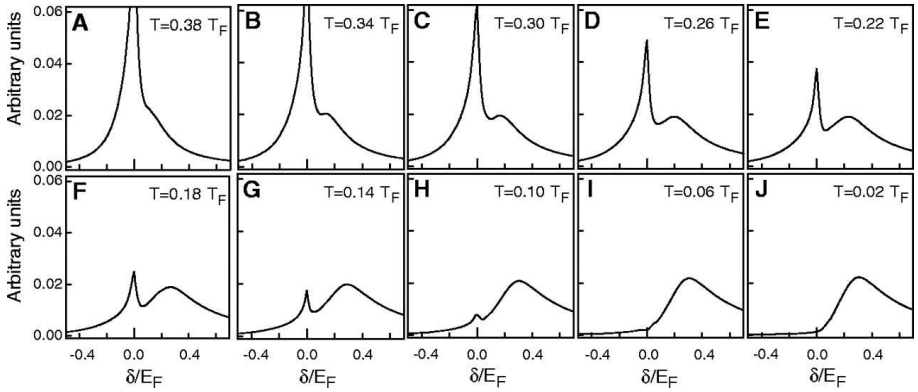

FIGURE 5.11 The rf-spectra of a trapped superfluid at several temperatures obtained using the first-order perturbation theory [44] (Publication II). The spectra were in qualitative agreement with the experimental spectra, confirming the interpretations presented in figure captions in Figs. 5.9 and 5.10. The parameters used here correspond to Fig. 5.10, but the linewidths are too small. Compare with Fig. 5.14 where the linewidths correspond to the experimental values.

5.2.6 Coherent radio-frequency spectroscopy

The absence of the mean-field shift in the radio-frequency spectroscopy of the ultracold Fermi gas follows from the coherent transitions of the atoms. The simple picture of the rotation of the Bloch vector becomes insufficient when the atoms become paired. As seen also from the rf-spectra, different atoms are resonant with the field at different detuning energies, meaning that for a given detuning energy, only part of the atoms are affected. The idea of the coherent rotations of the atom states can be generalised to these asymmetric systems by defining different rotation operators $\hat{\mathcal{U}}_k(t)$ for different atoms, with the rotation frequency and the amplitude given by the common rf-coupling Ω but different energy differences ΔE_k. Now the question is, how to determine the energy difference ΔE_k?

The effect of the rf-field is to transfer atoms in the hyperfine state $|g\rangle$ to the hyperfine state $|e\rangle$. We define the rotation operator for an atom with momentum k as

$$\hat{\mathcal{U}}_k(t) = \alpha_k(t)\hat{c}^\dagger_{kg}\hat{c}_{kg} + \alpha_k(t)\hat{c}^\dagger_{ke}\hat{c}_{ke} + \beta_k(t)\hat{c}^\dagger_{kg}\hat{c}_{ke} - \beta_k(t)\hat{c}^\dagger_{ke}\hat{c}_{kg}. \tag{5.29}$$

Here $\alpha_k(t)^2 + \beta_k(t)^2 = 1$ for all times t. The simple Bloch rotation (meaning that all atoms are rotating symmetrically) would be obtained with the choice $\alpha_k(t) = \cos(\omega t)$ and $\beta_k(t) = \sin(\omega t)$.

Assume that the state of the system before the rf-pulse (and the rotation) is given by the BCS ground state

$$|\Psi(t=0)\rangle = \prod_k \left(u_k + v_k\hat{c}^\dagger_{kg}\hat{c}^\dagger_{-kg'}\right)|0\rangle. \tag{5.30}$$

Operating on all atoms in the hyperfine state $|g\rangle$ with the corresponding rotation

operators would produce the state

$$\begin{aligned}|\Psi(t)\rangle &= \prod_k \left(u_k + v_k \hat{\mathcal{U}}_k(t)\hat{c}^\dagger_{kg}\hat{c}^\dagger_{-kg'}\right)|0\rangle \\ &= \prod_k \left[u_k + v_k\left(\alpha_k(t)\hat{c}^\dagger_{kg} - \beta_k(t)\hat{c}^\dagger_{ke}\right)\hat{c}^\dagger_{-kg'}\right]|0\rangle.\end{aligned} \tag{5.31}$$

In general, the energy of the system is given by the Hamiltonian $\hat{H} = \hat{H}_0 + \hat{H}_{\rm int}$, where $\hat{H}_0 = \sum_{k\sigma}\epsilon_k \hat{c}^\dagger_{k\sigma}\hat{c}_{k\sigma}$ and

$$\hat{H}_{\rm int} = \sum_{\sigma.\sigma'} U_{\sigma\sigma'} \sum_{kk'q} \hat{c}^\dagger_{k\sigma}\hat{c}^\dagger_{q-k\sigma'}\hat{c}_{q-k'\sigma'}\hat{c}_{k'\sigma}. \tag{5.32}$$

This is the same Hamiltonian as in Eq. (3.3) but now generalised to several interacting components. Neglecting the single particle energies, the interaction energy of the initial state is now

$$\begin{aligned}E_{\rm i} = \langle\Psi(0)|\hat{H}_{\rm int}|\Psi(0)\rangle &= U_{gg'}\sum_{k\neq k'} u_k v_k u_{k'} v_{k'} + U_{gg'}\sum_k v_k^2 \\ &= U_{gg'}\left(\sum_k u_k v_k\right)^2 + U_{gg'}\sum_k v_k^4 \\ &= \frac{\Delta^2}{U_{gg'}} + U_{gg'}\sum_k v_k^4\end{aligned} \tag{5.33}$$

Likewise, the energy after the rotation is

$$\begin{aligned}E_{\rm f}(t) = \langle\Psi(t)|\hat{H}_{\rm int}|\Psi(t)\rangle &= \sum_{k\neq k'}\left(\alpha_k(t)\alpha_{k'}(t)U_{gg'} + \beta_k(t)\beta_{k'}(t)U_{eg'}\right)u_k v_k u_{k'} v_{k'} \\ &+ \sum_k \left(\alpha_k(t)^2 U_{gg'} + \beta_k(t)^2 U_{eg'}\right)v_k^2.\end{aligned} \tag{5.34}$$

The U_{eg}-interaction term is invariant in the rotation, in harmony with the absence of the mean-field shift, although now generalised to an asymmetric setting in which different atoms are rotated at different rates and amplitudes (the mean-field shift is absent here because the $|e\rangle$-states are initially empty, but the result is more general).

The energy difference is now

$$\begin{aligned}\Delta E = E_{\rm f} - E_{\rm i} = &\sum_{k\neq k'}\left[\alpha_k(t)\alpha_{k'}(t)U_{gg'} + \beta_k(t)\beta_{k'}(t)U_{eg'} - U_{gg'}\right]u_k v_k u_{k'} v_{k'} \\ &+ \sum_k \beta_k(t)^2\left(U_{eg'} - U_{gg'}\right)v_k^2,\end{aligned} \tag{5.35}$$

in particular the energy change of an atom with momentum p is

$$\begin{aligned}\Delta E_p = &\sum_{k'\neq p} \left[\alpha_p(t)\alpha_{k'}(t)U_{gg'} + \beta_p(t)\beta_{k'}(t)U_{eg'} - U_{gg'}\right] u_p v_p u_{k'} v_{k'} \\ &+ \beta_p(t)^2 \left(U_{eg'} - U_{gg'}\right) v_p^2.\end{aligned} \tag{5.36}$$

If the elements α and β of the rotation matrix would be independent of k (this is the Bloch rotation), the energy difference would become

$$\Delta E = \beta^2 \frac{U_{eg'} - U_{gg'}}{U_{gg'}} \frac{\Delta^2}{U_{gg'}} + \beta^2 \left(U_{eg'} - U_{gg'}\right) \sum_k v_k^4, \tag{5.37}$$

For weakly interacting gas, the first term on the right dominates. The energy difference depends on the rotation angle β, describing how the pairing is gradually broken (if $U_{eg'} = 0$), or at least altered (for a finite $U_{eg'} \neq 0$). This is in stark contrast to the Bloch rotation of an unpaired system, where the rf-transition does not require any additional energy. We define the resonance detuning energy $\delta_{\max}$ as the energy difference of the $\pi/2$-pulse (meaning $\beta = 1$)

$$\delta_{\max} = \frac{U_{eg'} - U_{gg'}}{U_{gg'}} \frac{\Delta^2}{U_{gg'}}. \tag{5.38}$$

This same result has been obtained also in Ref. [87] for a weakly interacting gas using a completely different approach. For a strongly interacting gas, the excitation spectrum is much broader and we expect the Bloch rotation picture to break down as the atoms will be rotated at different frequencies.

This simple calculation suggests us how to include the interactions of the $|e\rangle$-state in the perturbative calculation, at least in a qualitative level. The initial and the target state have the same form, meaning that the target state of the atom exhibits the same energy gap as the initial state (i.e. only the hyperfine state of the atom is changed, not the spatial shape of its state). However, because the interaction strengths $U_{eg'}$ and $U_{gg'}$ are different, these states correspond to different energies. The problem is how to determine the energy difference ΔE, or especially the final energy E_{f}, as this is the energy that the rf-field needs to supply. The energy of the final state for a fully rotated system ($\beta = 1$) is

$$\begin{aligned}E_{\mathrm{f}}(t) &= U_{eg'} \left(\sum_k u_k v_k\right)^2 + U_{eg'} \sum_k v_k^4 \\ &= \frac{\left(U_{eg'} \sum_k u_k v_k\right)^2}{U_{eg'}} + U_{eg'} \sum_k v_k^4\end{aligned} \tag{5.39}$$

The first term has almost the form $\tilde{\Delta}^2/U_{eg'}$, where $\tilde{\Delta}$ is the BCS gap equation for

interaction $U_{eg'}$. The only difference is that the Bogoliubov coefficients do not correspond to the gap $\tilde{\Delta}$ but to the gap Δ. However, the coefficients u_k and v_k vary as Δ^2, so that for a weakly interacting gas these coefficients are affected only slightly. Thus we can calculate the energies and the spectrum of the target states by using the simple equilibrium BCS (or some extension of BCS) theory. The transfer rates between these initial and target states are then calculated perturbatively.

Notice that the discussion above applies only in the limit of weak interactions. However, below we apply these ideas also to strongly interacting gases and therefore the effects must be considered on a qualitative level. On the other hand, in the unitarity regime (close to resonance) the pairing gap is insensitive to small changes in the interaction strength U, and therefore the assumptions above may be valid also in the strongly interacting regime.

5.2.7 The collective transition picture

The perturbative approach is by design best suited for describing single particle effects. However, with certain modifications the perturbative approach can be used to obtain qualitative results and insight on collective transitions (collective referring to the coherent transition of a large number of atoms, as for example in the rotation of the Bloch vector).

A collective transition of N atoms during the rf-pulse is at least of order N in the perturbative expansion (of the time evolution of the whole many-body state). Thus we need to consider the perturbative approach in a more general setting. The expectation value for the number of transferred atoms (measured at time T) is in the (real) S-time loop picture

$$N_{\mathrm{trans}} = \langle \hat{S}_{\mathrm{int}}(T,0)^\dagger \hat{N}_e \hat{S}_{\mathrm{int}}(T,0) \rangle, \tag{5.40}$$

where the $\hat{S}_{\mathrm{int}}(T,0)$ is the scattering matrix using the full many-body Hamiltonian as the operator $\hat{H}_0$ and the light-atom coupling $\hat{H}_{\mathrm{a-l}}$ in Eq. (5.25) as the perturbation. The operator $\hat{N}_e$ describes the measurement by calculating the number of atoms in the excited state $|e\rangle$. And finally, the whole expectation value is calculated for the ground state (or some other initial state) in the absence of the rf-field.

Writing the number operator as $\hat{N}_e = \sum_k \hat{c}^\dagger_{ke} \hat{c}_{ke}$ yields (dropping the time arguments)

$$N_{\mathrm{trans}} = \sum_k \langle \hat{S}^\dagger_{\mathrm{int}} \hat{c}^\dagger_{ke} \hat{c}_{ke} \hat{S}_{\mathrm{int}} \rangle. \tag{5.41}$$

Each term in the sum on the right hand side describes the transition probability for the transfer of a single atom of momentum k, regardless of what is happening to the

rest of the atoms. The same thing can also be written in the form

$$N_{\mathrm{trans}} = \sum_n n P^n_{\mathrm{trans}}, \tag{5.42}$$

where each P^n_{trans} is the probability that *exactly* n atoms are transferred. Notice that now we are looking at the system globally, not each atom separately. Eq. (5.41) is the form usually used, but the nonstandard form in Eq. (5.42) can be shown to be equal, and it is more useful in the present context. While in Eq. (5.41) the transfer probability is calculated for each single atom without considering the rest of the system, the probability that rest of the atoms are *not* transferred must be included in Eq. (5.42). This point is clarified by writing

$$P^n_{\mathrm{trans}} = \sum_{(k_i)_{i=1,\ldots,n}} P_{\mathrm{trans}}(\{k_1, \ldots, k_n\}) \tag{5.43}$$

where the summation is over all sets $\{k_1, \ldots, k_n\} = \{k_n\}$ of n available atoms, and the probability $P_{\mathrm{trans}}(\{k_n\})$ is the probability that all the atoms with momentum $k \in \{k_n\}$ are transferred *but* all other atoms remain untouched. For uncorrelated atoms, this can be written as

$$P_{\mathrm{trans}}(\{k_n\}) = \prod_{k\in\{k_n\}} p_k \prod_{k\in\{k_n\}^c} (1 - p_k), \tag{5.44}$$

where p_k is the probability that atom k is transferred.

If the transfer probability of all of the atoms would be the same, p, the transfer probability of (any) set of n atoms would follow a binomial distribution

$$P^n_{\mathrm{trans}} = \binom{N}{n} p^n (1-p)^{N-n}, \tag{5.45}$$

where N is the number of atoms in the $|g\rangle$-state. This can be easily derived from Eq. 5.44. The expectation value for the number of transferred atoms is now

$$N^{binomial}_{\mathrm{trans}} = \sum_n n \binom{N}{n} p^n (1-p)^{N-n} = pN, \tag{5.46}$$

for large N ($\gg 1$). In this limit, the distribution forms a very narrow peak centered at the expectation value, as shown in Fig. 5.12.

The advantage of this alternative view is that it gives an idea of the many-body state after the rf-pulse. Especially the energy difference due to the rf-pulse as calculated in Eq. (5.35) depends on how many and how much the atoms are 'rotated' by the pulse, i.e. what are the actual rotation angles $\alpha_k(t)$ and $\beta_k(t)$. Only when all atoms behave identically in the presence of the field, i.e. when the rotation angles

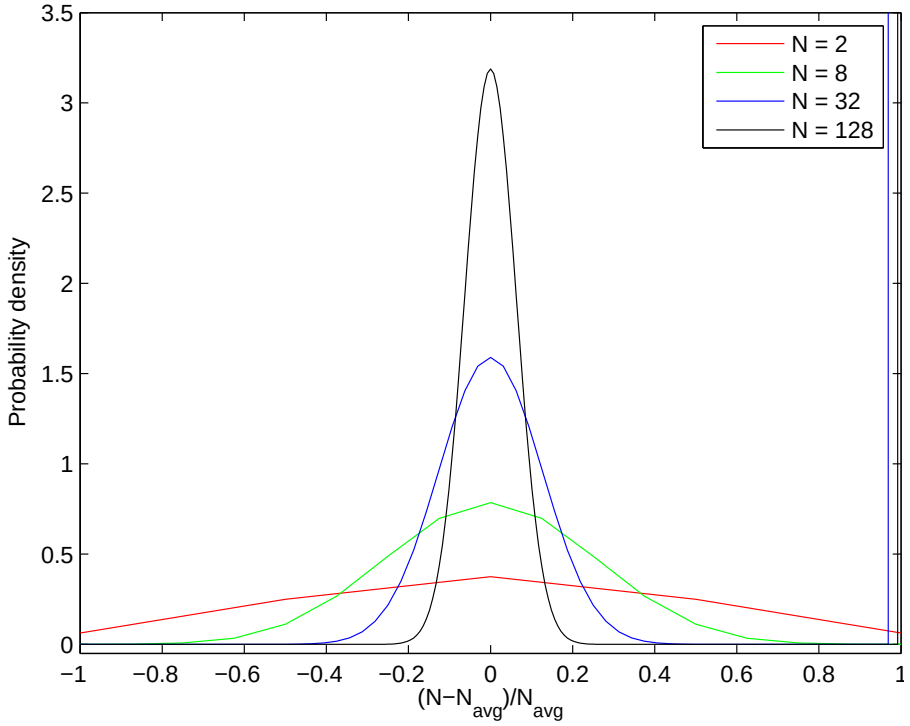

FIGURE 5.12 The binomial distribution becomes a narrow peak when the number of repetitions N (or the number of atoms) becomes large. Here the probability for each trial is $p = 0.50$ and $N_{\mathrm{avg}} = pN$.

are k-independent, the final many-body state can be easily deduced from the single-particle transition (the two pictures are of course equal, but the determination of the final many-body state is more straightforward in the many-body picture). Next I will formulate the perturbative theory in this many-body framework.

5.2.8 Coherent rf-spectroscopy using perturbative approach, simple and generalised first order theories

Here I will start by assuming that all the rotation angles $\beta_k(t)$ are either 0 or 1, meaning that all atoms that are on resonance with the field, will be transferred but all the other atoms remain in their initial state. I denote the set of atoms with $\beta_k(t) = 1$ by $S = \{k_1, \ldots, k_N\}$.

Assuming that the atoms are noncorrelated, the probability that one of the atoms (of momentum k_1) is transferred by a pulse of length T is (in the first-order perturbation theory)

$$P_{\mathrm{trans}}(\{k_1\}) = \frac{1}{\hbar^2}\int_0^T dt_1 \int_0^T dt_1' \, \langle e^{i\hat{H}_0 t_1'/\hbar}\hat{V}(k_1)e^{-i\hat{H}_0(t_1'-t_1)/\hbar}\hat{V}(k_1)e^{-i\hat{H}_0 t_1/\hbar}\rangle, \quad (5.47)$$

where $V(k) = \Omega c_{ek}^\dagger c_{gk} + h.c.$. Likewise, the probability that the whole set S will be

transferred is

$$P_{\rm trans}(S) = \left(\frac{1}{\hbar^2}\right)^N \prod_{n=1}^{N} \left[\int_0^T dt_n \int_0^T dt'_n \, \langle e^{i\hat{H}_0 t'_n/\hbar} \hat{V}(k_n) e^{-i\hat{H}_0(t'_n - t_n)/\hbar} \hat{V}(k_n) e^{-i\hat{H}_0 t_n/\hbar} \rangle \right], \tag{5.48}$$

which is of order N in V^2 in the many-body picture but of the first-order in the single particle picture of each atom.

In analogy to the Bloch rotation, all the atoms in set S should behave symmetrically. Therefore, we assume that all transfer events $V(k_n)$ will take place at the same moment t', i.e. all $t_n \to t$ and all $t'_n \to t'$. This yields

$$P_{\rm trans}(S) = \frac{1}{\hbar^2} \left(\frac{T^2}{\hbar^2}\right)^{N-1} \int_0^T dt \int_0^T dt' \, \langle e^{i\hat{H}_0 t'/\hbar} \prod_{n=1}^{N} \hat{V}(k_n) e^{-i\hat{H}_0(t'-t)/\hbar} \prod_{n=1}^{N} \hat{V}(k_n) e^{-i\hat{H}_0 t/\hbar} \rangle. \tag{5.49}$$

Operating with the unperturbed time evolution operators $e^{iH_0 t}$ will give a phase factor of the type $e^{i\Delta E t}$, where $\Delta E = E_{\rm f} - E_{\rm i}$ is the energy difference for the transfer of all atoms in S. If the operators H_0 include interactions between the atoms, and especially the interactions of the state $|e\rangle$, the energy difference will be given by equation similar to Eq. (5.35). The time integrals will now give the total energy conservation of the many-body rf-transition. For a pulse of finite length T, the transition probability for a $\pi/2$-pulse ($\Omega T/\hbar = \pi/2$) is

$$P_{\rm trans}(S) = 4\Omega^2 \frac{\sin^2\left(\frac{\Delta E T}{2\hbar}\right)}{\Delta E^2}. \tag{5.50}$$

Analogously to the Rabi oscillations of a single atom, higher order theory would introduce the linewidth Ω.

The transition probability in Eq. (5.49) can be formally obtained using coherent coupling Hamiltonian $H_{\rm coh}$, that explicitly transfers several atoms at the same time

$$\hat{H}_{\rm coh} = \Omega \sum_{n=1}^{\infty} \left(\sum_k \hat{c}^\dagger_{ke} \hat{c}_{kg} + h.c. \right)^n. \tag{5.51}$$

This Hamiltonian has been introduced, and the corresponding linear response theory has been studied in Ref. [46] (Publication III). The main point in those studies was the relaxation of the single-particle energy conservation. In the Bloch rotation picture the energy difference in Eq. (5.35) does not uniquely specify the many-body rf-transition. By imposing single-particle energy conservation (through equation similar to Eq. (5.36)), we regain the results from the first-order perturbation theory. However, higher order processes allow transfers through virtual states, relaxing the single-particle energy conservation by allowing energy exchange between the atoms. We expect these effects to be important in the limit of long and weak pulses

where the linewidth of the rf-transition is very small. For a strongly interacting gas with a broad excitation spectrum, the small linewidth will suppress the uncorrelated single-particle transfer processes. In such case, the higher order processes will be dominating.

The role of different higher order theories needs to be clarified here. The theory described by Hamiltonian (5.51), describing a many-body system, is different from the higher order theory discussed in Section 5.2.3 that considers the perturbative expansion of the time evolution of a single atom. Eq. (5.50) describes the time-evolution of the many-body state in which the time evolution of each single atom is treated in the first-order. Therefore the theory is (formally) of the first order in the coherent coupling Hamiltonian (5.51) but of higher order in the atom-light coupling Hamiltonian (5.25). Below I will refer by generalised (first order) theory to the first order theory in the many-body picture, allowing the energy transfer between the atoms and relaxing the single-particle energy conservation.

As an example of the generalised first order theory, assume that the system has 6 atoms with the excitation energies $\epsilon_{ig} - \epsilon_{ie}$ as shown in the Fig. 5.13. If the rf-field detuning energy is $\delta = 0$, the possible combinations of atoms that can be transferred while conserving (only) the total energy are:

$$\begin{aligned} &B, D \\ &B, E \\ &B, C, F \\ &A, D, F \\ &A, E, F \\ &A, B, D, E, F \end{aligned} \tag{5.52}$$

In contrast, if the linewidth of the rf-transition is sufficiently small, none of the atoms can be transferred in the single-particle picture as they are all off-resonant (simple first-order theory). Notice, that except for the third line, all other sets are subsets of the last line, which corresponds to the transfer of all atoms except for the C-atom. Because the transfer probability of a given set S includes the probability that rest of the atoms are *not* transferred, only the maximally large sets will contribute (since we are assuming that the transition probability of each atom is either 0 or 1). The sets $\{B, C, F\}$ and $\{A, B, D, E, F\}$ are maximal sets and the probability of each is a priori the same. The expectation value for the number of transferred atoms is then $\frac{5+3}{2} = 4$, using the generalised theory (5.51).

The transition probability in Eq. (5.49) requires only the total energy conservation for the many-body rf-transition (just like in the Bloch picture in Eq. (5.35)). A process which conserves all single-particle energies trivially conserves also the total energy. On the other hand, the single-particle energy conservation can be relaxed when the atoms are interacting. The interaction channel allows the atoms to

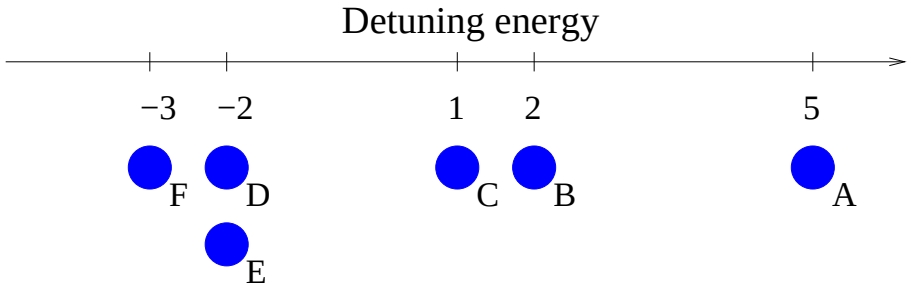

FIGURE 5.13 A trial system of 6 atoms with different excitation energies. The two maximal energy conserving sets are $\{A, B, D, E, F\}$ and $\{B, C, F\}$.

redistribute the excess or missing excitation energies between themselves.

However, the mean-field effects such as studied in Ref. [89] can be explained without such interaction channels (because the single-particle energy conservation is enough). For an unpaired system in which the rf-excitation spectrum is very narrow, all atoms behave symmetrically, meaning that all atoms can be transferred at the same time in the perturbative approach described above. This means that the energy difference $\Delta E = E_{\mathrm{f}} - E_{\mathrm{i}}$ is calculated between the initial state and a state into which all applicable atoms have been transferred. Indeed, this reproduces the absence of the mean-field shift, as the mean-field energies of the two states are the same.

5.2.9 Comparison with the experiments

Now we are ready to compare the different theoretical approaches we have developed to the experiments. The two key experimental results are the absence of the mean-field shift [89] and the probing of the pairing gap [19].

In the first experiment [89], the system was composed of ^{6}Li atoms in two hyperfine states $|g\rangle$ and $|g'\rangle$ in an 80%-20% mixture (meaning 80% in state $|g\rangle$ and 20% in state $|g'\rangle$). The fermionic atoms were weakly interacting (with $(k_{\mathrm{F}}a)^{-1} \approx -5$) through the s-wave interaction potential, and the external rf-field was used to transfer atoms between the two states $|g\rangle$ and $|g'\rangle$ (notice that now the transfer is between two populated states $|g\rangle$ and $|g'\rangle$ instead of an initially empty state $|e\rangle$). For a 50-50% mixture the atom transfer is blocked at low temperatures because of the Pauli exclusion (but also because of cancelling particle currents for $|g\rangle \to |g'\rangle$ and $|g'\rangle \to |g\rangle$).

The experimental spectrum is shown in Fig. 5.8, showing a peak in the particle transfer at frequency $74\,159\,\mathrm{MHz}$, matching exactly with the energy splitting of the two hyperfine states. The figure shows also the data for an inverted system, in which the population ratios have been reversed. The observed peak (or actually a dip, since now atoms are transferred out from the state $|g'\rangle$) coincides with the peak in the original setting, showing that the resonance detuning is indeed immune to mean-

field shifts.

As already discussed earlier, in the mean-field level the expected mean-field energy shift for the particle transfer between the two hyperfine states would have been

$$\Delta E = E_g + gN_e - E_e - gN_g = E_g - E_e + g(N_e - N_g). \tag{5.53}$$

Because the rf-field does not provide any additional momentum to the atoms, the single-particle energies of the two hyperfine states are the same (neglecting the hyperfine splitting), i.e. $E_g = E_e = \frac{\hbar^2 k^2}{2m}$, where $\vec{k}$ is the momentum of the atom. For the parameters used in the experiment [89], the energy shift should have been $\Delta E \approx 20\,\mathrm{kHz}$. Since the observed splitting was (34 ± 146) Hz, the mean-field level treatment is completely inadequate (despite the weak interaction strength!).

Now, can our theoretical approach explain this phenomenon? Yes, it can. Since (locally) all atoms are necessarily resonant with the rf-field at the same frequency (in the absence of a pairing gap all atoms are symmetric as the energies E_g and E_e are equal), only the term that transfers all atoms at the same time contributes from the coherent coupling Hamiltonian (5.51). Therefore the energy difference ΔE in Eq. (5.50) is determined by the initial state with $(20/80)\%$ mixture and the final state with $(80/20)\%$ mixture. Since the total interaction energies for these two states are the same, the energy difference is zero (neglecting the hyperfine energy splitting). Hence, our generalised perturbation theory agrees with the absence of the mean-field shift observed in the experiment [89]. Note that ΔE in Eq. (5.50) contains the final state energy of *all* atoms transferred (i.e. $(20/80)\% \rightarrow (80/20)\%$ mixture) also in the case where the experiment transfers much less atoms due to a shorter or weaker pulse (for example $(20/80)\% \rightarrow (40/60)\%$ for which the total mean-field energies would be different). Therefore the absence of the mean-field shifts is independent of the amount of the atoms transferred (or the length of the pulse), just like observed in the experiment.

The next experiment [19] that we aim to explain studied a superfluid Fermi gas in which the atoms in the two hyperfine states $|g\rangle$ and $|g'\rangle$ have formed pairs (molecules or Cooper pairs). The rf-field couples the atoms in state $|g\rangle$ to a third state $|e\rangle$, and the transfer of the atoms requires breaking of the pairs. Thus, the rf-spectrum measured the binding energy or the pairing gap of the pairs. The experimental spectra are shown in Fig. 5.9.

Indeed, the spectra show that the resonance peak is shifted from the zero detuning (that would correspond to the hyperfine energy splitting). In addition, at higher temperatures an additional peak appears at the zero detuning. This has been interpreted to originate from the edges of the trap where the density is low and the local pairing gap is small [44] (Publication II). The atoms in this region can then be transferred at very small detuning energies, producing a distinct peak. The central region of the trap has a large pairing gap that is relatively insensitive to thermal effects, and therefore the broad shifted peak is unaffected.

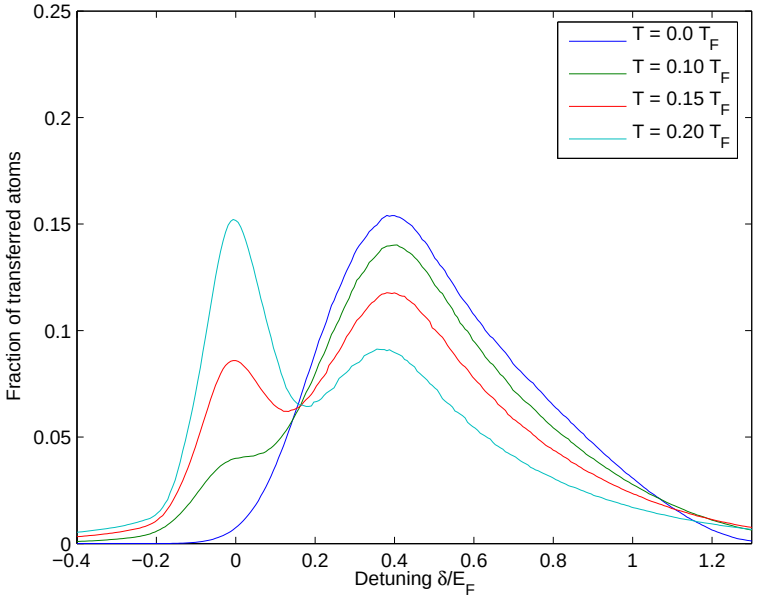

FIGURE 5.14 The rf-spectra obtained from the simple first order theory for both zero and finite temperatures. The data is for an on-resonant gas ($(k_{\mathrm{F}}a_{gg'})^{-1} = 0.0$) and the excited state is assumed to be non-interacting ($(k_{\mathrm{F}}a_{eg'})^{-1} = -\infty$). Here, and in the spectra below, the calculations are done using the BdG-approach in the harmonic oscillator basis.

The relevant timescales in the experiment were $t_{\mathrm{Pulse}} = 1\,\mathrm{s}$ and $t_{\mathrm{dec}} < 1\,\mathrm{ms}$. The decoherence has been interpreted to arise from three-body collisions, and the decoherence rate is the rate at which the transferred atoms in state $|e\rangle$ vanish from the trap [31]. The perturbative approach is expected to be valid due to the short decoherence time, even though the Rabi oscillation timescales t_{Rabi} are not known. The homogeneous linewidth of the narrow peak at the zero detuning would suggest $t_{\mathrm{Rabi}} < 1\,\mathrm{ms}$, since the width of the peak comes mainly from the homogeneous broadening due to the rf-coupling Ω (power broadening). In contrast, the broadness of the pairing peak is a result of an inhomogeneous broadening caused by the pairing of the atoms, as different atoms have different resonant frequencies but also because of the inhomogeneous trapping potential as atoms closer to the center will feel a larger pairing gap.

The rf-spectroscopy of a superfluid Fermi gas has been studied by several groups. First-order perturbation theory in a uniform gas has been used in [84,14,45] (the last one is the Publication I). Trapped gases have been studied using both first-order perturbation theory and the local density approximation in [44,35,61,62,34] (the first one is the Publication II). The Bogoliubov-deGennes approach discussed earlier has been used together with the first-order perturbation theory in [61,62]. In addition, beyond linear response or non-perturbative theories have been done in [46,87] (first one is Publication III). Basically all theories are in good agreement with the experimental results but only the last two theories agree with the absence

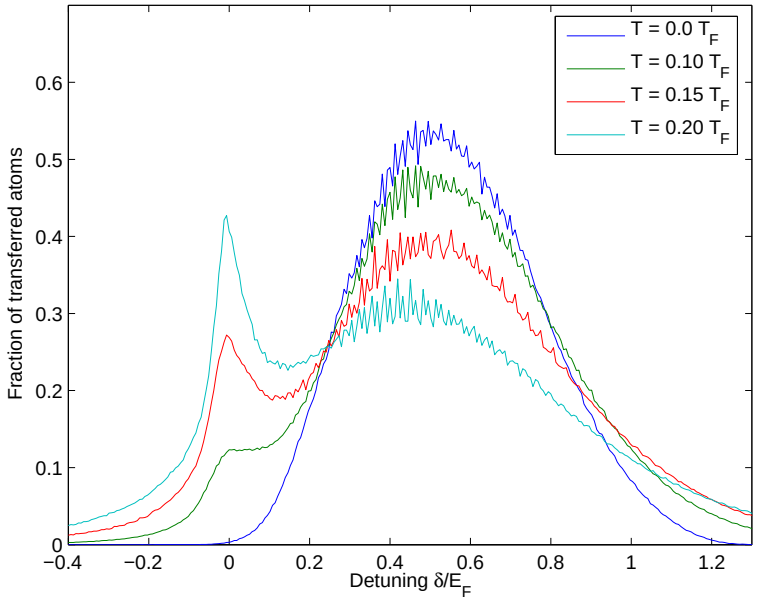

FIGURE 5.15 The rf-spectra obtained from the generalised first order theory for both zero and finite temperatures. The data is for an on-resonant gas ($(k_{\mathrm{F}}a_{gg'})^{-1} = 0.0$) and the excited state is assumed to be non-interacting ($(k_{\mathrm{F}}a_{eg'})^{-1} = -\infty$).

of the mean-field effect.

Fig. 5.14 shows the rf-spectra obtained using the simple first-order perturbation theory together with the Bogoliubov-deGennes technique in the harmonic oscillator basis. The parameters correspond to a magnetic field value $83.4\,\mathrm{mT}$ (on resonance) and linewidth of $\Gamma = 0.07\,E_{\mathrm{F}}$. Comparing this with the experimental spectra in Fig. 5.9 for $B = 83.7\,\mathrm{mT}$ shows qualitatively correct features such as a broad shifted peak at low temperatures and the appearance of a narrow peak at the zero detuning for higher temperatures. However, the lineshape does not have quite the correct shape, showing a strong tail at high detuning energies.

Fig. 5.15 shows the rf-spectra obtained using the generalised theory that allows the relaxation of the single-particle energy conservation through the use of virtual states. Compared to the first-order perturbation theory, these spectra have higher transfer rates and the strong tail is missing.

However, for both theories, the pairing peak is located at too high detuning energies, at $\delta = 0.4\,E_{\mathrm{F}}$ with first order theory and at $\delta = 0.5\,E_{\mathrm{F}}$ with generalised first order theory (compare with roughly $0.2\,E_{\mathrm{F}}$ observed in the experiment). As the atoms are excited into the state $|e\rangle$, the system becomes polarised and the creation of holes in the Fermi sea effectively increases the temperature of the gas. Since the pulse is very long, the system has time to equilibrate making the pairing gap possibly decrease in time, shifting the pairing peak to lower detunings. More importantly, the calculation neglects the interactions between the excited state $|e\rangle$ and the states $|g\rangle$ and $|g'\rangle$. However, all these states are strongly interacting, and especially $|e\rangle$ and $|g'\rangle$ states have a broad Feshbach resonance nearby (at $81.1\,\mathrm{mT}$). Including these

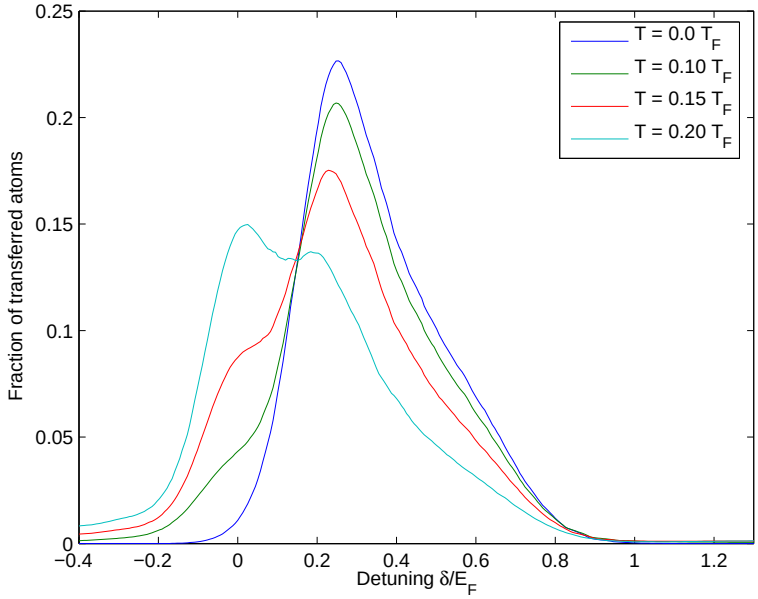

FIGURE 5.16 The rf-spectra obtained from the first order theory for both zero and finite temperatures but now the excited state is also interacting. The data is for an on-resonant gas with $(k_{\mathrm{F}}a_{gg'})^{-1} = 0.0$ and $(k_{\mathrm{F}}a_{eg'})^{-1} = -0.20$.

interactions would shift the energy levels of the $|e\rangle$-state down by creating a gap in the excitation spectrum.

Based on the discussion in section 5.2.6, I have incorporated the effect of $|e\rangle - |g'\rangle$ pairing by calculating the energy spectrum of the $|e\rangle$-state assuming a two-component gas in the $|e\rangle$- and $|g'\rangle$-states (I neglect the interactions between the $|e\rangle$ and $|g\rangle$-states based on the invariance of the $|e\rangle - |g\rangle$ interaction in the Bloch rotation). The spectra for the $|g\rangle \rightarrow |e\rangle$ rf-transition obtained using the simple first order theory is shown in Fig. 5.16. Comparing with Fig. 5.14, the effect of interactions in the $|e\rangle - |g'\rangle$ channel is to shift the pairing peak towards lower detunings as expected. Here the pairing peak is located at around $\delta = 0.25\,E_{\mathrm{F}}$, which is in good agreement with the experimental spectra. However, the effect of including these interactions should be considered only in a qualitative level, as the interaction strength $(k_{\mathrm{F}}a_{eg'})^{-1} = -0.20$ is much stronger than the real experimental interaction strength (for $B = 83.7\,\mathrm{mT}$ we have $(k_{\mathrm{F}}a_{eg'})^{-1} \approx -0.70$ [8]). On the other hand, the excitation gap for the $|e\rangle$-state, using experimental values, would be much smaller than for the $|g\rangle$ state. This would mean that the approximations in section 5.2.6 (namely that the pairing gap is the same for both states) fail. The choice of the interaction strength $(k_{\mathrm{F}}a_{eg'})^{-1} = -0.20$ is somewhat arbitrary here and the choice is based on convenience rather than any approximations.

Fig. 5.17 shows the corresponding spectra for the generalised theory. As with the simple first order theory, the pairing peak is shifted towards lower detuning energies, located at around $\delta = 0.3\,E_{\mathrm{F}}$. Comparing the spectra from the two theories (simple and generalised first order theories) shows that the effect of interaction

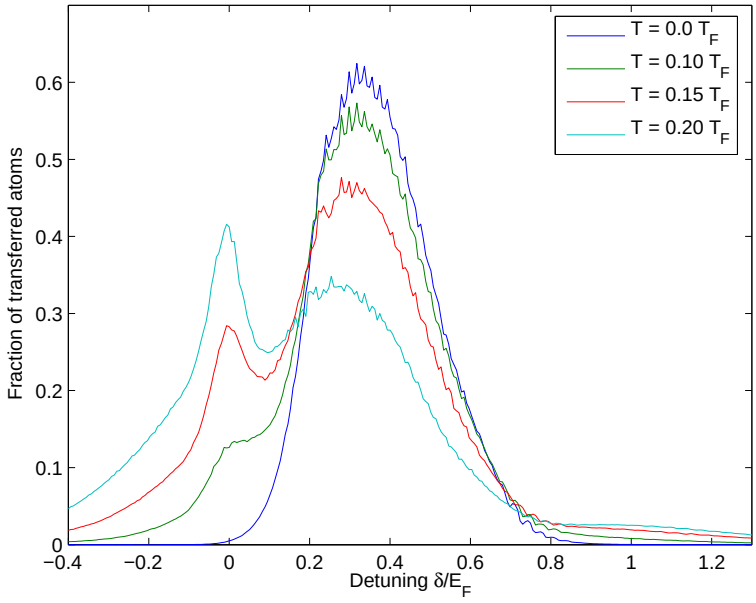

FIGURE 5.17 The rf-spectra obtained from the generalised first order theory for both zero and finite temperatures with an interacting excited state. The data is for an on-resonant gas with $(k_{\mathrm{F}}a_{gg'})^{-1} = 0.0$ and $(k_{\mathrm{F}}a_{eg'})^{-1} = -0.20$.

channel between the atoms is to increase the number of transferred atoms. The first order theory produces transfer fractions of roughly 0.25 at the peak value while the generalised theory exceeds 0.60. This transfer fraction is a measure of fraction of atoms that are on-resonant with the field. Neglecting any relaxation effects, extending the length of pulse does not allow any higher fractions as the on-resonant states become depleted. On the other hand, increasing the rf-field power does increase the fractions by enlarging the linewidth due to homogeneous power broadening. The effect is seen most dramatically in the limit of very small linewidth (the earlier spectra were for $\Gamma = 0.07\, E_{\mathrm{F}}$). Fig. 5.18 shows spectra for both theories using a smaller linewidth ($\Gamma = 0.01\, E_{\mathrm{F}}$). The first order theory gives tiny transfer fractions due to the broad excitation spectrum of the $|g\rangle$ atoms. On the other hand, the generalised first order theory is not constrained by the small linewidth as the atoms are allowed to exchange energy through collisions. Since these high order processes require interactions between two atoms of the same hyperfine state (although mediated through atoms in different hyperfine states), they are expected to be important only in strongly interacting gases.

The power of the rf-field in the experiment [19, 10] varied for different spectra, making the determination of the homogeneous linewidths and the rf-coupling tricky. In addition, the power broadening is not the only source of broadening, with the experimental setup, decoherence, and phenomena such as Doppler shifts providing other sources of broadening, although these effects are expected to be very small. However, under certain approximations, the linewidths can be deduced from the experimental spectra and from the knowledge of relative rf-powers [10], as dis-

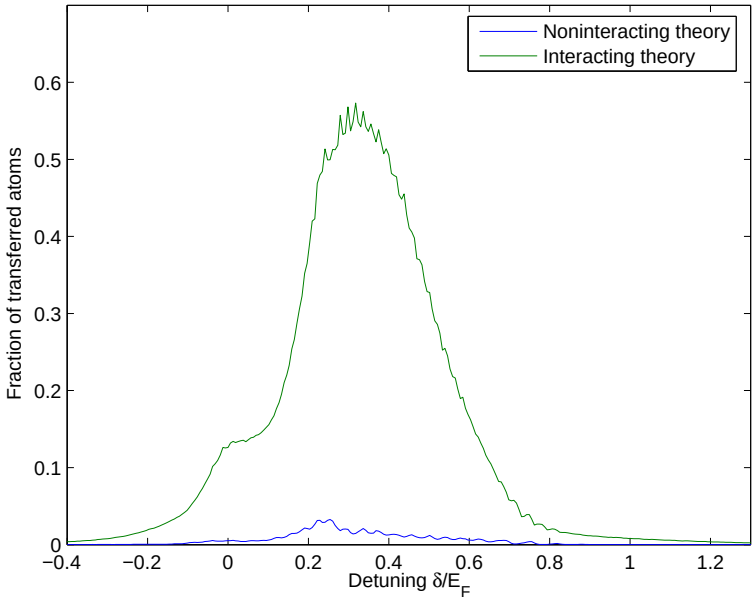

FIGURE 5.18 A small homogeneous linewidth gives very small transfer fractions in the simple first order theory because only a few atoms are on-resonant with the field at a given detuning. On the other hand, the spectrum from generalised first order theory is relatively insensitive to linewidths as the atoms are able to transfer excess energy to the environment (the other atoms). The parameters used in the plot are $(k_{\mathrm{F}}a_{gg'})^{-1} = 0.0$, $(k_{\mathrm{F}}a_{eg'})^{-1} = -0.20$, and temperature $T = 0.10\,T_{\mathrm{F}}$.

cussed in Appendix A.

Here the finite temperature spectra are obtained with a simple mean-field theory (the Bogoliubov-deGennes approach described above) neglecting any fluctuations of the order parameter. In contrast, the spectra in Refs. [45, 44] (Publications I and II) and in Fig. 5.11 were based on an extended (BCS) theory that included the effect of pseudogap. The pseudogap in turn follows from the fluctuations of the order parameter that are present already above the critical temperature when the average value of the order parameter is zero.

5.3 Physics of the generalised first order theory

The implications of the generalised first order theory can be studied further. A better insight can be attained by 'deriving' the theory using simple arguments.

In the perturbative approach, the transfer of N atoms is necessarily of at least order N in the coupling $\hat{H}_{\mathrm{a-l}}$. Neglecting the back and forth oscillations of the atoms (in the spirit of the linear response theory), the transfer of the atoms is described by

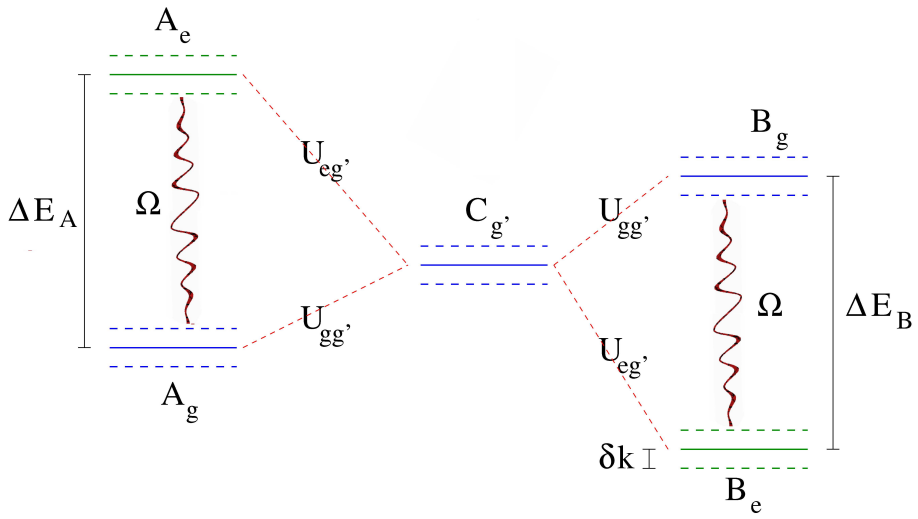

FIGURE 5.19 A simulation using three atoms. The atoms A and B are coupled by the rf-field (coupling strength Ω) to excited states $|e\rangle_A$ and $|e\rangle_B$, respectively. In addition, atom C interacts with the atoms A and B, conserving the total momentum but allowing momentum exchange δk between the atoms. The coupling strength between atoms in state $|g'\rangle$ and state $|g\rangle$ (states $|g'\rangle$ and $|e\rangle$) is $V_{gg'}$ ($V_{eg'}$).

the term

$$\langle \hat{N}_e(t)\rangle_N = \frac{1}{\hbar^{2N}}\Big\langle \int_0^t dt_1 \ldots \int_0^{t_{N-1}} dt_N\, \hat{H}_{\text{a-l}}(t_N)\ldots\hat{H}_{\text{a-l}}(t_1)\hat{N}_e(t) \int_0^t d\tau_N \ldots \int_0^{\tau_2} d\tau_1\, \hat{H}_{\text{a-l}}(\tau_N)\ldots\hat{H}_{\text{a-l}}(\tau_1)\Big\rangle. \tag{5.54}$$

If the number of transferred atoms N is large (and the atoms are uncorrelated), the transfer events occur at roughly even intervals. This means that each intermediate state lasts for the same time $t_{\text{inter}} = \frac{T}{N-1}$, where T is the length of the rf-pulse. The energy imprecision of the intermediate state is therefore $\Delta E \approx hN/T$. If a one-second pulse ($T = 1\,\text{s}$) transfers $N = 10^5$ atoms, the energy imprecision will be $\Delta E/h \approx 10^5\,\text{Hz}$, which well exceeds the typical Fermi energies. Therefore, the energy cost of a single-particle excitation is irrelevant, as the energy imprecision is enough to transfer any atom in the system. On the other hand, the energy imprecision of the total pulse is roughly $1\,\text{Hz}$, showing that the total energy of the system must be conserved.

The pulse length T enters the picture only through the uncertainty relation, by introducing an effective energy cutoff δ_c for the maximum energy cost of an atom transferred through an intermediate state. This allows us to simplify Eq. (5.54) by fixing the cutoff δ_c. Now the actual duration of the intermediate state t_{inter} becomes irrelevant for $t_{\text{inter}} \leq \frac{\hbar}{\delta_c}$ and we can choose $t_{\text{inter}} \to 0$. This produces the coherent coupling Hamiltonian $\hat{H}_{\text{coh}}$ (5.51).

The relaxation of the single-particle energy conservation is now clear. How-

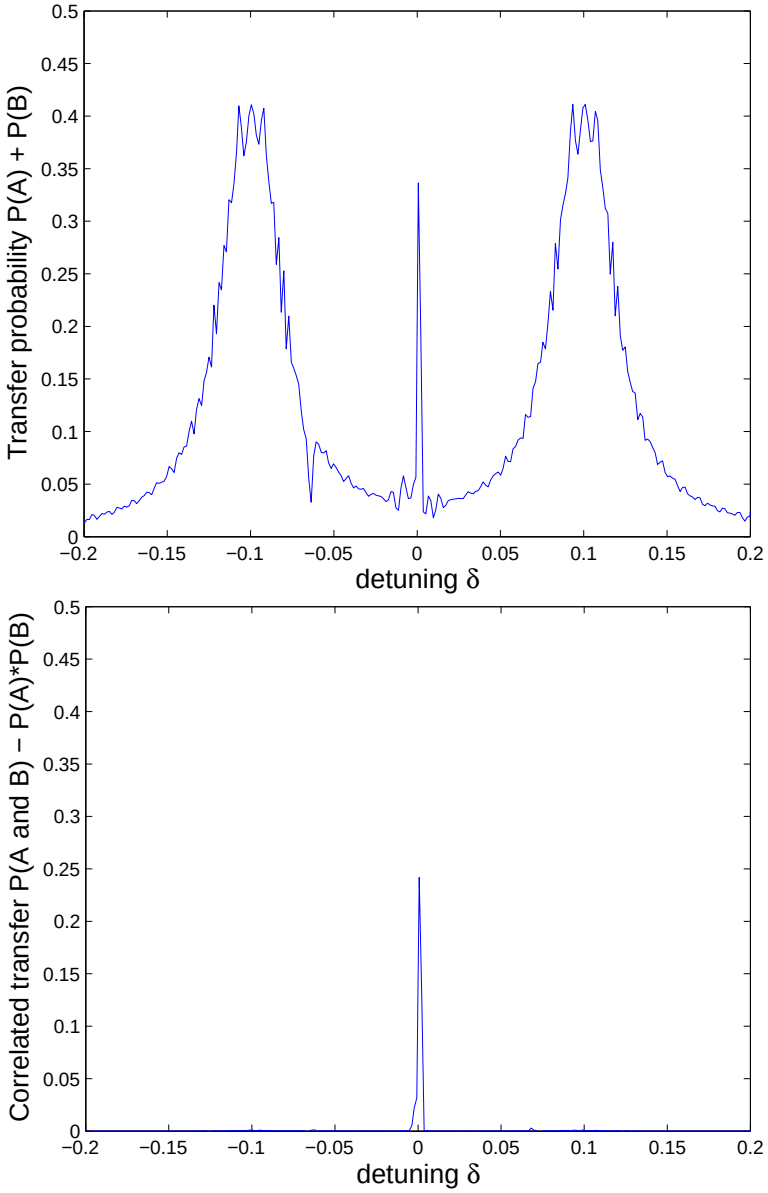

FIGURE 5.20 Top: the spectrum of the three-body system. The narrow peak at the zero detuning is described by the correlated two-atom transfer process. Bottom: the spectrum of correlated two-atom transfer processes.

ever, as discussed earlier, without correlations (that is, interactions) between the atoms, there is no channel for the atoms to share the excess energy. In order to study this effect, I have made a simulation using three atoms: one atom in state $|g'\rangle$ and two atoms in state $|g\rangle$. The atoms A and B in the hyperfine state $|g\rangle$ are coupled by the rf-field to an excited state $|e\rangle$ and the atom in state $|g'\rangle$ interacts with atoms in all other states. The system with the interaction and rf-coupling channels is shown schematically in Fig. 5.19. Each atom state is split into three different momentum states $k - \delta k$, k, and $k + \delta k$. In addition, the energy differences between the ground ($|g\rangle$) and the excited state ($|e\rangle$) for the two atoms have been chosen as $\Delta E_A = 0.1$

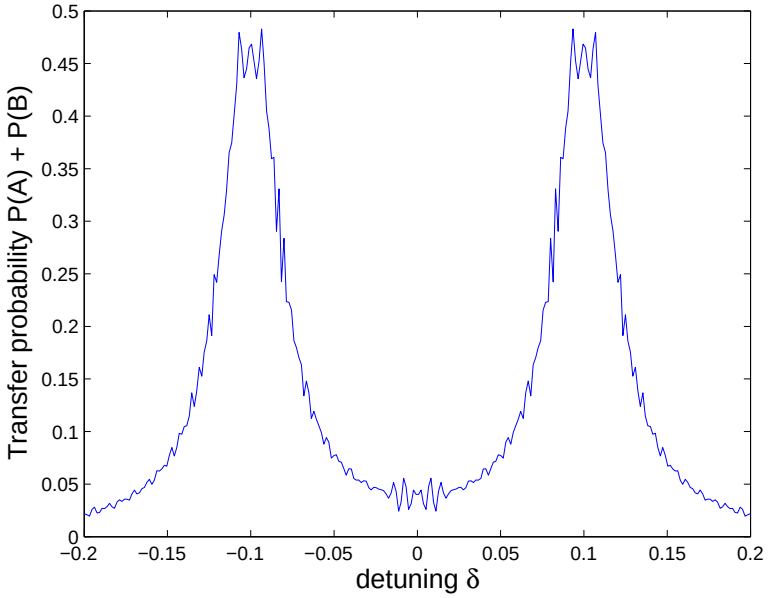

FIGURE 5.21 The spectrum of two noninteracting atoms.

and $\Delta E_B = -0.1$. The goal is to see the coherent transfer process of the two atoms in which the total energy is conserved (corresponding to the detuning $\omega = 0$). The coupling parameters used below are $\Omega = 0.01$, $V_{gg'} = 0.01$, $V_{eg'} = 0.005$, and $\delta k = 0.13$, and the momenta of the atoms are $k_A = k_B = 0.5$, and $k_C = 1.0$ (and the kinetic energy is k^2).

The time evolution of the system is solved exactly and Fig. 5.20 (top) shows a typical spectrum with two large, broad peaks at energies $\omega = 1.0$ and $\omega = -1.0$ corresponding to the excitations of single particles into the state $|e\rangle$. In addition, a sharp peak appears at the zero detuning. This peak originates from two processes: incoherent process in which atom B scatters from the atom in state $|g\rangle$ and is excited by the rf-field (and the same for atom A), and a coherent process in which both atoms A and B are scattered by the atom in state $|g\rangle$ and subsequently transferred to state $|e\rangle$. The incoherent contribution is given by the product of the transfer probabilities of the two atoms $P_a \cdot P_b$. Removing this from the spectrum, one obtains the spectrum of correlated processes shown in Fig. 5.20 (bottom). Indeed, a sharp peak remains at the zero detuning, corresponding to the total energy conserving process in which the two atoms are transferred. For comparison, Fig. 5.21 shows the spectrum when the interactions between the atoms have been removed. Now the two atoms are genuinely uncorrelated, and the sharp coherence peak vanished.

For weak interactions, the sharp coherence peak is very sensitive to the momentum difference δk of the atom states. The Fig. 5.22 shows the height of the coherence peak as a function of δk. Increasing the interaction strength allows a larger phase space for the correlated scattering process. Including more momentum states would enhance the narrow central peak by allowing more interaction channels that

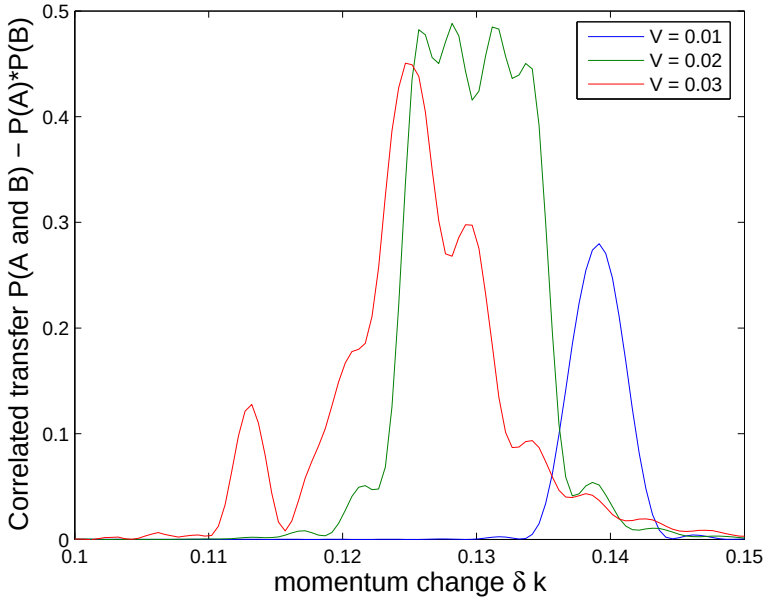

FIGURE 5.22 The height of the correlated peak as a function of the momentum change δk. Increasing the interaction strength makes the spectrum wider, creating correlations between the atoms in a wider range of momenta.

create correlations between the atoms A and B. Moreover, by including more atoms, the coherent peak becomes both broader (as different combinations of atoms are on-resonance at different detuning energies δ) and higher (as even higher order processes become available and the phase space grows).

This simple calculation shows that indeed there is a coherent process that is constrained only by the total energy conservation. The presence of an interaction channel between the atoms is crucial but for a strongly interacting gas the energy exchange processes should be strong.

An analogous idea of transport through virtual states is also encountered in solid state applications. Cotunnelling in a single electron transistor is a second order process in which an electron tunnels through two tunnel junctions [4]. Between the two tunnelling events, the system is in a virtual state in which the energy conservation is violated. If the tunnelling rate is sufficiently high, the energy imprecision due to short lifetime of the virtual state allows the transport of the electron and the current flow.

Transport through a virtual state is also used in Raman process, shown in Fig. 5.23. In the process, two lasers Ω_{12} and Ω_{23} create couplings between states. However, due to some conservation laws, the direct transition from state $|1\rangle$ to state $|2\rangle$ may be forbidden. In this case, the transition between the two states must take place through an additional state $|3\rangle$. However, if the lasers are off-detuned with respect to the transitions $|1\rangle \rightarrow |3\rangle$ and $|3\rangle \rightarrow |2\rangle$, the intermediate state is virtual.

The generalised first order perturbation theory described in this thesis can be understood as a many-body version of the Raman process, the two couplings pro-

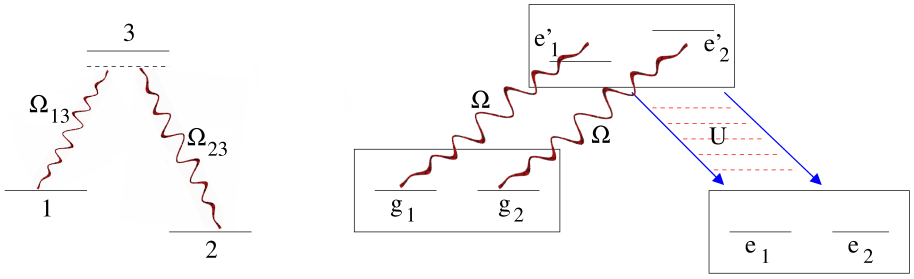

FIGURE 5.23 a) Raman transition from state $|1\rangle$ to state $|2\rangle$ applies an intermediate virtual state $|3\rangle$. The state $|3\rangle$ is a real state, but the two coupling lasers are off-detuned with respect to transitions $|1\rangle \rightarrow |3\rangle$ and $|3\rangle \rightarrow |2\rangle$. However, the combination of the two lasers is in resonance with the transfer $|1\rangle \rightarrow |2\rangle$, thus conserving the energy in the total process. b) The two atom transfer process described by the generalised perturbation theory also takes place through a virtual state. The first coupling between the states $|g_1, g_2\rangle \rightarrow |e_1', e_2'\rangle$ is created by the rf-field, and the coupling $|e_1', e_2'\rangle \rightarrow |e_1, e_2\rangle$ is provided by the atom-atom interactions U.

vided by the rf-field and the atom-atom interactions. Fig. 5.23 shows a two-atom process, in which the probing rf-field couples two atoms in hyperfine state $|g\rangle$ to hyperfine state $|e\rangle$. If this transition does not conserve energy, the target state is virtual. The relaxation into a real physical state takes place through an atom-atom interaction channel.

5.4 RF-spectroscopy of a polarised Fermi gas

The Bogoliubov-deGennes calculation described in this thesis is applicable also to polarised (or spin imbalanced) Fermi gases [91,65], when the chemical potentials of the two components are different, $\mu_{\mathrm{g}} \neq \mu_{\mathrm{g}'}$. Fig. 5.24 shows the density and order parameter profiles of a strongly interacting polarised Fermi gas at zero temperature [43] (Publication IV), revealing interesting oscillations of the order parameter at the edge of the atom cloud of the minority component (the atom species with less atoms). These oscillations are associated to FFLO-type pairing [28,49,56,86,17,52,43], in which the Cooper pairs have nonvanishing momentum (or angular momentum in the harmonic trap).

We have proposed the use of rf-spectroscopy to detect these oscillations [43] (Publication IV). The theories predict radio-frequency spectra shown in Fig. 5.25. At zero temperature, the spectrum of the majority component (the component with more atoms) shows a broad pairing peak and a narrow peak at the zero detuning energy. The narrow peak originates from the unpaired (excess) atoms at the edge of the trap. However, the spectrum of the minority component shows also a narrow peak at the zero detuning. This corresponds to a tail in the density distribution that combines with the oscillations of the order parameter. Since the amplitude of these oscillations is very small, these atoms are very weakly bound. Furthermore, the os-

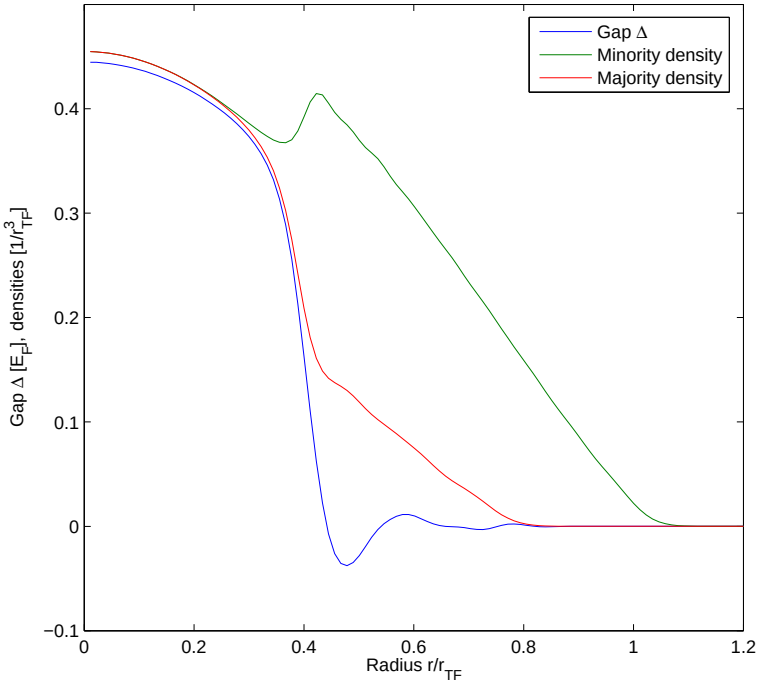

FIGURE 5.24 The densities of the two components $|g\rangle$ and $|g'\rangle$ and the order parameter profile $\Delta(r)$ of a polarised Fermi gas obtained using the Bogoliubov-deGennes approach. The data is for zero temperature and $(k_{\mathrm{F}}a)^{-1} = -0.5$. The numbers of atoms in the two components are $N_{\mathrm{g}} = 14555$ and $N_{\mathrm{g}'} = 3790$, yielding a total polarisation $P = \frac{N_{\mathrm{g}}-N_{\mathrm{g}'}}{N_{\mathrm{g}}+N_{\mathrm{g}'}} \approx 0.59$. The center of the trap exhibits ordinary BCS-type superfluidity with equal densities, but the edge of the cloud of minority atoms shows a polarised superfluid phase with a finite order parameter coexisting with a density difference. The oscillations of the order parameter are associated to FFLO-type pairing in a polarised superfluid.

cillating order parameter reaches zero at the nodes, so there are even completely unpaired atoms (in the local density approximation sense). The appearance of the zero detuning peak in the spectrum of the minority component is therefore a signature of the long oscillating tail of the order parameter, and of the zeroes of the order parameter.

5.5 Further experiments?

In order to confirm our predictions on the importance of the coherent transfer of atoms in the pairing gap experiments, a new set of experiments is needed.

The higher order processes, in which the atoms can exchange energy, thus relaxing the single-particle energy conservation, become relatively more important in the limit of narrow linewidth. Because of the broad excitation spectrum, the single-particle processes will give a very small contribution because only a small number of atoms can be on resonance with the field at a given frequency. On the other hand,

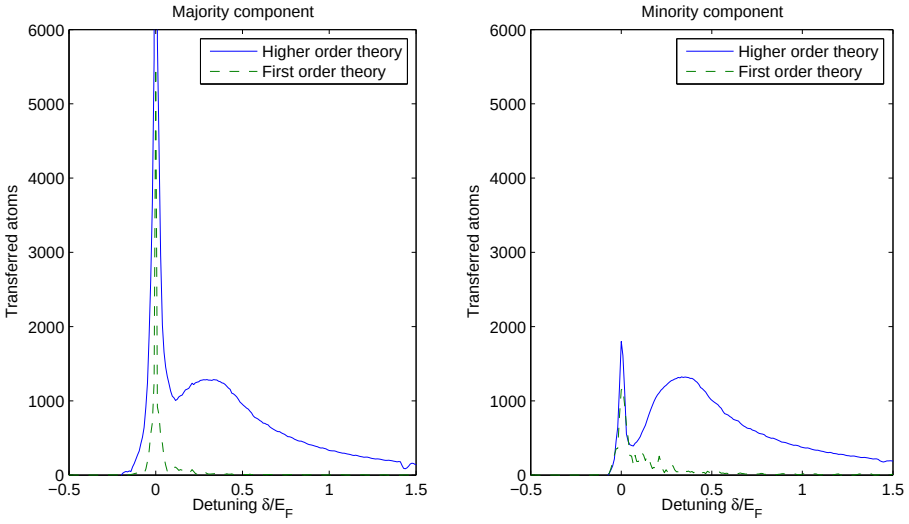

FIGURE 5.25 The rf-spectrum of a polarised Fermi gas, using the same parameters as in Fig. 5.24, and assuming the target state $|e\rangle$ to be noninteracting. The plot on the left shows the spectrum of the majority component. The zero detuning peak at zero temperature originates from the unpaired atom at the edge of the trap. The plot on the right shows the spectrum of the minority component. Here the zero detuning peak originates from atoms in the region with a small oscillating order parameter, signaling the presence of FFLO-type oscillations. The higher order theory corresponds to the generalised first order theory. The plain first order theory does not produce a visible pairing peak because of small linewidth $\Gamma = 0.005\, E_{\mathrm{F}}$. For larger linewidths the two theories produce spectra similar to the solid lines here.

the higher order processes are not limited by the linewidth but rather by the interaction and decoherence timescales. The importance of these higher order processes can thus be studied with strongly interacting gases using long weak pulses.

The theory outlined in this thesis should be applicable also to laser spectroscopy. The main difference between the use of radio-frequency and laser fields is the wavelength of the probing field. The laser fields can have significantly shorter wavelengths, meaning that the photons carry a higher momentum. The energy $\hbar\omega$ and the momentum δk given to the atoms in a two-photon process can be varied by changing the angle between two laser beams. This allows particle transfer between the $|g\rangle$ and $|g'\rangle$ states even in the $(50/50)\,\%$ mixture (compare with the spin-flip experiment [89]), or even between different momentum states of the same hyperfine state. This kind of Bragg spectroscopy has been applied in BEC experiments [80,78,79,81] for measuring the dynamic structure factor. The Bragg spectroscopy of superfluid Fermi gases has been considered theoretically in the BCS regime [55, 63, 15], optical lattices [36, 48], and the BCS-BEC crossover [60, 25, 13]. Since the spectroscopy can be performed between the $|g\rangle$ and $|g'\rangle$ states, there are no additional complications from the interactions with a third component. And finally, the laser beams can be targeted into a small region, helping to mitigate the inhomogeneous broadening effects from the trapping potential.

6 Conclusions

The spectroscopy of atom gases using radio-frequency or laser fields is well understood in the ideal case of noninteracting atoms. However, already in the case of weak mean-field type interactions, the simplest approach, using the Fermi Golden Rule or the first order perturbation theory, fails. This implies the need for a self-consistent solution that can describe collective processes, such as the coherent rotation of the states of all atoms.

The theory of rf-spectroscopy outlined in this thesis is a merge of the first order perturbation theory and the idea of the coherent Bloch rotation. The resulting theory is able to effectively describe all aspects in the two experiments in Refs. [89] and [19]. The introduction of the coherent coupling Hamiltonian (5.51) or the assumption of simultaneous transfer in the many-body perturbation theory are consequences of the inapplicability of the perturbative approach to collective phenomena. A rigorous approach would be to apply self-consistent methods that are by design well suited for collective effects.

A self-consistent theory for the rf-spectroscopy for a weakly interacting gas was suggested in Ref. [87]. The theory was able to explain the absence of the mean-field shift, because the self-consistency for symmetric atoms implies that if one atom is transferred, then all of them are, thus producing the correct spectrum. In addition, it can elegantly explain the pairing gap experiment, giving good agreement in the spectra. A future work would be to extend the self-consistent approach to strongly interacting gases where the virtual energy exchanging processes should be present. These effects can be included in a self-consistent theory by explicitly calculating the many-body rf-transitions (in the spirit of Section 5.2.7), or by including in the single particle picture such correlated effects that go beyond the mean-field theory.

Bibliography

[1] ALTMEYER, A., RIEDL, S., KOHSTALL, C., WRIGHT, M., GEURSEN, R., BARTENSTEIN, M., CHIN, C., HECKER DENSCHLAG, J., AND GRIMM, R., *Precision measurements of collective oscillations in the BEC-BCS crossover*. cond-mat/0609390 (2006).

[2] ANDERSON, M. H., ENSHER, J. R., MATTHEWS, M. R., WIEMAN, C. E., AND CORNELL, E. A., *Observation of Bose-Einstein Condensation in a Dilute Atomic Vapor*. Science **269** (1995) 198.

[3] ASHCROFT, N. W. AND MERMIN, N. D., *Solid state physics* (Saunders College, New York, 1976).

[4] AVERIN, D. V. AND NAZAROV, Y. V., *Macroscopic quantum tunneling of charge and co-tunneling, in "Single Charge Tunneling", edited by H. Grabert and M.H. Devoret* (Plenum, New York, 1992).

[5] BALDO, M., LOMBARDO, U., AND SCHUCK, P., *Deuteron formation in expanding nuclear matter from a strong coupling BCS approach*. Phys. Rev. C **52** (1995) 975.

[6] BARDEEN, J., COOPER, L. N., AND SCHRIEFFER, J. R., *Theory of Superconductivity*. Phys. Rev. **108** (1957) 1175.

[7] BARTENSTEIN, M., ALTMEYER, A., JOCHIM, S., CHIN, C., HECKER DENSCHLAG, J., AND GRIMM, R., *Collective excitations of a degenerate gas at the BEC-BCS crossover*. Phys. Rev. Lett. **92** (2004) 203201.

[8] BARTENSTEIN, M., ALTMEYER, A., RIEDL, S., GEURSEN, R., JOCHIM, S., CHIN, C., DENSCHLAG, J. H., GRIMM, R., SIMONI, A., TIESINGA, E., WILLIAMS, C. J., AND JULIENNE, P. S., *Precise determination of ^{6}Li cold collision parameters by radio-frequency spectroscopy on weakly bound molecules*. Phys. Rev. Lett. **94** (2005) 103201.

[9] BARTENSTEIN, M., ALTMEYER, A., RIEDL, S., JOCHIM, S., CHIN, C., HECKER DENSCHLAG, J., AND GRIMM, R., *Crossover from a molecular Bose-Einstein condensate to a degenerate Fermi gas*. Phys. Rev. Lett. **92** (2004) 120401.

[10] BARTENSTEIN, M. AND GRIMM, R., *personal communication* (2006).

[11] BOURDEL, T., KHAYKOVICH, L., CUBIZOLLES, J., ZHANG, J., CHEVY, F., TEICHMANN, M., TARRUELL, L., KOKKELMANS, S. J. J. M. F., AND SALOMON, C., *Experimental study of the BEC-BCS crossover region in lithium 6*. Phys. Rev. Lett. **93** (2004) 050401.

[12] BRUUN, G., CASTIN, Y., DUM, R., AND BURNETT, K., *BCS Theory for Trapped Ultracold Fermions*. Euro. Phys. J. D **7** (1999) 433.

[13] BRUUN, G. M. AND BAYM, G., *Bragg spectroscopy of cold atomic Fermi gases*. cond-mat/0607334 (2006).

[14] BRUUN, G. M., TÖRMÄ, P., RODRIGUEZ, M., AND ZOLLER, P., *Laser probing of Cooper-paired trapped atoms*. Phys. Rev. A **64** (2001) 033609.

[15] BÜCHLER, H. P., ZOLLER, P., AND ZWERGER, W., *Spectroscopy of Superfluid Pairing in Atomic Fermi Gases*. Phys. Rev. Lett. **93** (2004) 080401.

[16] BULGAC, A. AND YU, Y., *Renormalization of the Hartree-Fock-Bogoliubov equations in the case of a zero range pairing interaction*. Phys. Rev. Lett. **88** (2002) 042504.

[17] CASTORINA, P., GRASSO, M., OERTEL, M., URBAN, M., AND ZAPPALA, D., *Non-standard pairing in asymmetric trapped Fermi gases*. Phys. Rev. A **72** (2005) 025601.

[18] CHEN, Q., STAJIC, J., TAN, S., AND LEVIN, K., *BCS-BEC Crossover: From High Temperature Superconductors to Ultracold Superfluids*. Phys. Rep. **412** (2005) 1.

[19] CHIN, C., ALTMEYER, M. B. A., RIEDL, S., JOCHIM, S., DENSCHLAG, J. H., AND GRIMM, R., *Observation of the Pairing Gap in a Strongly Interacting Fermi Gas*. Science **305** (2004) 1128.

[20] CHIN, J. K., MILLER, D. E., LIU, Y., STAN, C., SETIAWAN, W., SANNER, C., XU, K., AND KETTERLE, W., *Superfluidity of ultracold fermions in an optical lattice*. cond-mat/0607004 (2006).

[21] COHEN-TANNOUDJI, C., DUPONT-ROC, J., AND GRYNBERG, G., *Atom-Photon Interactions* (Wiley, New York, 1992).

[22] COOPER, L. N., *Bound Electron Pairs in a Degenerate Fermi Gas*. Phys. Rev. **104** (1956) 1189.

[23] DAVIS, K. B., MEWES, M.-O., ANDREWS, M. R., VAN DRUTEN, N. J., DURFEE, D. S., KURN, D. M., AND KETTERLE, W., *Bose-Einstein condensation in a gas of sodium atoms*. Phys. Rev. Lett. **75** (1995) 3969.

[24] DE GENNES, P. G., *Superconductivity of Metals and Alloys* (Addison-Wesley Publishing, New York, 1989).

[25] DEB, B., *Light scattering in Cooper-paired Fermi atoms*. J. Phys. B **39** (2006) 529.

[26] EAGLES, D. M., *Possible Pairing without Superconductivity at Low Carrier Concentrations in Bulk and Thin-Film Superconducting Semiconductors*. Phys. Rev. **186** (1969) 456.

[27] FETTER, A. L. AND WALECKA, J. D., *Quantum theory of many-particle systems* (Dover publications, New York, 2003).

[28] FULDE, P. AND FERRELL, R. A., *Superconductivity in a strong spin-exchange field*. Phys. Rev. **135** (1964) A550.

[29] GRASSO, M. AND URBAN, M., *Hartree-Fock-Bogoliubov theory versus local-density approximation for superfluid trapped fermionic atoms*. Phys. Rev. A **68** (2003) 033610.

[30] GREINER, M., REGAL, C. A., AND JIN, D. S., *Emergence of a molecular Bose-Einstein condensate from a Fermi gas*. Nature **426** (2003) 537.

[31] GRIMM, R., *personal communication* (2004).

[32] GUPTA, S., HADZIBABIC, Z., ZWIERLEIN, M. W., STAN, C. A., DIECKMANN, K., SCHUNCK, C. H., VAN KEMPEN, E. G. M., VERHAAR, B. J., AND KETTERLE, W., *Radio-Frequency Spectroscopy of Ultracold Fermions*. Science **300** (2003) 1723.

[33] HAUSSMANN, R., RANTNER, W., CERRITO, S., AND ZWERGER, W., *Thermodynamics of the BCS-BEC crossover*. cond-mat/0608282 (2006).

[34] HE, Y., CHEN, Q., AND LEVIN, K., *Radio frequency spectroscopy and the pairing gap in trapped Fermi gases*. Phys. Rev. A **72** (2005) 011602.

[35] HEISELBERG, H., *Pairing gaps in atomic gases at the BCS-BEC crossover*. New J. Phys. **6** (2004) 137.

[36] HOFSTETTER, W., CIRAC, J. I., ZOLLER, P., DEMLER, E., AND LUKIN, M. D., *High-temperature superfluidity of fermionic atoms in optical lattices*. Phys. Rev. Lett. **89** (2002) 220407.

[37] HOLLAND, M., KOKKELMANS, S. J. J. M. F., CHIOFALO, M. L., AND WALSER, R., *Resonance superfluidity in a quantum degenerate Fermi gas*. Phys. Rev. Lett. **87** (2001) 120406.

[38] JENSEN, L. M., KINNUNEN, J., AND TÖRMÄ, P., *Non-BCS superfluidity in trapped ultracold Fermi gases*. cond-mat/0604424 (2006).

[39] JOCHIM, S., BARTENSTEIN, M., ALTMEYER, A., HENDL, G., RIEDL, S., CHIN, C., HECKER DENSCHLAG, J., AND GRIMM, R., *Bose-Einstein condensation of molecules*. Science **302** (2003) 2101.

[40] KADANOFF, L. P. AND BAYM, G., *Quantum statistical mechanics* (WA Benjamin, New York, 1962).

[41] KINAST, J., HEMMER, S. L., GEHM, M. E., TURLAPOV, A., AND THOMAS, J. E., *Evidence of superfluidity in a resonantly interacting Fermi gas*. Phys. Rev. Lett. **92** (2004) 150402.

[42] KINAST, J., TURLAPOV, A., THOMAS, J. E., CHEN, Q., STAJIC, J., AND LEVIN, K., *Heat capacity of a strongly interacting Fermi gas*. Science **307** (2005) 1296.

[43] KINNUNEN, J., JENSEN, L. M., AND TÖRMÄ, P., *Strongly interacting Fermi gases with density imbalance*. Phys. Rev. Lett. **96** (2006) 110403.

[44] KINNUNEN, J., RODRÍGUEZ, M., AND TÖRMÄ, P., *Pairing gap and in-gap excitations in trapped Fermionic superfluids*. Science **305** (2004) 1131.

[45] KINNUNEN, J., RODRÍGUEZ, M., AND TÖRMÄ, P., *Signatures of superfluidity for Feshbach-resonant Fermi Gases*. Phys. Rev. Lett. **92** (2004) 230403.

[46] KINNUNEN, J. AND TÖRMÄ, P., *Beyond linear response spectroscopy of ultracold Fermi gases*. Phys. Rev. Lett. **96** (2006) 070402.

[47] KOKKELMANS, S. J. J. M. F., MILSTEIN, J. N., CHIOFALO, M. L., WALSER, R., AND HOLLAND, M. J., *Resonance superfluidity: renormalisation of resonance scattering theory*. Phys. Rev. A **65** (2002) 053617.

[48] KOPONEN, T., MARTIKAINEN, J., KINNUNEN, J., AND TORMA, P., *Sound velocity and dimensional crossover in a superfluid Fermi gas in an optical lattice*. Phys. Rev. A **73** (2006) 033620.

[49] LARKIN, A. I. AND OVCHINNIKOV, Y. N., *Inhomogenous state of superconductors*. Sov. Phys. JETP **20** (1965) 762.

[50] LEGGETT, A. J., *Theory of a superfluid Fermi liquid. I. General formalism and static properties*. Phys. Rev. **140** (1965) 1869.

[51] LEGGETT, A. J., , *in Modern Trends in the Theory of Condensed Matter, edited by A. Pekalski and R. Przystawa* (Springer-Verlag, Berlin, 1980).

[52] MACHIDA, K., MIZUSHIMA, T., AND ICHIOKA, M., *Generic Phase Diagram of Fermion Superfluids with Population Imbalance*. cond-mat/0604339 (2006).

[53] MAHAN, G. D., *Many-Particle Physics* (Kluwer academic, New York, 2000).

[54] MARTIN, A. G., BAGNATO, V. S., LAFYATIS, G. P., AND PRITCHARD, D. E., *rf Spectroscopy of Trapped Neutral Atoms*. Phys. Rev. Lett. **61** (1988) 2431.

[55] MINGUZZI, A., FERRARI, G., AND CASTIN, Y., *Dynamic structure factor of a superfluid Fermi gas*. Eur. Phys. J. D **17** (2001) 49.

[56] MIZUSHIMA, T., MACHIDA, K., AND ICHIOKA, M., *Direct Imaging of Spatially Modulated Superfluid Phases in Atomic Fermion Systems*. Phys. Rev. Lett. **94** (2005) 060404.

[57] NOZÍERES, P. AND SCHMITT-RINK, S., *Bose condensation in an attractive fermion gas: from weak to strong coupling superconductivity*. J. Low Temp Phys. **59** (1985) 195.

[58] OHASHI, Y. AND GRIFFIN, A., *BCS-BEC crossover in a gas of Fermi atoms with a Feshbach resonance*. Phys. Rev. Lett. **89** (2002) 130402.

[59] OHASHI, Y. AND GRIFFIN, A., *Superfluid transition temperature in a trapped gas of Fermi atoms with a Feshbach resonance*. Phys. Rev. A **67** (2003) 033603.

[60] OHASHI, Y. AND GRIFFIN, A., *Superfluidity and collective modes in a uniform gas of Fermi atoms with a Feshbach resonance*. Phys. Rev. A **67** (2003) 063612.

[61] OHASHI, Y. AND GRIFFIN, A., *Single-particle excitations in a trapped gas of Fermi atoms in the BCS-BEC crossover region*. Phys. Rev. A **72** (2005) 013601.

[62] OHASHI, Y. AND GRIFFIN, A., *Single-particle excitations in a trapped gas of Fermi atoms in the BCS-BEC crossover region. II. Broad Feshbach resonance*. Phys. Rev. A **72** (2005) 063606.

[63] PARAOANU, G., RODRÍGUEZ, M., AND TÖRMÄ, P., *Cooper-pair coherence in a superfluid Fermi-gas of atoms*. J. Phys. B **34** (2001) 4763.

[64] PARISH, M. M., MIHAILA, B., TIMMERMANS, E. M., BLAGOEV, K. B., AND LITTLEWOOD, P. B., *BCS-BEC crossover with a finite-range interaction*. Phys. Rev. B **71** (2005) 064513.

[65] PARTRIDGE, G. B., LI, W., KAMAR, R. I., LIAO, Y. A., AND HULET, R. G., *Pairing and phase separation in a polarised Fermi gas*. Science **311** (2006) 503.

[66] PARTRIDGE, G. B., LI, W., KAMAR, R. I., LIAO, Y. A., AND HULET, R. G., *Response to comment on "Pairing and Phase Separation in a Polarized Fermi Gas"*. Science **314** (2006) 54.

[67] PARTRIDGE, G. B., LI, W., LIAO, Y. A., HULET, R. G., HAQUE, M., AND STOOF, H. T. C., *Deformation of a trapped Fermi gas with unequal spin populations*. cond-mat/0608455 (2006).

[68] PARTRIDGE, G. B., STRECKER, K. E., KAMAR, R. I., JACK, M. W., AND HULET, R. G., *Molecular probe of pairing in the BEC-BCS crossover*. Phys. Rev. Lett. **95** (2005) 020404.

[69] PETHICK, C. J. AND SMITH, H., *Bose-Einstein Condensation in Dilute Gases* (Cambridge University Press, Cambridge, 2002).

[70] PETROV, D. S., GANGARDT, D. M., AND SHLYAPNIKOV, G. V., *Low-dimensional trapped gases*. J. Phys. IV France **116** (2004) 3.

[71] PIERI, P., PISANI, L., AND STRINATI, G. C., *Pairing fluctuation effects on the single-particle spectra for the superconducting state*. Phys. Rev. Lett. **92** (2004) 110401.

[72] RAJAGOPAL, K. AND WILCZEK, F., *The Condensed Matter Physics of QCD, in "At the Frontier of Particle Physics / Handbook of QCD", edited by M. Shifman* (World Scientific, Singapore, 2001).

[73] REGAL, C. A., GREINER, M., AND JIN, D. S., *Observation of resonance condensation of fermionic atom pairs*. Phys. Rev. Lett. **92** (2004) 040403.

[74] REGAL, C. A. AND JIN, D. S., *Measurement of positive and negative scattering lengths in a Fermi gas of atoms*. Phys. Rev. Lett. **90** (2003) 230404.

[75] SCHUNCK, C. H., ZWIERLEIN, M. W., SCHIROTZEK, A., AND KETTERLE, W., *Superfluid expansion of a strongly interacting Fermi gas*. cond-mat/0607298 (2006).

[76] SHIN, Y., ZWIERLEIN, M. W., SCHUNCK, C. H., SCHIROTZEK, A., AND KETTERLE, W., *Observation of phase separation in a strongly-interacting imbalanced Fermi gas*. Phys. Rev. Lett. **97** (2006) 030401.

[77] STAJIC, J., MILSTEIN, J. N., CHEN, Q., CHIOFALO, M. L., HOLLAND, M. J., AND LEVIN, K., *The nature of superfluidity in ultracold Fermi gas near Feshbach resonances*. Phys. Rev. A **69** (2004) 063610.

[78] STAMPER-KURN, D. M., CHIKKATUR, A. P., GÖRLITZ, A., INOUYE, S., GUPTA, S., PRITCHARD, D. E., AND KETTERLE, W., *Excitation of phonons in a Bose-Einstein condensate by light scattering*. Phys. Rev. Lett. **83** (1999) 2876.

[79] STEINHAUER, J., OZERI, R., KATZ, N., AND DAVIDSON, N., *Excitation spectrum of a Bose-Einstein condensate*. Phys. Rev. Lett. **88** (2002) 120407.

[80] STENGER, J., INOUYE, S., CHIKKATUR, A. P., STAMPER-KURN, D. M., PRITCHARD, D. E., AND KETTERLE, W., *Bragg spectroscopy of a Bose-Einstein condensate*. Phys. Rev. Lett. **82** (1999) 4569.

[81] STÖFERLE, T., MORITZ, H., SCHORI, C., KÖHL, M., AND ESSLINGER, T., *Transition from a strongly interacting 1D superfluid to a Mott insulator*. Phys. Rev. Lett. **92** (2004) 130403.

[82] TIMMERMANS, E., TOMMASINI, P., HUSSEIN, M., AND KERMAN, A., *Feshbach resonances in atomic Bose-Einstein condensates*. Phys. Rep. **315** (1999) 199.

[83] TINKHAM, M., *Introduction to superconductivity* (Dover publications, New York, 2004).

[84] TÖRMÄ, P. AND ZOLLER, P., *Laser probing of Atomic Cooper Pairs*. Phys. Rev. Lett. **85** (2000) 000487.

[85] WALLS, D. F. AND MILBURN, G. J., *Quantum optics* (Springer-Verlag, Berlin, 1994).

[86] YANG, K., *Realization and detection of Fulde-Ferrell-Larkin-Ovchinnikov superfluid phases in trapped atomic fermion systems*. Phys. Rev. Lett. **95** (2005) 218903.

[87] YU, Z. AND BAYM, G., *Spin-correlation functions in ultracold paired atomic-fermion systems: Sum rules, self-consistent approximations, and mean fields*. Phys. Rev. A **73** (2006) 063601.

[88] ZWIERLEIN, M. W., ABO-SHAEER, J. R., SCHIROTZEK, A., SCHUNCK, C. H., AND KETTERLE, W., *Vortices and Superfluidity in a Strongly Interacting Fermi Gas*. Nature **435** (2005) 1047.

[89] ZWIERLEIN, M. W., HADZIBABIC, Z., GUPTA, S., AND KETTERLE, W., *Spectroscopic insensitivity to cold collisions in a two-state mixture of fermions*. Phys. Rev. Letters **91** (2003) 250404.

[90] ZWIERLEIN, M. W., SCHIROTZEK, A., SCHUNCK, C. H., AND KETTERLE, W., *Comment on "Pairing and Phase Separation in a Polarized Fermi Gas"*. Science **314** (2006) 54.

[91] ZWIERLEIN, M. W., SCHIROTZEK, A., SCHUNCK, C. H., AND KETTERLE, W., *Fermionic superfluidity with imbalanced spin populations*. Science **311** (2006) 492.

[92] ZWIERLEIN, M. W., SCHUNCK, C. H., SCHIROTZEK, A., AND KETTERLE, W., *Direct observation of the superfluid phase transition in ultracold Fermi gases*. Nature **442** (2006) 54.

[93] ZWIERLEIN, M. W., STAN, C. A., SCHUNCK, C. H., RAUPACH, S. M. F., KERMAN, A. J., AND KETTERLE, W., *Condensation of pairs of fermionic atoms near a Feshbach resonance*. Phys. Rev. Lett. **92** (2004) 120403.

Appendixes

A. Determination of the linewidth

The linewidth due to homogeneous broadening can be deduced (under a few assumptions) from experimental data in Ref. [19] together with the knowledge of relative rf-field powers [10], shown in Table 1. The total linewidth and shape of the spectra follows from many factors, but important for the present purposes is the linewidth of the narrow peak at zero detuning observed at finite temperatures, see Fig. 5.9.

The high temperature spectrum ($T \approx 6\,T_{\mathrm{F}}$, first row) for $B = 83.7\,\mathrm{mT}$ has linewidth of $640\,\mathrm{Hz}$. Increase of the rf-field power by $+11\,\mathrm{dB}$ (as in the intermediate temperature spectrum for the same interaction strength) corresponds to increasing the electric field intensity by factor 12.5. Increasing the field intensity increases the linewidth due to power broadening, i.e. the linewidth $\Gamma \propto \Omega$, where Ω is the atom-rf-field coupling as discussed in Section 5.1.2.

Factor of 12.5 would yield linewidths of $640\,\mathrm{Hz} \cdot 12.5 \approx 8\,\mathrm{kHz}$ which is much more than observed in the spectra at intermediate temperatures. Thus, it is clear that the linewidths at high temperatures have also other ingredients than the simple homogeneous power broadening. On the other hand, assuming that all these other broadening effects are independent of the rf-field power (and in principle all broadening effects that are directly proportional to the rf-field power can be dubbed as power broadenings), the linewidth at the high field powers would be completely dominated by the power broadening.

On the other hand, the width of the narrow peak at the zero detuning in the spectrum in the first column and the middle row ($72.0\,\mathrm{mT}$ and $T' \approx 0.5\,T_{\mathrm{F}}$) is ap-

	720G	822G	837G	875G
Top row ($T' \approx 6\,T_{\mathrm{F}}$)	$+0\,\mathrm{dB}$	$+0\,\mathrm{dB}$	$+1\,\mathrm{dB}$	$+0\,\mathrm{dB}$
Middle row ($T' \approx 0.5\,T_{\mathrm{F}}$)	$+17\,\mathrm{dB}$	$+10\,\mathrm{dB}$	$+12\,\mathrm{dB}$	$+8.5\,\mathrm{dB}$
Bottom row ($T' < 0.22\,T_{\mathrm{F}}$)	$+15.5\,\mathrm{dB}$	$+10.5\,\mathrm{dB}$	$+8\,\mathrm{dB}$	$+6\,\mathrm{dB}$

TABLE 1 The relative powers of the rf-field, corresponding to the spectra shown in Fig. 5.9. [10].

proximately $6\,\mathrm{kHz}$. The corresponding relative rf-power is $+17\,\mathrm{dB}$. Decreasing the field power is now expected to reduce the linewidth linearly with the rf-field intensity, and for relative rf-power of $+12\,\mathrm{dB}$ ($83.7\,\mathrm{mT}$ and $T' \approx 0.5\,T_\mathrm{F}$) this would yield linewidth of less than $2\,\mathrm{kHz}$. Since all other sources of broadening were assumed to be smaller (on the grounds of the narrowness of the peak at high temperatures), this gives the total homogeneous linewidth. Notice, that although the interaction strength at the resonance is much stronger than in the BEC side, any additional broadening due to simple mean-field interactions are already included in the high temperature spectrum at the same magnetic field value.

However, the linewidth of the narrow peak at the zero detuning in the spectrum for $83.7\,\mathrm{mT}$ and $T' \approx 0.5\,T_\mathrm{F}$ is roughly $5 - 6\,\mathrm{kHz}$. The source of this additional broadening is not clear. However, the generalised first order theory discussed in this thesis effectively provides an additional broadening that originates from the pairing of the atoms.

The Fermi energies at the intermediate temperatures were $T_\mathrm{F} \approx 3.4\,\mu\mathrm{K}$, giving as the linewidth in Fermi units $\Gamma/E_\mathrm{F} \approx 0.03$. This is smaller than the linewidths used in the calculations in this thesis by factor of 2. The effect of smaller linewidths would be to reduce the fraction of transferred atoms in all simple first order spectra by factor of 2. In contrast, the generalised first order spectra are insensitive to narrow linewidths and therefore they remain unchanged.